Template for Submission of Manuscripts to American Chemical Society Journals

Word 2010, single-column, double-spaced (2013)

This template is a guide to be used to prepare manuscripts for submission. Please consult the Instructions to Authors or a recent issue of the journal for detailed guidelines and procedures for submission. This template is intended to benefit to the author in that the entire manuscript (text, tables, and graphics) may be submitted in one file. Inserting graphics and tables close to the point at which they are discussed in the text of the manuscript can also be a benefit for the reviewer.

When you submit a manuscript using this template, you will not actually see the page formatting that appears in the printed journal. This will occur as part of the editorial production process. Abbreviated instructions for using the template follow. Consult the documentation for your specific application and version for more information. Additional instructions can be found in the readme file at the web page where you downloaded this template.

Using the template

In ACS publications there are many different components of a manuscript (i.e., title, abstract, main text, figure captions, etc.) that are represented in the template. See the Guide, Notes, Notice, or Instructions for Authors on the journal's homepage to determine which parts should be included for the manuscript that you are preparing

1. If typing your manuscript directly into the template, select (highlight) the text of the template that you want to replace and begin typing your manuscript (i.e., select the Title section for typing in your title).

2. If you have already prepared your document in a Word file, you will need to attach the template to your working document in order to apply the Word Style tags. Further instructions can be found in the readme file at the web page where you downloaded this template.

    a. Go to the Add-Ins tab and you will see all the Word Styles from the template that has now been imported into the current document. A Styles toolbar has been generated that will display the different Styles for you to choose from. If this is not present, type in the following command (Alt+Ctrl+Shift+S) and it should appear. You can close this at any time and then reopen it when needed.

    b. Click in the sentence or paragraph and then go to the Add-Ins tab and select the relevant Word Style. This will apply the Word Style to the entire text (sentence or paragraph). Do this for all sections of the manuscript.

3. To insert graphics within the text or as a figure, chart, scheme, or table, create a new line and insert the graphic where desired. If your graphic is not visible, ensure that the Word Style is "Normal" with an automatic height adjustment. If the size of the artwork needs to be adjusted, re-size the artwork in your graphics program and re-paste the artwork into the template (maximum width for single-column artwork, 3.3 in. (8.5 cm); maximum width for double-column artwork, 7 in. (17.8 cm)). **NOTE**: If you are submitting a Table of Contents graphic, please insert the graphic at the end of the file.

4. Ensure that page numbers are present on all pages before submitting your manuscript.

5. Delete these instructions and any sections that are not needed.

6. Save the file with the graphics in place: select **Save As** (**File** menu) and save it as a document file (not a .dot template file).

7. Proof the manuscript to ensure that all parts of the manuscript are present and clearly legible.

Down the Microporous Rabbit Hole of Silicoaluminophosphates, Recent Developments on Synthesis, Characterization and Catalytic Applications

*Matthew E. Potter**

Department of Chemistry, University of Southampton, Southampton, Hampshire, UK, SO17 1BJ. Email: M.E.Potter@soton.ac.uk

ABSTRACT: Since their invention silicoaluminophospates (SAPOs) have become by far the most researched class of aluminophosphates due to their commercial use as solid acid catalysts. Currently over 25 different SAPO frameworks have been synthesized, providing a diverse range of confined nanoporous topologies, with distinct acid sites. When combined with emerging synthetic techniques to further modulate these species, there are endless possibilities to tailor SAPO materials for specific catalytic applications. Herein this review focusses on developments, and possibilities, from the last decade in the field of SAPO research, with particular attention paid to synthesis, characterization, theoretical studies and case studies of their catalytic

applications. I aim to simultaneously educate and inspire readers at all stages of their career and hope that this review helps further interest and research into the exciting field of SAPOs.

Introduction to SAPOs

Silicon doped aluminophosphates (SAPOs),[1] a subclass of aluminophosphates (AlPOs)[2] represent a large family of materials. Since SAPOs discovery in the 1980s by Union Carbide Corporation, they have widely been studied as heterogeneous Bronsted acid catalysts. This is partly due to their use in the methanol to olefin (MTO) process,[3-6] but also due to the wider range of synthetic variables that allow careful tuning of catalytic behavior.

AlPOs are microporous materials, with pore diameters spanning 3-12 Å. They are constructed by alternating AlO_4 and PO_4 tetrahedra, known primary building units (PBUs). These PBUs bind through Al-O-P bonds, forming simple shapes, known as secondary building units (SBUs), including hexagons (s6r), squares (s4r) or stacked hexagons (d6r). The SBUs then orientate and combine to create distinct frameworks, labelled with a unique number and a 3-letter code. AlPO-18 (AEI) and AlPO-34 (CHA) show how slight differences in SBU alignment form different frameworks. Both species contain d6r, bound by s4r, though in AlPO-34 the d6r are all aligned (AAA, Figure 1) whereas the d6r layers alternate in AlPO-18 (ABA, Figure 1), though the change is subtle, this significantly influences the properties of the systems.[7-10]
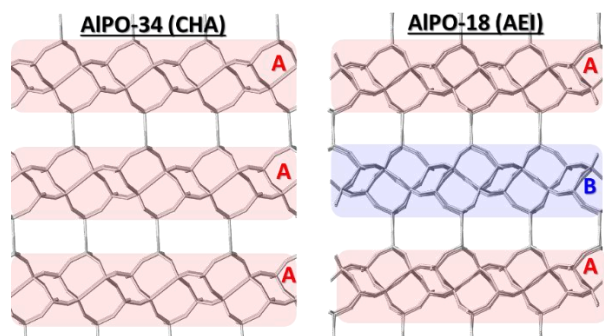
Figure 1. Highlighting the subtle structural difference in AlPO-34 (CHA) and AlPO-18 (AEI) based on the orientation of d6r layers.

Undoped AlPOs have limited catalytic potential, as the ever-present Al-OH and P-OH defect species are very weakly-acidic, and ineffective for many transformations.[11-12] The interest in AlPOs comes from the ability to isomorphously substitute framework Al or P atoms with dopants, creating a range of possible active sites within the microporous framework.[13] The nature of these sites depends on many parameters, including framework topology, dopant choice, dopant quantity and synthesis protocol. A variety of dopants have been isomorphously substituted into AlPOs, but not all elements can be substituted, as there are restrictions on size and charge.[13-14] Dopants must be similar in size to the framework Al and P species to be included in the framework, as deviation from the ideal geometry distorts the local framework. Significant deviation comes with a greater energy cost, and therefore limits incorporation. Charge also plays a major role in framework substitution. M^{2+} or M^{3+} dopants will exclusively substitute the framework Al^{3+}, known as *Type I substitution*.[15] M^+ species cannot isomorphously substitute, as the lower charge means weaker coulombic interactions with framework oxygen, which cannot justify the energy cost of distortion to accommodate it. Substituting an M^{3+} dopant for Al^{3+}, is charge neutral. But M^{2+} substituting Al^{3+}, creates a negative charge, which is balanced by a

proton binding to an oxygen atom, adjacent to the dopant, creating a M-O(H)-P Bronsted acid site, which is commonly stronger than the Al-OH and P-OH defects.[16-18] Similarly, M^{4+} and M^{5+} dopants substitute framework P^{5+}, via *Type II substitution* (Figure 2B). An isolated M^{4+} dopant substituting P^{5+} will also create a Bronsted acid species.[19] M^{4+} dopants, primarily Si, can also undergo *Type III substitution*, where an adjacent Al^{3+} and P^{5+} are both substituted with a Si^{4+} species (Figure 2C). This is a neutral substitution, so no protons are generated. The existence of an isolated $(AlO)_3Si-O-Si(OP)_3$ species has not been reported in an AlPO, thus when Type III substitution occurs, it is accompanied by Type II substitution, leading to the formation of Si-islands in SAPO materials (Figure 2D).[19-21]
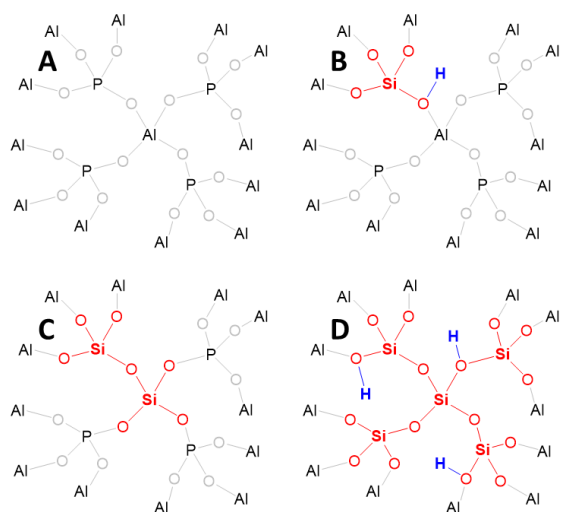
Figure 2. Si substitution mechanisms in SAPOs showing A) Bare undoped framework, B) Type II substitution, C) Type III substitution and D) The combination of type II and III substitution giving a 5-silicon island.

Whether Si forms islands or isolated sites, is determined by many factors, though each framework has a preference. SAPO-34 and SAPO-37 favor isolated sites, whereas SAPO-5 often favors Si islands.[19] The Si quantity also influences the mechanism, with smaller quantities favor

isolated sites, whereas greater quantities often lead to islanding. The reasons behind these factors are still unclear, likely it is affected by the energetics of silicon distorting the framework, which could be calculated computationally. However, this approach would prematurely dismiss the crystallization processes, and rate of Si-O-Si bond breaking versus framework formation. Specific investigation into this would require a combination of in-depth *in situ* and *operando* characterization and theoretical methods on the synthesis of SAPO materials. Therefore, despite significant interest in SAPOs, there are still many important fundamental questions to answer.

Given that SAPOs are microporous solid acid species, they are naturally compared to zeolite materials, which are prevalent catalysts in industrial petrochemical processes. Despite, in principle, both species deriving from the same basic building blocks, there are few examples of SAPOs and zeolites forming identical frameworks. The most common examples being the CHA (SAPO-34 and Chabazite) and FAU (SAPO-37 and Faujasite) frameworks. Despite this there are countless examples of frameworks that are unique to zeolites such as FER, MFI and BEA. Similarly, there are also frameworks that are unique to SAPOs, with no analogous zeolite species including SAPO-31 (ATO), SAPO-39 (ATN) and SAPO-40 (AFO). There are several reasons for this disparity, perhaps the simplest of which is due to Lowensteins rule, which prohibits Al-O-Al and P-O-P bonds. Thus SAPOs (and AlPOs in general) cannot form structures that include odd numbered rings, such as MFI (ZSM-5), which contains 5-membered rings. The preference for different frameworks also lies in the electronic structures of the different materials. While zeolites have been shown to possess more covalent character, AlPOs (and SAPOs) are more ionic, existing more as Al^{3+} and PO_4^{3-} ions.[22] This fundamental difference may lead to some frameworks being more energetically favourable than others. Finally the synthesis procedures are also different, as zeolites are predominantly formed under basic conditions, whereas SAPOs

form under more acidic conditions.[23] This will influence the rates of formation of different building units, ultimately leading to different frameworks being formed.

Focussing on acidity, the Bronsted acid sites in SAPOs (as discussed) derive from Si being doped into the Al, P and O framework. Whereas in zeolites it is the Al dopants being introduced into the Si and O lattice which creates the Bronsted acidity. The acid sites in SAPOs are typically weaker than in zeolites,[24] while this may be unhelpful in some reactions, it can increase catalyst lifetime by limiting coking, which occurs primarily on stronger acid sites. While SAPO chemistry almost exclusively concerns Bronsted acidity, Lewis acidity is not uncommon in zeolites, deriving from extra framework aluminium. As such one could argue that it is more straightforward to form one uniform acid site in a SAPO, than a zeolite, which would help target one specific reaction and intermediate.

While zeolites are more common industrial catalysts than SAPOs, the different frameworks offered by SAPO materials could provide unique options for tailoring the selectivity of processes towards desired products. Further the weaker acid sites in SAPOs have already been shown to be beneficial for some reactions.[25] As such wherever zeolites are employed, SAPOs must always be considered as a viable alternative.

The synthesis of SAPO materials

Hydrothermal synthesis of SAPOs

Traditionally SAPO materials are synthesized hydrothermally, where an aqueous gel is formed from aluminum, phosphorus and silicon precursors and a structure directing agent (SDA).[3] The

initial acidity helps decompose the precursors into MO_4 tetrahedra within the gel, which combine to give small oligomers, that later form the framework.[26-28] The SDA, typically an amine or ammonium ion (though alternatives have been investigated[29-33]) serves as a template for the framework to form around, thus SDA choice helps dictate SAPO structure will be formed. One can rationalize that small SDAs, such as isopropylamine, form systems with small pores, while larger SDAs such as a tetrapropylammonium form larger pored systems. In some cases this idea holds, indeed elegant computational studies have focused on this idea,[34-35] predicting the ideal SDA for a framework, by optimizing the fit for molecule within the pore space. However, in many cases this is an oversimplification, as it cannot account for the influence the SDA basicity has on framework choice. Nor can it consider interactions between SDA and reagents, or how this would influence the crystallization kinetics of different frameworks. Finally, and importantly for SAPO materials, it cannot investigate the role of dopants. In wider AlPO chemistry, SDA choice is a significant factor in whether a dopant is isomorphously substituted or not.[36] Computational techniques encompassing this would be highly valuable, it would require a multi-scale approach to establish even a general case. This would realistically span crystallization kinetics, molecular dynamics to consider the arrangement of framework species around the SDA and finally quantum mechanical calculations looking at the interactions between the various species. A challenge for sure, but a worthwhile one. Many syntheses also use a 'mixed-template' approach, such as SAPO-37, the SAPO equivalent of faujasite.[37-38] This species contains sodalite cages, linked together by d6r to form a supercage. This uses both tetramethyl and tetrapropyl ammonium ions as SDAs, as the tetramethyl ammonium ions encouraging formation of the sodalite cages, while the tetrapropyl ammonium ions reside in the supercages (Figure 3).
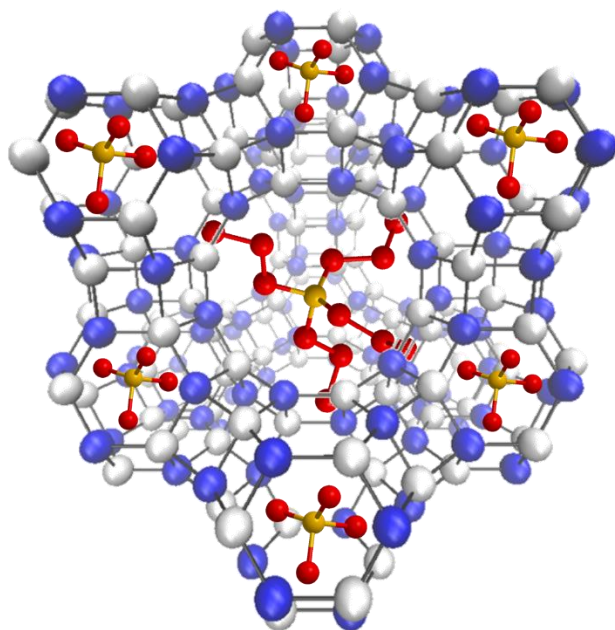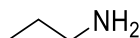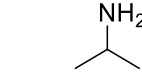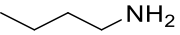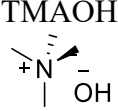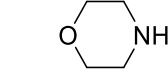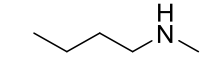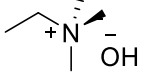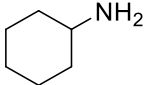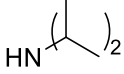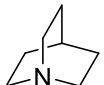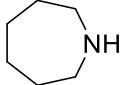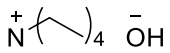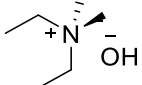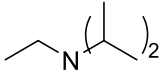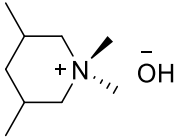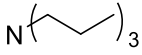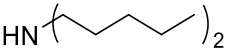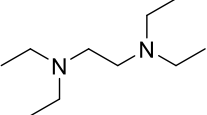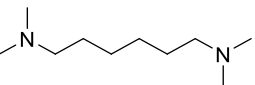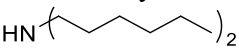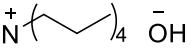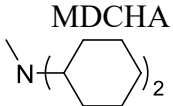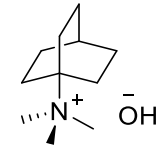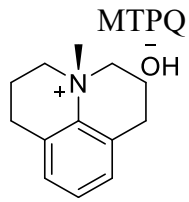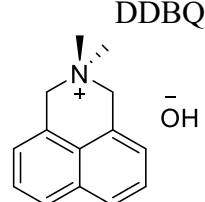
Figure 3. SAPO-37 FAU framework showing TPAOH residing in the supercage and TMAOH in the sodalite cages. White = Al, Blue = P, Red = C & Yellow = N.

Many different nitrogen containing species have been used as SDAs (Table 1) for SAPOs, though few SDAs can be considered 'structure specific', meaning that they will target only one specific framework, regardless of the other synthetic parameters. Perhaps one of the few examples of this is N,N-methyldicyclohexylamine, which regardless of reaction conditions will almost exclusively form the AFI framework; SAPO-5. However, some SDAs such as dipropylamine, have been shown to form 8 different frameworks, showing its versatility as an SDA, and the influence of other synthetic factors.

Table 1. Known SDAs for single templated hydrothermal synthesis of phase pure SAPOs.

Template	SAPO formed	Ref	Template	SAPO formed	Ref
n-Propylamine $\diagdown\diagup\diagdown$ NH$_2$	47	[39]	iso-Propylamine	43	[40]

Compound	Values	Refs
n-Butylamine	34	41
sec-Butylamine	47	42
Diethylamine	5, 11, 34, 41, 44, 47	43-47
TMAOH	20, 42	48-49
Morpholine	34, 47	50-51
Piperidine	34	52
N-Methylbutylamine	47	53
ETMAOH	59, 67, 69	33, 54-55
Methyldiethanolamine	5, 35, 35, 44	56
Triethylamine	5, 34, 47	46, 49, 51
Dipropylamine	5, 11, 31, 34, 39, 41, 46, 47	46, 51, 57-61
Diisopropylamine	5, 11, 34, 41	62-64
Cyclohexylamine	17, 35, 44	65-67
Hexamethyleneimine	5, 16, 35, 44	68-70
Quinuclidine	16, 17, 35	1
DEDMAOH	57, 79	33, 54
TEAOH	5, 18, 34	46, 49, 71
Dibutylamine	5, 11, 31, 41	57, 72-74
Diisopropylethylamine	18	7
Tripropylamine	5	59
DMDMPOH	18	75
TEEDA	5, 34	76
Dipentylamine	31	57
Dihexylamine	31	57
TMHD	17, 56	77-78
TPAOH	40	79

MDCHA   5   [16]   TMAdaOH   34   [80]

MTPQ   42   [81]   DDBQ   42   [81]

    Once the synthesis gel is sufficiently homogenized with the SDA it is transferred to a closed system, typically a Teflon-lined steel autoclave, where it is heated above the boiling point of water, for either hours or weeks (Figure 4). Steam tables predicts that significant pressure is generated, 3.7 barG is formed at 150 °C, at 200 °C this rises to 14.5 barG, so care should always be taken! Systems designed to hold such pressures are typically heavily reinforced, meaning they are unlikely to instantly reach the desired temperature, creating a heating gradient across the vessel. Thus, it may take many minutes for the synthesis gel to equilibrate at the desired temperature, during which time, many different products could form, so it is important to minimize this length of time as much as possible. After crystallization step, the systems are cooled, again, this step should be minimized to quench all possible reactions. After the sample is typically washed and collected via filtration of centrifugation, and finally calcined by flowing air over the material at over 500 °C, to remove the SDA from the pores.
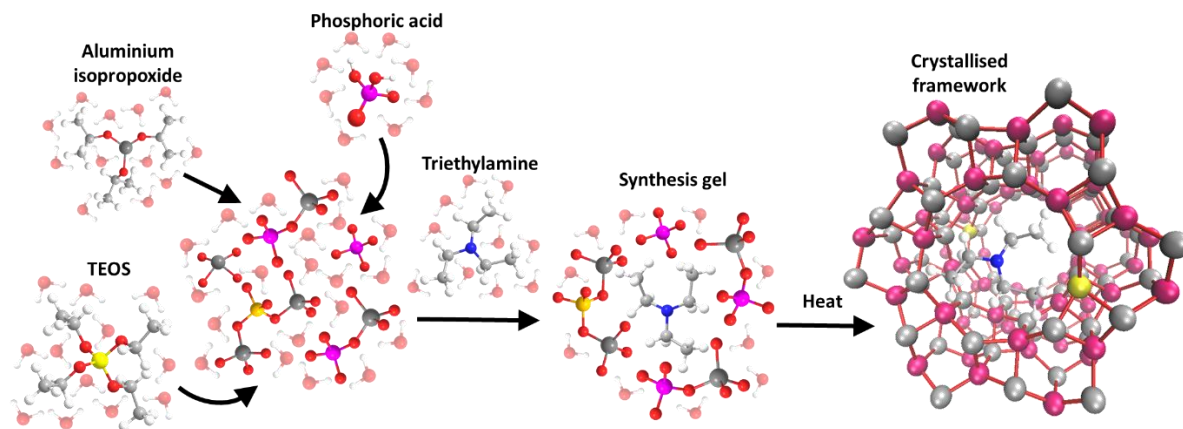
Figure 4. Typical protocol for a hydrothermal synthesis.

Synthesizing a phase pure SAPO material without a known procedure is challenging, iterative, and repetitive, with many parameters to consider and harmonize, mainly because many variables influence multiple factors (Table 2). A recent example comes from Zhu *et al* who probed the influence of the Si/Al ratio, with triethylamine (TEA) as an SDA, on phase formation.[82] A gel ratio of $xAl_2O_3:1.0P_2O_5:4.5TEA:0.4SiO_2:80H_2O$ was used, where x varied to give Si/Al ratios of 0.03, 0.08, 0.1, 0.2 and 0.4. All gels were heated at 200 °C for two days, so the only variable was the quantity of pseudoboehmite added. For the Si/Al ratio of 0.03 phase pure SAPO-5 was formed, whereas at 0.4 phase pure SAPO-34 was formed, with a progression from AFI to CHA seen in between.[82] Such studies emphasize the need for careful design of the synthesis procedures, and highlight, in some cases, how little room for error there is, creating a unique synthesis protocol, typically requires an expansive 'design of experiments' approach.

Table 2. Influence of synthetic variables in SAPO synthesis.

Synthesis parameters	Variables

Template choice
Al/P ratio
Precursor choice
Silicon dopant quantity
Crystallisation temperature
Ageing time
Heating rate
Cooling Rate
Crystallisation time

Framework choice
Phase purity
Particle size
Crystallinity
Silicon substitution mechanism
Acid site strength
Acid site density
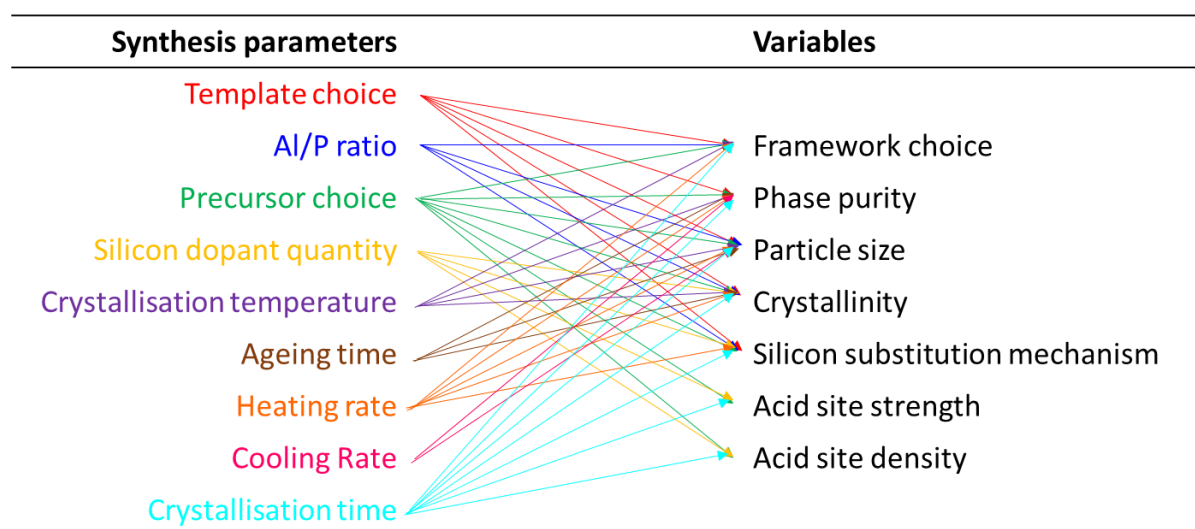
While hydrothermal methods are the most established method for SAPO synthesis (Figure 4), there are flaws. Firstly, the need for specialist equipment that can withstand the pressure generated is costly, and on a lab-scale can only be done in batch, taking significant time to synthesis large quantities of material. Secondly the process is incredibly energy intensive, the heated crystallization step can last for days, and the calcination process typically runs for over 6 hours. Finally, the requires costly SDAs which are rarely recovered. Therefore, inspiration has been taken from zeolite synthesis into SDA-free methods with some success. In many cases the necessity of the SDA can be reduced (though rarely completely removed), by using seed crystals.[3, 83-85] Adding small quantities of the desired framework into the synthesis gel provides ready-made nucleation sites for the framework, this speeds up the crystallization kinetics for that species, as a blueprint has already been supplied.

It is often desirable to also control particle size as porous materials typically benefit from smaller particles,[86] as this improves diffusion through the pores, increasing access of active sites. Many approaches have been used to try to modulate particle size and shape. Work from Pham Thanh *et al* explored the influence of a mixed-template approach for SAPO-34 synthesis.[87]

Specifically focusing on triethylamine (TEA), tetraethylammonium hydroxide (TEAOH) and morpholine on a 48 hour, 200 ºC hydrothermal synthesis. Despite different combinations all resulting in phase pure SAPO-34, the particles were found to have different properties (Figure 5). Morpholine alone produced larger 38 μm cubic particles, whereas tetraethylammonium hydroxide gave smaller cubic 5 μm particles. Combining the three SDA's retained crystallinity, but reduced particle size further, with an average size of 3 μm (Figure 5). This suggests mixtures of SDAs can either promote nucleation, or hinder crystallization, causing smaller particles.
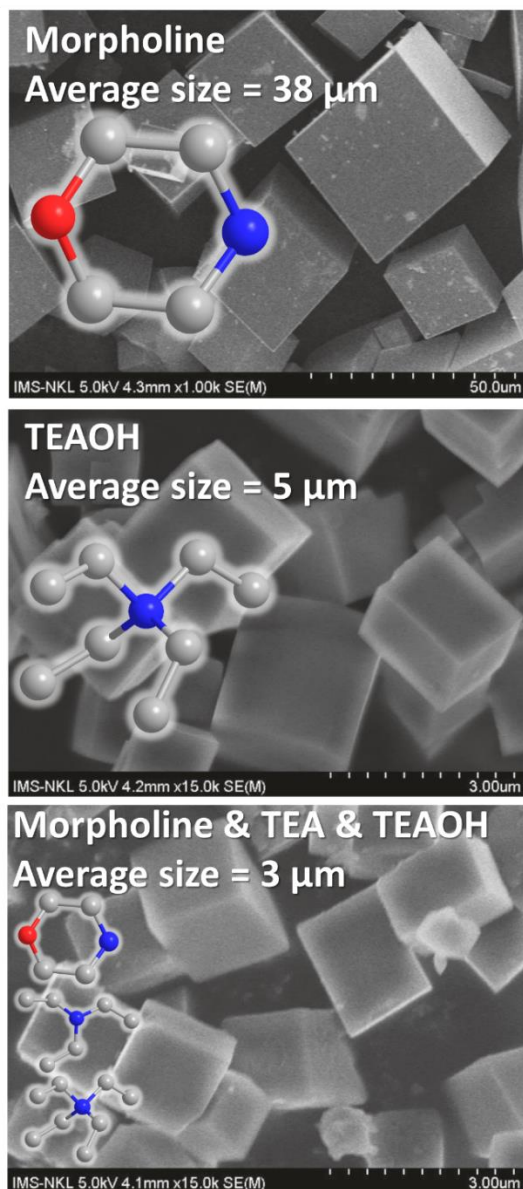
Figure 5. Showing the influence of templating agent, and combinations thereof, on the particle size of phase-pure SAPO-34. Adapted from reference [87], with permission from Hindawi publishing.

Yang *et al* probed the influence of phase transfer on the formation of SAPO-31.[88] Conventional hydrothermal SAPO-31 formed with dihexylamine was found to give rod-like crystals 1-2 μm in length. Introducing toluene into the synthesis gel, drastically increased the

nucleation rate, producing 55 nm spheroids of SAPO-31 using a phase-transfer synthesis procedure. These smaller SAPO-31 particles were found to have superior selectivity and lifetime for the hydroisomerization of n-heptane compared to conventional SAPO-31, due to improved mass transfer. Others have included surfactants to control particle size, such as pluronic F127 in a SAPO-34 synthesis.[89] Here an optimized amount of pluronic F127 lowered the particle size from 5 to 1.5 μm, which increased the MTO catalytic lifetime fourfold, as the larger external surface area prevented the build-up of coke precursors. Others have adopted an alternative approach by carefully controlling the crystallization temperature (Figure 6). Luo *et al* prepared a conventional SAPO-34 species by crystallizing at 200 ºC for 24 hours.[90] They modified the procedure by introducing two pre-heating steps, in the first step the sample was heated at 200 ºC for 0.5, 1 or 2 hrs. In the second step the sample was heated for 2 hours at either 40, 70, 100 or 130 ºC, before finally being crystallized at 200 ºC for 24 hours, as per the conventional sample. The rationale being that the sample would undergo rapid nucleation and then hindered crystallization to create smaller particles.[90]
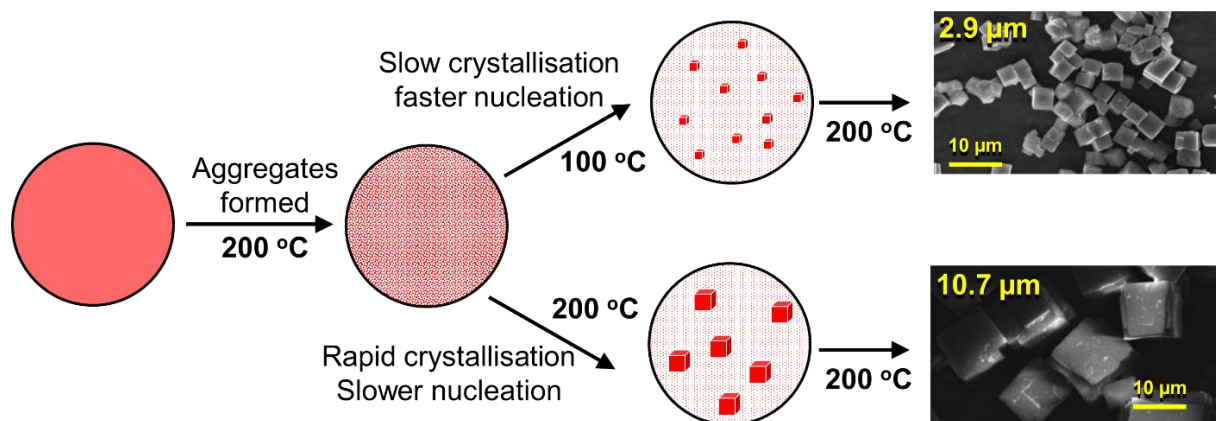
Figure 6. Three stage crystallization showing the influence on particle size of SAPO-34, adapted from reference [90] with permission from Wiley publishing.

This three-step approach successfully engineered smaller SAPO-34 particles than the conventional method, reducing the particle sizes from 10.7 μm to 2.9 μm (Figure 6).[90] This greatly increased the number of weak acid sites in the SAPO-34 system, however had a limited effect on the stronger acid sites. Again, these systems were tested in the MTO reaction, showing the smaller particles had a longer catalytic lifetime and improved selectivity to ethylene and propylene. Overall, some degree of control on the particle size can be achieved with hydrothermal synthesis, however this often results in extra costly steps that may not be viable on a larger scale.

The influence of microwave synthesis

Microwave synthesis is expanding among the inorganic community, due to its energy efficient and shorter crystallization times, typically 5-10 times faster than conventional heating.[91] Microwave synthesis is not simply an alternative heating method, as it plays a major role on framework selection. Park *et al* showed the same gel, with triethylamine as an SDA, crystallized at 180 ºC, gave different frameworks on microwave and conventional heating.[92] Microwave heating prompted the kinetic SAPO-5 product, whereas conventional heating gave the thermodynamic SAPO-34. Microwaves controlling framework formation was further investigated, as other researchers demonstrated that for a synthesis gel containing a mixture of TEAOH and dipropylamine (DPA) SDAs, heated at 150 ºC, SAPO-5 is the dominant product after 30 minutes (Figure 7).[93] After 60 minutes SAPO-34 impurities form, with phase pure SAPO-34 achieved after 500 minutes, highlighting the time resolution achieved with microwave heating (Figure 7).
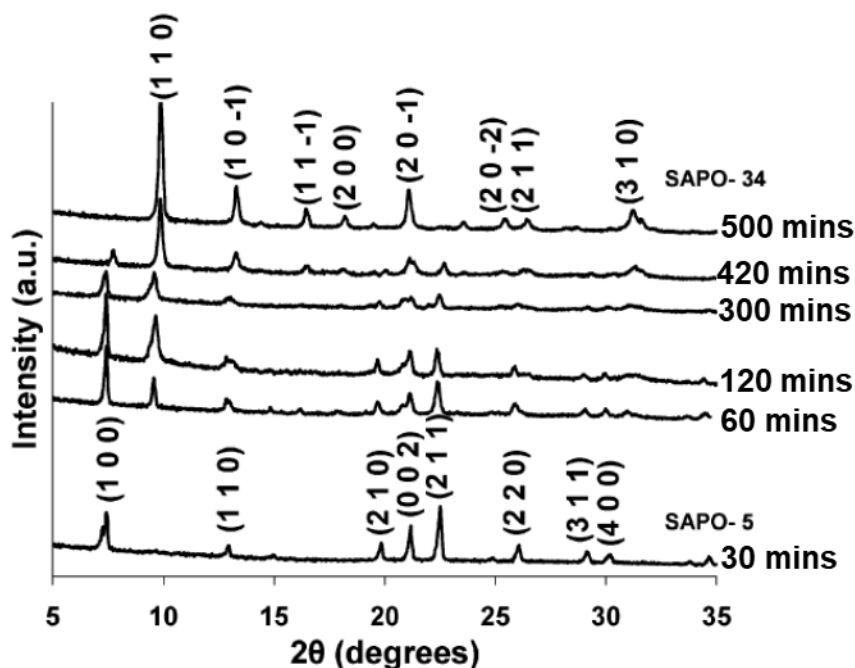
Figure 7. Showing the phase transition of SAPO-5 to SAPO-34 using a microwave assisted approach, modified from reference [93], with permission from RSC publishing.

Reports on microwave SAPO synthesis concur it creates smaller particles with narrower size distributions.[91, 94-96] This is attributed to more uniform heating of the synthesis gel, prompting faster nucleation. However, it is unclear how microwave heating influences crystallization kinetics. A study on SAPO-11 synthesis found the activation energy of microwave crystallization was 1.5 times larger than conventional heating.[97] Despite this the microwave crystallization pre-exponential factor was 8 orders of magnitude larger, accounting for the faster crystallization rate. This was attributed to more collisions between active sites, as microwave heating makes a much larger fraction of reacting surfaces active, leading to greater reactive sites. Particle size is not the only difference observed in SAPOs on conventional and microwave heating. Parallel studies on SAPO-5 and SAPO-34 found differences in acidity, despite identical silicon loadings, depending on whether microwave or conventional heating was used.[98-99] Microwaved SAPO particles were

much smaller, resulting in higher external surface area and mesopore pore volume, however, conventional samples contained a greater number of stronger acid sites. This was attributed to the differing silicon distributions of the two species, as conventional heating favoring isolated active sites (type II substitution, Figure 2), with a 1:1 ratio between silicon and protons. Microwave synthesis formed larger silicon islands, with fewer acid sites due to increased type III substitution, increasing the silicon to proton ratio (Figure 8).[98-99] This suggests rapid crystallization, from microwave heating, gives silicon less opportunity to enter the framework as isolated sites.[98-99] Thus, as crystallization occurs there are fewer available AlO_4 and PO_4 species, encouraging Si-O-Si bond formation and silicon islands. This shows that silicon distribution, and acidic properties (Figure 8), can also be tailored by microwave heating time, with longer times required to form stronger acid sites, akin to those from conventional synthesis.
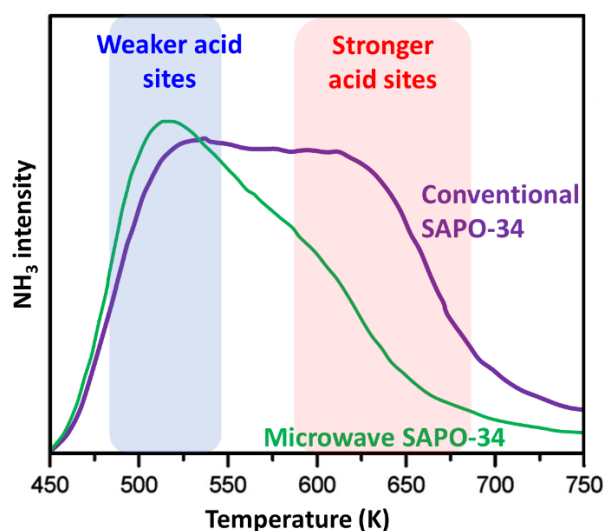
Figure 8. Showing the NH_3-TPD data comparing conventional SAPO-34, with microwave heated SAPO-34, both with a Si/Al ratio of 0.6, adapted from reference [99] with permission from RSC publishing.

Despite the seeming simplicity of microwave heating, this method has its own variables, including precursor volume, reactor size, applicator type and frequency (Table 3). A study on SAPO-11 and AlPO-11 considered the influence of these variables on the final products, showing that increasing the reaction volume decreased the crystallization rate.[97] This was due to a lower surface area-to-volume ratio of the precursor solution, giving a less homogeneous temperature distribution, when over 15 g of solution was used, despite microwave heating. As a result, larger reaction volumes lead to longer times to achieve 1% crystallinity. To further probe the reactor configuration, 10 g of identical of precursor solution were heated to 160 °C in cylindrical reactor vessels, with diameters of 11 and 33 mm. The 33 mm reactor was found to give particles of 2.14 ± 0.76 μm in size, whereas the smaller 11 mm reactor gave smaller more uniform particles; 1.38 ± 0.18 μm in size (Table 3). This was attributed to a less homogeneous temperature distribution in the larger reaction, encouraging nucleation and crystallization to occur simultaneously. Whereas the smaller reactor lead to slower nucleation, separating the two processes. Therefore, giving smaller more uniform particles. The choice of microwave applicator, frequency and sweeping rate were also both shown to influence particle formation. Comparing crystallinity as a function of time at 2.45, 5.8, 8.7 and 10.5 GHz showed little difference between the three higher frequencies, but the rate of growth was noticeably slower for the 2.45 GHz frequency. This is likely due to 2.45 GHz not having enough penetration depth to uniformly heat the whole vessel (33 mm diameter), whereas 5.8 GHz is enough.

Table 3. Comparing microwave heating variables, and their influence on particle size and crystallization rate in SAPO-11 synthesis, adapted from reference [97].

Precursor Mass (g)	Reactor diameter (mm)	Frequency (GHz)	Nucleation time (min)	Crystallization rate (min^{-1})	Particle size (μm)
10	33	2.45	4	0.035	2.14 ± 0.76
15	33	2.45	10	0.035	3.50 ± 0.73
30	33	2.45	25	0.010	2.35 ± 0.66
10	11	2.45	10	0.060	1.38 ± 0.18
15	33	2.45	17	0.015	3.77 ± 0.55
15	33	5.8	15	0.025	3.68 ± 0.46
15	33	8.7	15	0.025	2.63 ± 0.24
15	33	10.5	15	0.025	2.70 ± 0.23

Conditions: 160 ^{o}C crystallization temperature, gel ratio of 1.0 Pr_2NH: 0.5 $(TBA)_2O$: Al_2O_3: P_2O_5: $0.4SiO_2$: 50 H_2O.

To tailor particle size, two step protocols are being developed that combine microwave and conventional heating.[100-101] Here a SAPO-11 gel was exposed to either 15 hrs conventional heating, 2 hrs microwave heating, and combinations thereof. Samples made purely from microwave heating were found to give small 2 μm crystals, with a narrow size distribution. Those from conventional heating gave larger particles, with less uniform shape and size distribution. Mixing microwave and conventional heating an intermediate particle size was achieved. Performing microwave heating first, then conventional heating, gave a more uniform particle size, due to the uniform nucleation rates of microwave synthesis. In contrast performing the conventional heating first lead to similar size particles, but with a much broader size and shape distribution, as conventional heating favors particle growth. This shows the possibilities for combined synthesis techniques.[100-101]

Microwave synthesis has many possible advantages over conventional synthesis, not just in powder synthesis, but also in coatings and membrane formation.[96, 102-103] While it is undoubtedly a more energy efficient route, maintaining that efficiency on a larger (industrial) scale may be challenging, especially given the still considerable pressure build up. Balancing these factors must surely be a goal for the future of sustainable microwave synthesis.

Inclusion of ionic liquids with ionothermal synthesis
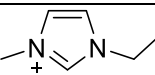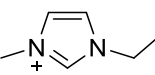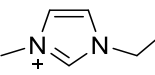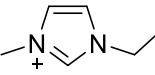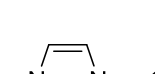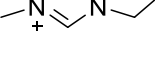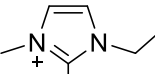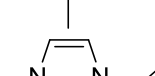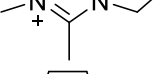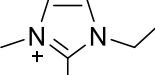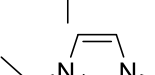
While many synthesis procedures utilize water (hydrothermal) or organic (solvothermal) solvents, their low (< 120 ºC) boiling points create pressure during crystallization above 150 ºC. In 2004 Morris *et al* devised a strategy to utilize ionic liquids as solvents, coining the term 'ionothermal'.[104] Ionic liquids, typically substituted imidazoliums, have high boiling points and low vapor pressure, allowing zeolite and AlPO synthesis to be performed in open vessels. This approach has obvious safety benefits, avoiding pressure build up, and has the potential to be converted into a continuous process.
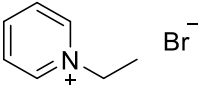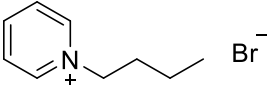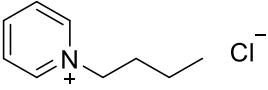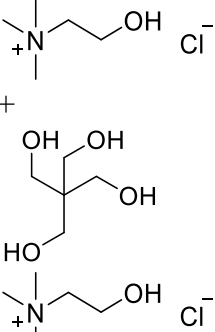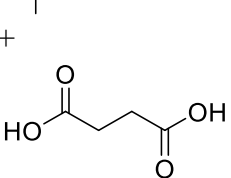
One of the earlier reports of ionothermal SAPO synthesis comes from Xu *et al*, where SAPO-11 was synthesized with microwave heating, using 1-ethyl-3-methylimidazolium bromide as both a solvent and SDA.[105] It was found that HF was needed for phase purity, yet excessive amounts increased the crystallinity, but greatly lowered the product yield. This was attributed to the Al and Si precursors in the SAPO gel competing with one another to react with the fluoride ions in solution to form intermediate species.[105] Contrasting microwave and conventional heating showed, as expected, microwave synthesis required significantly less time, to achieve more crystalline species.[105]

The influence of ionothermal synthesis was recently investigating, comparing SAPO-5 synthesized ionothermally with 1-ethyl-2,3-dimethylimidazolium bromide, with the conventional approach.[106] Key differences were seen in the silicon distribution with conventional SAPO-5 showing far more isolated (type II) Si sites than ionothermal SAPO-5, which primarily showed Si-O-Si bonds. This was also reflected in the total acidity, with hydrothermal SAPO-5 showing a greater number of total acid sites and stronger acid sites, allowing it to selectively form C_2 to C_4

alkenes in the MTO reaction. In contrast ionothermal SAPO-5 principally formed dimethyl ether.[106] This has since been attributed to the excellent conductivity and high polarity of ionic liquids, allowing the temperature to be more effectively dispersed in the solution, speeding up the rate of growth. Again, allowing less time for the Si to substitute into the framework.

Table 4. Ionic liquids used in the ionothermal of SAPO systems.

Ionic liquid	Structure	Co-SDA	SAPO structure	Ref
[emim]Cl	Cl⁻	None	SAPO-34	[107]
[emim]Br	Br⁻	None TPAOH	SAPO-11 SAPO-42	[105, 108-109] [110]
[allylmim]Br	Br⁻	None	SAPO-11	[108]
[bmim]Cl	Cl⁻	None	SAPO-5*	[108]
[bmim]Br	Br⁻	None 1-Methylimidazole TMAF	SAPO-5 SAPO-34 SAPO-42	[108] [108] [111]
[edmim]Br	Br⁻	None TEA	SAPO-5 SAPO-5	[108] [106]
[allyldmim]Br	Br⁻	None	SAPO-5	[108]
[bdmim]Br	Br⁻	None	SAPO-5	[108]
[teim]OH	OH⁻	None	SAPO-5 SAPO-34	[112] [112]
[etmim]OH	OH⁻	None	SAPO-34	[112]
[temim]OH	OH⁻	None	SAPO-11	[112]

[epy]Br		None	SAPO-5	[108]
[bpy]Br		None	SAPO-5	[108]
[bpy]Cl		None	SAPO-42	[108]
Choline chloride + Pentaerythritol		None	SAPO-5*	[113]
Choline chloride + Succinic acid		TEABr	SAPO-5	[114]

* = Small impurity phases also detected.

The choice of ionic liquid has a significant effect on the framework formed (Table 4). In 2018 Azim and Stark performed a systematic study to investigate the effect of ionic liquid choice, synthesis times and gel ratio on the SAPO formed.[108] Using 1-butyl-3-methylimidazolium bromide ([bmim]Br), showed that despite SAPO-5 readily converting to SAPO-34 under hydrothermal methods, SAPO-5 was stable on crystallization up to 24 hours using this ionothermal method. Likely this is due to the bulky ionic liquid limiting the formation of the smaller pored CHA phase. Varying the initial Si/Al ratio also controlled the phases formed, at a low Si/Al ratio (0.2) both AEL and AFI phases formed, however above 0.2 AFI was exclusively formed.[108] Modifying the imidazolium substituents also influenced phase formation. While the 1-butyl-3-methylimidazolium bromide ([bmim]Br) formed phase pure SAPO-5, it was shown that 1-ethyl- and 1-allyl-3-methylimidazolium bromide ([emim]Br and [allylmim]Br, respectively) favored SAPO-11. Further, a combination of 1-butyl-3-methylimidazolium bromide ([bmim]Br)

and 1-methylimidazole formed SAPO-34. While the organic species clearly had a significant effect, the anions also had a structure directing property. Changing from bromide to chloride had little influence with the imidazolium species. However, changing from 1-butyl pyridinium bromide ([bpy]Br) to 1-butyl pyridinium chloride ([bpy]Cl) caused the SAPO material to change from phase pure SAPO-5, to phase pure SAPO-LTA. This was attributed to the anion's involvement in during the crystallization with pyridinium species, whereas clearly this has less of an influence in imidazolium species.[108]

Ionothermal synthesis is an elegant and simple way to avoid pressure build up, and closed batch synthesis. As with microwave synthesis, the faster crystallization times limit type II silicon substitution in the framework, which is key for acid catalysis, and is something that must be addressed moving forward. While questions remain over the economic effects of large-scale processes involving ionic liquids, such methods clearly have logistical merits.

Solvent-free synthesis of SAPOs

To limit issues of water consumption and wastewater generation, solvent-free methods have been investigated. The most common being dry-gel conversion (DGC), which has been successful for both SAPO-11 and SAPO-34 synthesis.[115-117] In DGC, a regular aqueous synthesis gel is made, but before crystallization the water is evaporated, leaving a "dry-gel". The dry-gel then undergoes crystallization at elevated temperatures, without pressure build up from solvent evaporation. As this gel is more concentrated, faster crystallization occurs. For SAPO-11, researchers focused on the influence of temperature at which the initial aqueous synthesis gel is formed, prior to evaporation, which varied between 5–30 °C, before crystallization at 200 °C

(Figure 9).[117] Samples from gels synthesized at 5 and 30 °C showed no significant differences in particle size, all having irregular shaped particles. The 30 °C samples showed AEL framework after 2 hours of crystallizing, whereas those formed at 5 °C required 4 hours. Comparing the acidity of the systems showed a lower gel formation temperature (5 °C), gave greater framework silicon incorporation, leading to more stronger acid sites. Microscopy showed (Figure 9) that the 30 °C system had an uneven distribution of silicon over the SAPO particles, due to silicon islanding. This shows the importance of the gel formation temperature, something commonly overlooked. However, such a method is not without flaws. Firstly, evaporation to form the dry-gel, is energy intensive, further, irregular particle shapes are also likely to form due to an uneven distribution of reagents within the dry-gel. Few take steps to form a completely homogeneous mixture at this stage, and unlike microwave synthesis, there is a pronounced temperature gradient throughout the dry-gel. This will lead to notably different crystallization and nucleation rates, producing uneven particles.
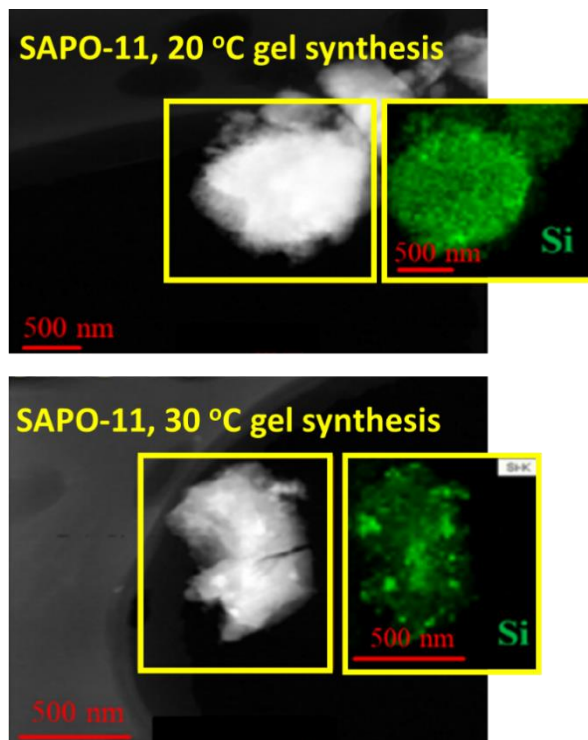
Figure 9. STEM (scanning tunneling electron microscopy) mapping images of SAPO-11 species formed with different gel synthesis temperatures, showing that higher temperatures (30 °C) lead to a less homogeneous silicon distribution. Adapted from reference [117] with permission from Elsevier publishing.

Collaborative efforts from China provided an alternative solvent-free method for SAPO (and AlPO) synthesis based on grinding.[118] Here there is no need for a separate evaporation step, as no additional water is added, creating a paste that is ground for 10-15 minutes into a solid, which is transferred to an autoclave for crystallisation.[83] This was shown to make particularly crystalline SAPO-34 species, which was easily followed as a function of crystallization time. Likely the more regular particles are due to the grinding, ensuring a homogeneous mixture of reagents. This method was also found to give impressive SAPO yields (94 %), making it a highly effective synthesis. The doped silicon was also found to be almost exclusively type II substituted, producing a large amount of strong acid sites. These species of SAPO-34 were found to have comparable activity to conventional SAPO-34, for the MTO reaction. To enhance the mixing of grinding methods, many have replaced the liquid SDA amines and H_3PO_4, with an ammonium phosphate salt, limiting the number of reagents to be evenly mixed while grinding.[119] This approach resulted in a more subtle mesopore hysteresis from N_2 physisorption, compared to traditional hydrothermal approaches. This was attributed to the faster grinding-based synthesis method, allowed rapid formation of the microporous material, with less time for mesopore incorporation. Further, grinding-based methods gave much smaller particles, with similar numbers of Bronsted acid sites to conventional synthesis. In 2018 Liu *et al* considered this approach, noting that ammonium phosphate salts, required significant purification with volatile solvents, which would be unfavorable for large scale processes.[120] They also again highlighted

that while solvent-free methods had many advantages, they struggled to achieve the same proportion of type II substituted Si in the SAPO-11 framework as hydrothermal methods.

Summary of synthetic methods

While this review has only focused on just four techniques, many other methods are emerging, including the use of ultrasound,[121-123] and developing composite materials.[124-125] While newer techniques can provide excellent control over particle sizes and crystallization rates, less focus is being paid to tailoring silicon incorporation, which remains a key catalytic factor. An ideal synthesis procedure moving forward would make it possible to select both the particle shape and substitution methods towards an optimized catalyst, whilst still being safe, scalable and sustainable.

Understanding SAPOs

Use of X-ray diffraction in studying SAPOs

Diffraction measurements are found in most works on SAPOs, as the primary technique for confirming phase purity, with each framework having its own unique powder X-ray diffraction (PXRD) pattern. Peak positions are based on lattice parameters and space group, whereas the peak intensities depend on the unit cell contents. Further in some cases, the particle size can be determined from the peak full width at half-maximum (FWHM). In many cases as synthesized and calcined pattern are collected only to confirm the desired framework has formed, but this

underrates the significant advances in diffraction technology, which can provide vast amounts of information.

As the peak positions are a function of the six unit cell parameters (a, b, c, α, β and γ), they unit cell parameters, and unit cell volume, can be calculated from the positions of PXRD peaks through Reitveld refinement.[126] Conversely, PXRD patterns can also be predicted for a given unit cell, to match the peak intensities to the unit cell contents. In practice synchrotron radiation is typically used, as the precision needed to differentiate between a hundredth of an angstrom demands excellent experimental resolution, which is not common among lab-based systems. XRD measurements have few demands on sample environment, so can accommodate a range of experimental parameters, including temperature and pressure.[127-128] This lends itself well to *in situ* and *operando* studies, particularly as patterns can be collected in a matter of seconds, and simultaneously alongside other characterization techniques.[9, 126, 129-132] One of the first *in situ* XRD studies with SAPOs focused on the formation of SAPO-34 in 2001.[133] Researchers followed the crystallization, leading to the isolation of a layered SAPO-34 pre-phase, which decayed above 150 °C, to SAPO-34. Further, tracking the peak intensities *in situ* permits calculation of crystallization rates, here the activation energy for crystallization was 157 kJ/mol, which was larger than for undoped AlPO-34 (120 kJ/mol), due to the added energy for silica incorporation. *Ex situ* analysis of the XRD samples confirmed that silicon was only gradually introduced into the framework, again highlighting the need for extended synthesis times.[133]

Slawinski *et al* expanded diffraction studies to understand the growth of competing phases, considering SAPO-34 and AlPO-18, with two main crystal faults; displacement and growth, considered (Figure 10).[134-135] A displacement fault occurs when the ideal crystal pattern (in this case a continuous stack of layer A; AAAAAAA), makes a solitary error, which is then corrected;

AAABAAA. A growth fault occurs when this this error is not corrected, leading to the formation of an incorrect phase; AAABBBB. By calibrating their proposed methods, they modelled a series of cases starting with 'perfect' SAPO-34 and AlPO-18, observing the influence on introducing increasing numbers of either fault. This led to subtle differences in the patterns (Figure 10), based on the peak intensities and width, which when compared to experimental spectra of 'real' SAPO-34 samples, showed intergrowth of AlPO-18 in SAPO-34 was primarily through displacement. This led to a simple method for investigating defect levels in samples, based of simple XRD parameters, and has since evolved beyond this to incorporate atomic force microscopy and solid-state nuclear magnetic resonance (NMR).[135] Thus, highlighting the precise mechanism (layer-by-layer growth) that the SAPO-34 and AlPO-18 phases intergrow.
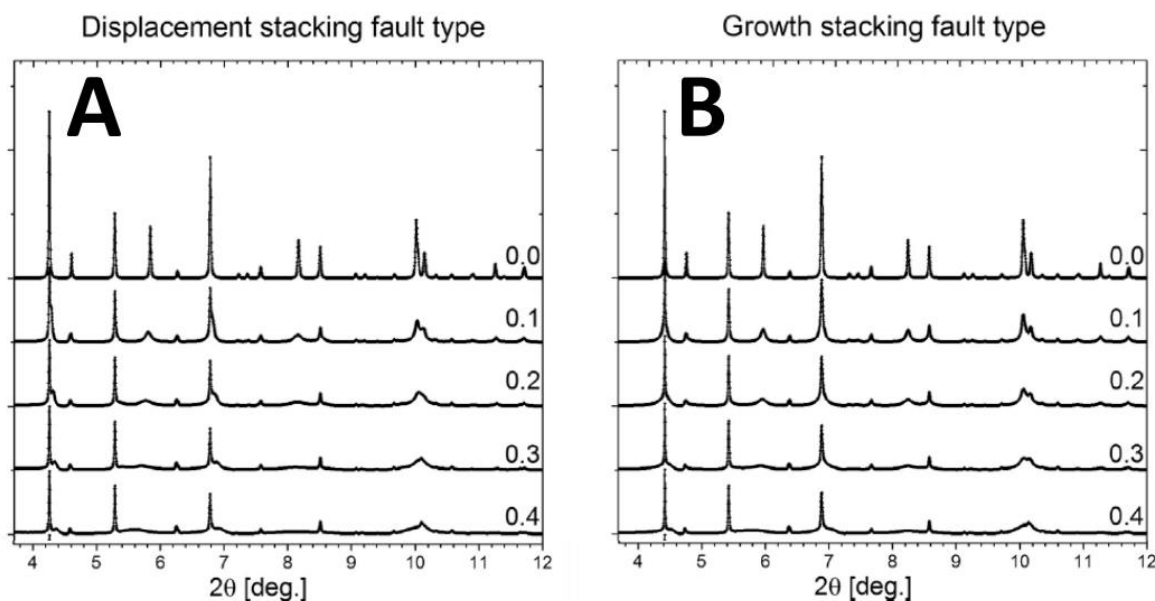
Figure 10. Showing the influence of incrementally introducing A) Displacement and B) Growth stacking defect faults into a pure SAPO-34 system (0.0), towards a pure AlPO-18 system (1.0), on the calculated XRD pattern. Adapted from reference [134] with permission from Elsevier publishing.

Calcination is a necessary step in most SAPO syntheses; so naturally researchers are curious about the transformations that occur during this process. Wragg *et al* focused on the calcination of SAPO-37, *in situ* at the BM01 beamline station at the European Synchrotron Radiation Facility.[127] Combining XRD with Mass Spectrometry (MS), Thermogravimetric Analysis (TGA) and Differential Scanning Calorimetry (DSC) correlated changes in structure with the removal of TMAOH and TPAOH SDAs (Table 1). As SAPO-37 has a cubic unit cell, it is well-suited to such studies, as only one unit cell parameter; a, varies, linking directly to the unit-cell volume (a^3). Initially no real change in unit cell parameter (or unit-cell volume) is seen on removal of water, below 375 K. However, the decomposition, and loss, of TPA^+ (tetrapropylammonium) ions from the supercages (Figure 3) caused a spike in unit-cell volume from 15086 to 15110 $Å^3$, between 600 and 660 K. After this the unit-cell volume decreased to 14939 $Å^3$ at 1000 K, attributed to the TMA^+ (tetramethylammonium) ions leaving the framework. It was concluded that TMA^+ species could not leave the SOD (sodalite) cages until the TPA^+ had mostly vacated the FAU (faujasite) supercages. The experimental data resolution allowed them to model the isotopic thermal parameters of both the oxygens and the collective T-atoms (Al/P/Si), representing the amount of motion of these species. It was shown that the thermal motion of the oxygen atoms increases on decomposition of TPA^+ (550 K). Yet, the T-atoms thermal motion did not increase until 660 K, coinciding with the spike in unit-cell volume. Further analysis decoupled the behavior of the FAU supercage and SOD cages. This showed the initial increase in unit-cell volume was due to expansion of the FAU cage, whereas the subsequent shrinking was due to the SOD cages contracting. This was probed further with an *in situ* XRD study focused on the stability of SAPO-37. The framework was found to be completely stable under an inert Ar environment, however subtle changes were seen in the XRD patterns on exposure to air,

attributed to water (Figure 11).[136] Combining XRD with DRIFTS (Diffuse Reflectance Infrared Fourier Transform Spectroscopy) and DFT (Density Functional Theory) it was shown that spaces within the SOD cages and d6r will hold trap molecules. This then puts strain on the rest of the framework, leading to the d6r breaking, triggering the decomposition of the framework (Figure 11). This goes some way to explaining the stability of SAPO-37, relative to other SAPOs.
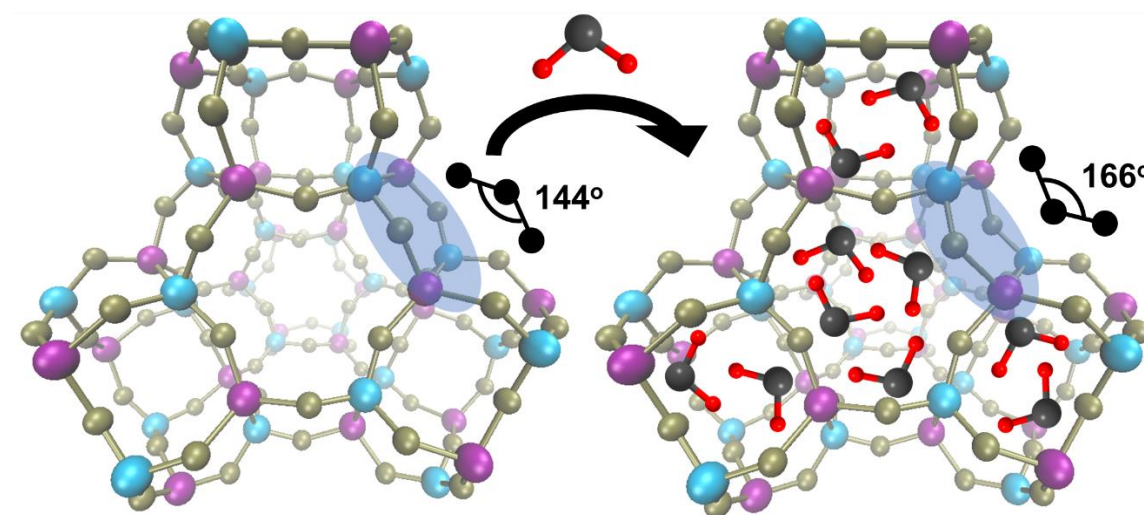
Figure 11. Showing the framework strain on introducing water into the SAPO-37 faujasite framework.

There is also interest in how the SDAs orientate within SAPO frameworks, as a guide for future template and catalyst design. Liu *et al* prepared CHA SAPOs (SAPO-34/44) from different SDAs.[41] Combining PXRD with ^{13}C NMR and DFT, showed that two cyclohexylamine or two n-butylamine molecules occupy a CHA cage, whereas just one diisopropylamine or dipropylamine would occupy the same cage. By creating this self-consistent model, there is scope for identifying the precise locations and binding modes of probe molecules within SAPOs. Beyond SDAs, the interactions between SAPOs and other molecules is of great interest, particularly methanol and water as vital components of the MTO process.[9, 137-138] *In situ* powder

XRD of SAPO-34 was able to show that the adsorption of methanol lead to a 0.5 % expansion of the unit cell, primarily due to an expansion of the a-parameter. In contrast the cell volume contracted by 2 % when water was added.[129] This difference shows that the SAPO-34 system has a stronger interaction with water, than methanol, with different adsorption mechanisms. Collection of high-resolution powder diffraction (HRPD) predicted crystal structures of methanol within the CHA cages, confirming these weaker interactions.[129]

In situ and *operando* XRD of SAPOs naturally lends itself to SAPO-34 and the MTO process. Impressive works by Wragg and co-workers have been dedicated to observing structural changes in rhombohedral SAPO-34 during the catalytic process, the build-up of coke and coke precursors, and the formation of methoxy intermediates.[9, 126, 129-132, 139] These combined works showed that during the MTO process, at 450 ℃, the unit cell volume of SAPO-34 increases, due to an increase in the c parameter.[9, 126, 130-132, 139] This complemented with Fourier maps, showing the differences in electron density within the CHA cages, as the reaction progressed, were attributed to coke build-up, showing excellent correlation between coke build up and the c parameter expansion. These changes were found to be reversible on oxidation, showing the catalyst could be regenerated. They expanded these studies to identify the types of coke, and their production mechanisms. One notable study contrasted SAPO-18 and SAPO-34 under *operando* conditions for the MTO reaction.[9] Despite being structurally similar, SAPO-18 has a longer catalytic lifetime than SAPO-34, albeit with less activity. It was shown that while coke deposits build up in SAPO-18, the unit cell volume only expands by 0.9 %, whereas for SAPO-34 the expansion is around 3 %, despite similar Si loadings. It was suggested that the continued activity of SAPO-18 was due to the cage size, which allowed bulky aromatics to form, but not

fill the cage. The smaller unit cell expansion was attributed to the more rigid d6r in SAPO-18, which translated to limited pore blockage.

The above studies have significant merit, but only capture the average sample behavior, yet constant improvements in computing power allow the simultaneous processing of thousands of data sets. This facilitates spatially resolved experiments of SAPO-34, leading to multi-dimensional mapping of structural parameters, during the MTO processes (Figure 12).[126, 139] This study focused on the c-parameter, as a function of bed height and time on stream, over a range of methanol flow rates. This revealed that the formation of the hydrocarbon pool (HCP) of intermediates begins at a single point within the catalyst bed, who's location depends on the flow rate. Eventually the HCP will begin a significant expansion of the c-parameter, at the top of the catalyst bed, leading to deactivation of the catalyst bed, while some areas remain coke free.[139] This allowed researchers to develop kinetic models, showing the build-up of coke, and the HCP independently, within the bed. This work was the expanded to incorporate XRD-computed tomography, with multiple 2D slices of the cylindrical reactor bed, from inlet to outlet (Figure 12).[139] The SAPO-34 systems were run under real conditions, and then quenched to room temperature, to collect data on the influence of coke deposits. Focusing on variations in time-on-stream and silicon content (as a measure of acidity), showed that the SAPO-34 sample with the lowest silicon quantity (4 wt%), had little variation in the c-parameter, showing an even distribution down the bed. Whereas, the 8 wt% Si SAPO-34 sample showed areas with significant build-up of coke within the cages, which correlated well with expansions in the unit cell parameters. This led the researchers to suggest that lower Si loadings would lead to improved catalytic lifetime for SAPO-34 in the MTO process.
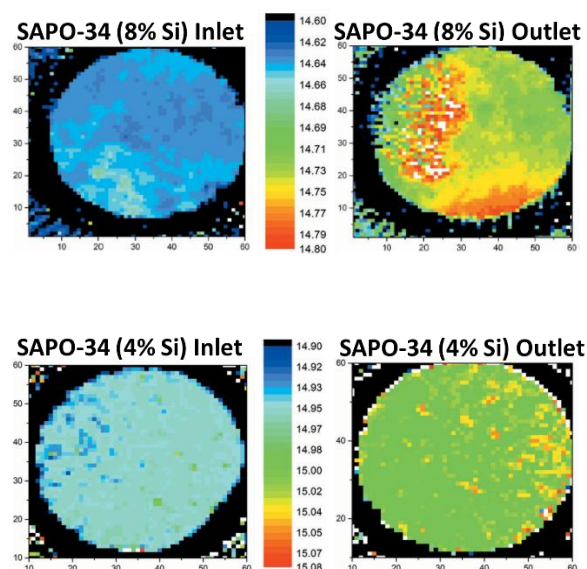
Figure 12. Showing the variation in the c-parameter of SAPO-34, across cross sections of an MTO bed after ~200 minutes on stream for the MTO process. The SAPO-34 (4% Si) system shows relative homogeneity, whereas uneven changes in the c-parameter are seen for the 8% Si SAPO-34. Figure adapted from reference [139] with permission from the International Union of Crystallography.

The high intensity of even commercial benchtop diffractometers allows reasonable quality XRD patterns to be collected in minutes. However, XRD occurs due to interactions with photons and protons, thus, the more protons an element has, the stronger the interaction. This makes XRD useful for looking at the SAPO framework, but not so useful for looking at lighter elements, such as hydrogen, which are vital in acidic SAPOs. Unlike X-rays, the neutron cross section, does not follow a loosely linear trend with the atomic number. Instead a more random pattern occurs, notably with hydrogen having a large neutron cross section, making neutron techniques well suited to probing acid sites in SAPOs. Neutron diffraction has previously been used to probe the four possible acid sites in SAPO-37.[140] Cheetham *et al* were able to calculate

the proton occupancies of each oxygen from neutron diffraction data, showing most (~ 75 %) protons are in the FAU supercage, but stronger acidic sites are from protons residing in SOD cages. This extended to observing the binding of d_6-Benzene in SAPO-37, were it was shown the stronger SOD cage protons migrate to interact with the benzene molecule, in a similar fashion to zeolite analogues.[8, 141] Similar studies were performed on partially deuterated SAPO-34, complemented with CO-probed FTIR. Again, four oxygen environments were considered, though only two were found at 15 K, corresponding to protons protruding from the 6 and 4 membered rings. Such measurements however could not explain the appearance of three different acid sites seen in the CO-probed FTIR spectra, which is likely due to the differences in temperature for the two measurements (15 and 77 K). Therefore, neutrons diffraction can provide complementary data to XRD.[8, 140-141] However, neutron diffraction will always be more of a niche technique for SAPOs, as it requires orders of magnitude more time, at a synchrotron, to collect data of the same quality as even benchtop X-ray diffractometers.

A further benefit to diffraction is the ability to extract accurate experimental bond lengths from a range of species, including SAPOs, through the Pair Distribution Function (PDF); D(r).[142-144] D(r) represents the probability of finding any atom at a distance r, from the center of any other atom, and is obtained through a variety of data processing steps. While PDF analysis can be challenging, it is derived from the same information as neutron and X-ray diffraction, so all the above studies could still be interpreted with PDF. The advantage of PDF is it can look at locally disordered species, which diffraction cannot, thus it has potential to look at silicon substitution within SAPOs. Previous work on SAPO-18 and AlPO-18 from Sankar *et al* compared the PDF of the two species to extract data relevant to the dopant, however only subtle differences were found.[143] In principle this approach is possible, but is complicated by low silicon quantities, and

the similarities in Al-O, P-O and Si-O bond lengths. PDF analysis is also highly dependent on computational models to explain changing bond distances, or similar variations, so a good understanding of the system is required. However, if known, PDF is an incredibly powerful technique for future studies, focusing on *in situ* crystallisation,[144] catalysis[142] or even determining dopant mechanisms and substitution. All of which would be of great benefit for the understanding of existing, and development of new, SAPO materials.

Examining SAPOs with Solid State NMR

Solid state nuclear magnetic resonance (ssNMR) is another technique that is widely used in probing the structure of SAPOs. The ability to selectively focus on Al, Si, P and H nuclei means one can probe the local environments of these elements. ^{31}P and ^{27}Al ssNMR are common in SAPO characterization, owing to large amounts of P and Al in the framework, further ^{31}P is 100% abundant and a dipolar nucleus (spin I = 1/2), making data collection relatively straight-forward. While ^{27}Al is quadrupolar (spin I = 5/2), its gyromagnetic ratio is large, meaning high quality data can be collected in a short space of time. In AlPOs, the data from 1D NMR spectra of ^{31}P and ^{27}Al is quite limited. ^{31}P shows a signal at around -28 ppm, attributed to P(OAl)$_4$, while ^{27}Al shows a primary signal at around 40 ppm, corresponding to Al(OP)$_4$, as expected.[145] In ^{27}Al some secondary signals can also appear at -15 ppm, due to octahedral alumina, or a signal at 15 ppm due to hydrated (or five-coordinate) aluminum.[145] These two measurements can confirm the correct formation of the intended AlPO framework, with some even explaining framework connectivity. However, ^{29}Si NMR is more useful for predicting acidity and catalytic performance, despite it appearing in lower loadings, with a lower gyromagnetic ratio, meaning

data collection lasts for many hours. The position of the ^{29}Si signal is sensitive to both its first and second coordination spheres (Table 5). This is incredibly fortunate, as in all cases we assume the silica will be tetrahedra, so SiO_4, however being able to distinguish between the five possible $Si(OAl)_x(OSi)_{4-x}$ species, where x is an integer from 0–4, provides a direct insight into the silicon substitution.

Table 5. Common Si species found in calcined, phase pure SAPO materials.

Species	Framework	Chemical shift (ppm)	Reference
$Si(OAl)_4$	SAPO-11	-90	[145]
	SAPO-31	-90	[145]
	SAPO-34	-90 to -92	[146-147]
	SAPO-35	-89 to -90	[148]
	SAPO-37	-91 to -93	[147, 149]
	DNL-6	-92	[150]
$Si(OAl)_3(OSi)$	SAPO-18	-95 to -96	[145, 151]
	SAPO-34	-96	[146]
	SAPO-35	-96	[148]
	SAPO-37	-98	[149]
$Si(OAl)_2(OSi)_2$	SAPO-18	-100	[151]
	SAPO-34	-101	[146]
	SAPO-37	-103	[149]
$Si(OAl)(OSi)_3$	SAPO-18	-106	[145]
	SAPO-34	-105	[146]
$Si(OSi)_4$	SAPO-11	-110	[145]
	SAPO-18	-112	[151]
	SAPO-31	-110	[145]
	SAPO-34	-115	[146]
	SAPO-37	-108	[149]

If type II substitution exclusively occurs one expects a single peak at -89 to -93 ppm, attributed to $Si(OAl)_4$. This, as discussed previously, would have a 1:1 relationship between Si dopants and acid sites (Figure 2). The degree of silicon islanding can be seen in the distribution of ^{29}Si NMR

signals and may also be quantified. Increasingly researchers use 2D ^{29}Si NMR to resolve individual signals, despite significantly longer acquisition times, this is a useful method for determining the true number of species in a sample.[149] To directly probe the acidity of a sample many have used solid state ^{1}H NMR, for this to occur the sample must be exceptionally dry, to remove signals from physisorbed water or other adsorbed species.[145-147, 151-153] However, in doing so this then makes cross-polarization measurements of other nuclei less effective. Investigations on the ^{1}H NMR of dry SAPO-34 and SAPO-37, by Hunger *et al*, showed that SAPO-34 only possessed one type of acid site (at 3.6 ppm), attributed to Si-OH-Al species.[147] However, SAPO-37 showed three different signals at 4.2, 3.6 and 1.7 ppm, which were assigned as protons in the sodalite cages, supercage and weak silanols respectively. It was later shown that SAPO-34 also possess two shoulder peaks at 2.6 and 1.6 ppm. Through the use of ^{1}H-^{27}Al TRAPDOR (Transfer of populations in double resonance) and ^{1}H-^{29}Si REDOR (Rotational double echo resonance) measurements these were assigned as Al-OH and Si-OH species respectively.[146] Further, more recent studies on SAPO-34, have shown the primary peak at 3.6 ppm can be deconvoluted into two peaks at 3.6 and 4.0 ppm. Both signals relate to Bronsted acid Si-OH-Al species, from the proton occupying the O2 and O4 positions of the CHA framework.[154] Aside from more routine measurements, SAPO ssNMR work can mostly be grouped into crystallization, catalysis, accessibility and acidity studies.

ssNMR has the benefit that it doesn't require crystallinity to produce a signal, elements only need to be present, making it a powerful tool for monitoring SAPO crystallization. Primarily ssNMR has been used *ex situ*, as multiple elements are of interest (Al, P and Si), which cannot be measured in a timely fashion simultaneously. Especially as good quality ^{29}Si NMR data takes many hours to collect, severely limiting the time resolution of an *in situ* approach. As such *ex*

situ methods have been used to explore a range of frameworks,[155-156] including SAPO-34[26-28, 157-161] and SAPO-37.[162] Tan *et al* tracked the hydrothermal synthesis of SAPO-34 over the course of 26 hours, with a silica sol, pseudoboehmite, triethylamine and phosphoric acid as precursors.[158] Solid samples were collected at a range of time points, collecting ^{27}Al, ^{31}P and ^{29}Si CP spectra on appropriate samples. After 30 minutes of crystallization the ^{27}Al NMR spectra showed primarily octahedral species, with a well-defined peak at 8 ppm, corresponding to hydrated alumina. Similarly the ^{31}P spectra showed a very broad peak centered at roughly -10 ppm, suggesting a wide range of disordered P states in the gel, with a shoulder, at -27.3 ppm assigned to P(OAl)$_4$.[158] The analogous ^{29}Si signal was also broad, centered at -85 ppm, with no discernible shoulder peaks. Associated XRD data showed framework formation after an hour, which prompted changes in all three NMR spectra. In the ^{27}Al spectra a peak at 28 ppm; Al(OP)$_4$, emerged, with the ^{31}P NMR signal becoming dominated by the sharp feature at -27.6 pp; P(OAl)$_4$, confirming framework formation. After one hour the ^{29}Si NMR shows a single signal at -90.9 ppm, due to Si(OAl)$_4$, suggesting Si exclusively underwent type II substitution to form isolated sites. Beyond 1 hour the ^{29}Si and ^{31}P spectra showed little change, though ^{27}Al showed a transition, as the 38 ppm signal increased, while the octahedral alumina species (12 ppm) diminished into a small shoulder. After 26 hours of crystallization some smaller features, due to Si-O-Si bond formation emerged, suggesting that type II substitution occurs during the crystallization step, and more rapidly than type III substitution in this case.[158]

   Huang *et al* used a similar approach to monitor the hydrothermal synthesis of SAPO-37 (Figure 13).[162] The associated XRD shows the crystallization kinetics of SAPO-37 were much slower than SAPO-34,[158] with SAPO-37 Bragg peaks only appearing after crystallizing for 16 hrs at 200 °C.[162] The ^{27}Al and ^{31}P ssNMR spectra agreed with the SAPO-34 findings, with ^{27}Al

initially showing a signal at 7 ppm, with a second peak at 41 ppm evolving on crystallization. Similarly, the ^{31}P shows a broad signal at -10 ppm, which transitions to a sharp signal at -26 ppm. The ^{29}Si spectra showed no noticeable signal before 22 hours, after which a peak at -90 ppm appears, with a shoulder at -94 ppm developing after 24 hours (Figure 13A). In this study the ^{13}C NMR was used to probe the templating agents (TMAOH and TPAOH). The initial gel showed four features, attributed to a range of TPA$^+$ environments, while no TMA$^+$ species were seen. On crystallization the peak positions shifted, showing TPA$^+$ becoming trapped in the supercage, and TMA$^+$ was now inside the sodalite cages (Figure 3). Huang *et al* also compared the conventional synthesis (above) of SAPO-37 to the DGC method.[162] XRD showed the formation of an intermediate phase at 6 ° after 0.5 hr, using the DGC method. This grew after 1 hr, but diminished once the SAPO-37 framework formed after just 5.5 hrs. This faster crystallization was also seen with ssNMR where the tetrahedral Al(OP)$_4$ signal; 41 ppm, is as intense as the octahedral species (6 ppm) in the initial gel.[162] Interestingly the ^{29}Si ssNMR dry-gel method (Figure 13B) showed the Si(OAl)$_4$ species at -90 ppm evolve from the broader Si(OSi)$_4$ signal at -112 ppm, suggesting that synthesis protocols significantly affect the silicon incorporation and crystallization times.[162]
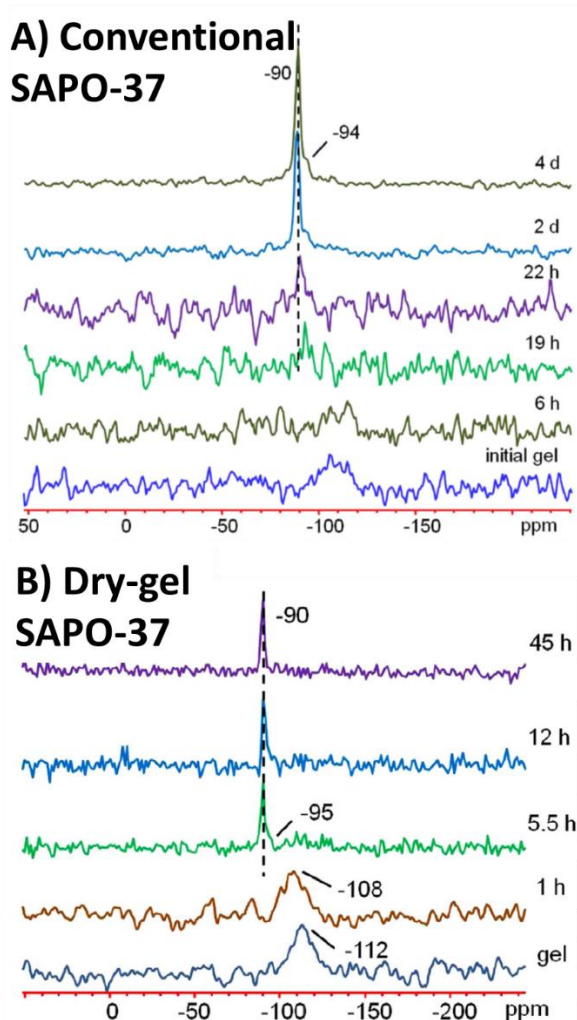
Figure 13. ^{29}Si NMR studies showing the variation in conventional (A) and dry-gel (B) synthesis methods for SAPO-37. The conventional hydrothermal method (A) shows a -90 ppm signal emerging from the baseline, whereas in the dry-gel method (B), this signal evolves from a silicate environment at -112 ppm. Adapted from reference [162] with permission from Elsevier publishing.

These studies have added significant insight into the crystallization mechanisms behind SAPO synthesis, laying the foundation for more advanced studies. More recently groups have been exploring isotopic doping, including measuring ^{17}O ssNMR,[26, 163] which is an emerging field in

microporous materials. Here a custom-made autoclave rehydrated dry-gel SAPO-34 with ^{17}O-enriched water. ^{17}O is sensitive to different environments, with peak position a function of its nearest neighbors. Using this approach, a wide range of ^{17}O sites were observed during the crystallization process.[26] Such studies exemplify how isotopes drastically enhance the resolution and information from ssNMR, paving the way for further studies. As ^{27}Al and ^{31}P are already close to 100% abundance, enriched ^{29}Si sources would be able to produce stronger signals, improving resolution in the spectra, and speeding up collection time, akin to the zeolite world.[164]

While challenging, *in situ* ssNMR synthesis have been developed, primarily with hydrothermal approaches, which requires tubes that contain the significant pressure build up. Taulelle *et al* showed one of the earliest studies of this kind,[165] focusing on SAPO-34 crystallization, with ^{27}Al, ^{31}P and ^{19}F ssNMR spectra. The ^{27}Al spectra shows the initial broad aluminum peak splits into two signals at 2 and -10 ppm, assigned to different hexacoordinated fluoroaluminophosphates. This signals then evolve and split into the expected tetrahedral $Al(OP)_4$ species and a broad peak due to hydrated octahedral aluminum oxide species.[165] Tracking the spectra as a function of time the team were able to show the influence of heating the gel (prior to crystallization), and the transition as a function of time. This led to the conclusion that bond-formation was not the determining step for framework formation but was for the activation energy of crystallization.

Given the importance of SAPOs in the MTO process, ssNMR has repeatedly been used for identifying coke precursors and reaction intermediates from the HCP.[166-168] One of the earliest examples introduced $^{13}CH_3OH$, CD_3OH or ethene to SAPO-34,[169] while being heated in a closed system, with samples analyzed as a function of reaction temperature. ^{13}C and ^{2}H NMR confirmed the formation of surface methoxy groups, which at low temperatures (< 473 K), are stable and involved in all hydrocarbon transformations.[169] It was noted that isobutane was among the initial

products observed, attributed to alkene methylation of these surface methoxy groups. Similarly, isopentane is also observed early in the reaction, likely due to the subsequent methylation of isobutane from the surface methoxy groups.[169] This work has been developed over the years primarily by Weckhuysen[170-171] and Hunger,[151-152, 172-174] who focused on early reaction products and coke precursors, respectively. Weckhuysen *et al* employed 2D ^{13}C-^{13}C and ^{1}H-^{13}C ssNMR to confirm the identity of a range of hydrocarbon intermediates and products with exceptional clarity (Figure 14), ultimately providing fundamental insights on the MTO mechanism.[170-171] This confirmed that the surface methoxy species indeed play a major role in the MTO process, as they react with CO to form acetate species, that initiate C-C- bond formation, a significant mechanistic finding.[170-171] Hunger *et al* employed an *in situ* approach, flowing nitrogen and ^{13}CH$_3$OH over a SAPO-34 packed rotor, whilst collecting ^{13}C ssNMR.[152, 172, 174] This study compared the spectra from a continuous flow and stopped flow systems, the latter purges the system, mid-reaction, to probe surface methoxy species. Focusing on SAPO-34 showed the formation of C$_6$-C$_{12}$ intermediates within the pores. To gain further insight the reagent flow was switched from ^{13}CH$_3$OH to ^{12}CH$_3$OH, to observe the influence this would have on the products formed. This resulted in a decrease in the ^{13}C abundance in the coke molecules, showing that methanol is continually contributing to the HCP.
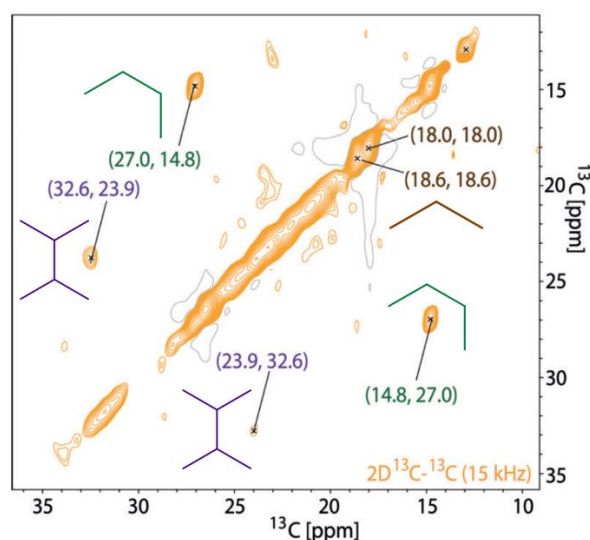
Figure 14. 2D ^{13}C-^{13}C solid state NMR correlation experiments probing the mobile molecules in the MTO process with SAPO-34. Adapted from reference [170] with permission from Wiley publishing.

^{129}Xe is an unlikely nucleus to explore for SAPO characterization, but a significant body of work, over many materials, describes how it can be used to probe accessibility and diffusion in microporous frameworks.[175-177] Here the ^{129}Xe peak positions, line shapes and shielding tensors are used to calculate Xe-Xe interactions, which are correlated to confinement of Xe molecules. Jokisaari *et al* confirmed theoretical findings on the change in line shape for Xe residing in circular or elliptical channels for a range of SAPO and AlPO materials.[176-177] Further this showed the acidic sites did not influence the diffusion. This was also applied to the MTO reaction with SAPO-34, which had been on stream for 0, 5, 10, 18 and 49 minutes, at 673 K.[178] The samples were then exposed to gaseous Xe and the ^{129}Xe spectra collected at 293, 233 and 193 K (Figure 15). Gaseous Xe could be seen at 0 ppm, though a second peak could at 84 – 134 ppm was attributed to Xe in the CHA (chabazite) cages. The peak position shifted significantly depending on the measurement temperature, but not with time-on-stream.[178] It was concluded this signal

corresponded to Xe in empty CHA cages only, showing that coke formation is not uniform across all areas of the catalyst. The peak intensity was also monitored, confirming that pores get rapidly blocked after 10 minutes, from coke build-up, reducing accessibility.[178] Recently this work has been developed further to probe the variation in Xe interactions across a large 15 μm cubic crystal of SAPO-34.[179] This revealed an inhomogeneous distribution of Xe throughout the particle, where the outer layers were readily accessible, but the inner layer was not. This again highlights the importance of controlling both mass-transfer and internal diffusion in microporous materials.
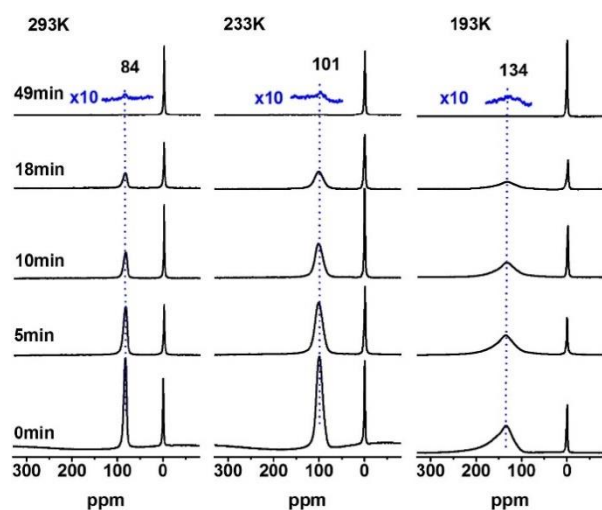
Figure 15. Showing the variations with MTO time on stream and temperature for the [129]Xe NMR spectra of Xe-loaded SAPO-34. Adapted from reference [178] with permission from Elsevier publishing.

A further NMR technique that has been utilized to probe diffusion is pulsed field gradient (PFG) NMR.[180] PFG NMR directly measures the self-diffusivity constants (D) of organic molecules, which, combined with observation time, determines the molecular displacement of these molecules. Varying the temperature of these measurements, thus varying D, means the

diffusion activation energy can then be calculated.[180] One can then observe the variation in diffusion activation energy from a fresh sample to a spent one. Hunger *et al* compared the diffusivity of ethane and ethene in fresh and used SAPO-34.[181] Diffusivity of both ethene and ethane drastically decreased in used species, confirming coking has a significant effect on diffusion, which has since been repeatedly observed.[178, 181]

ssNMR can also probe the acidity of different supports, primarily by comparing peak positions attributed to probe molecules before and after adsorption onto a support.[182] Here the strength of the acid site, in principle, relates to the strength of the acid site-probe interactions, which are measured by ssNMR. In theory, the ^{1}H ssNMR could be used, but the narrow chemical shift range and large ^{1}H-^{1}H dipole interactions makes it a challenge to resolve,[183] instead ^{13}C NMR of the hydrocarbon probes is typically used.[146, 182] Acetone is a common probe, with ^{13}C signals at 207 and 30 ppm from carbonyl and methyl carbons respectively. The carbonyl oxygen can hydrogen bond with Bronsted sites or interact with Lewis sites. Both interactions shift the carbon signal downfield, the extent of which relates to acid strength.[146, 182] Acetone was adsorbed onto two SAPO-34 species with different silicon loadings (8.7 and 3.6 wt%, Figure 16). The high loading SAPO-34 (8.7 wt% Si) showed two signals at 217 and 225 ppm, attributed to a moderately-strong and strong acid site respectively.[146] However, the lower loading species (3.6 wt% Si) showed a third signal at 240 ppm, showing Lewis acid sites were also present (Figure 16). Ammonia has also been used as an acid site probe for SAPO-34 and SAPO-37, following the ^{27}Al and ^{1}H signals as a function of ammonia loading, showed the different ammonium locations within the two frameworks, giving insights into acid site location.[147]
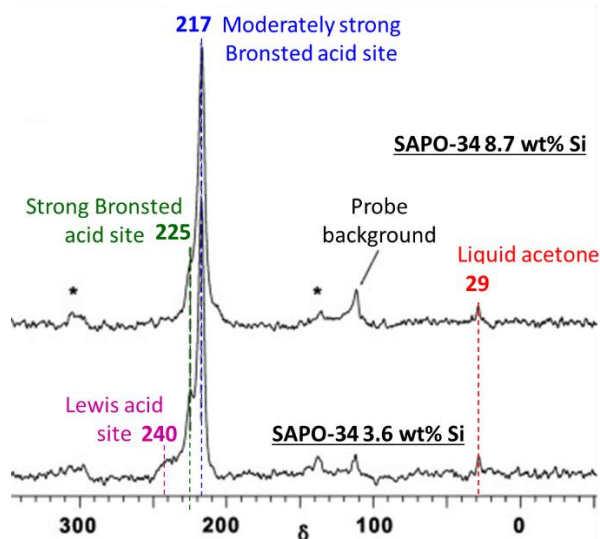
Figure 16. ^{13}C NMR of acetone bound to different Si loadings of SAPO-34. Adapted from reference [146] with permission form Elsevier publishing.

Overall NMR has immense possibility for studying SAPOs. The versatility of this technique can be increased further by isotopically labelled studies, especially ^{29}Si, allowing better resolution data to be collected. Using NMR to measure acidity is also an interesting prospect. While a range of techniques already exist to measure acidity, the strong influence of atomic proximity in NMR means that it may in future be able to expand on typical acid characterization techniques, to acidity, and the local geometry of the site, simultaneously.

Porosity, elemental analysis and microscopy techniques

A range of other techniques are vital for confirming the structural and textural integrity of SAPOs. Porosity is a key feature of SAPO, each framework will have a characteristic microporous surface area ranging from around $100 - 600$ m^2/g, that depends on the framework

topology. Typically, these measurements are performed through nitrogen physisorption at 77 K, as nitrogen is added to a known quantity of SAPO, quantifying the amount of nitrogen adsorbed as a function of pressure to build an adsorption isotherm. This continues until atmospheric pressure is reached, at which point the pressure then decreases back down to vacuum to construct the desorption isotherm. The surface area is typically calculated from the low-pressure regime using the BET (Brunauer-Emmett-Teller) model,[184] while total pore volume is calculated from the total nitrogen uptake at atmospheric pressure. A range of different isotherm shapes can occur, depending on the porosity of the system.[185] Typically, microporous species show a rapid uptake at low pressures, with minimal uptake beyond, known as a type I isotherm. However, variations occur when larger pores are introduced into the system to make hierarchical analogues. In this case the meso- and macropore width can be estimated using many different functions, with NLDFT (Non-linear density functional theory)[186-187] and BJH (Barrett, Joyner and Halenda)[188] among the most common. This can be used to investigate pore-blockage, for example researchers have calculated the surface areas and pore volumes of SAPO-34, at various times on stream for the MTO process, showing a decrease in both as time on stream increases.[189]

Elemental analysis of SAPOs is necessary for all samples, as the Si loading is required to calculate the catalytic efficiency, through turnover numbers or frequency. Beyond simply quantifying the amount of Si in a SAPO, the relative amounts of Si, Al and P can reveal which silicon substitution mechanisms have occurred (Figure 2). If silicon exclusively substitutes phosphorus (type II), then the sum of the moles of silicon and phosphorus should equal the moles of aluminum; $Si_xAl_1P_{1-x}O_4$. Commonly, researchers calculate some variation of: $X = (n_P + n_{Si})/n_{Al}$, where X should be close to unity, if type II has exclusively occurred. Deviation from unity suggests either extra framework Al is present, or type III substitution has occurred. Again,

in the other extreme, where type III substitution exclusively occurs the formula would be: $Si_{2x}Al_{1-x}P_{1-x}O_4$, thus the moles of alumina and phosphorus would be equal. As such it is possible to estimate the proportion of type II v type III Si substitution from the elemental analysis, which can guide ^{29}Si NMR interpretation.

Microscopy plays an essential role in measuring particle size and shape, particularly scanning electron microscopy (SEM). This is highly relevant for recent work on minimizing particle size to improve MTO performance, but also for assessing crystallinity, surface roughness and particle shape. Potentially this can be combined with synthetic studies to observe any macroscopic changes during synthesis. While this is important for all catalytic systems, SEMs use beyond this is limited, especially as the similarity between Al, P and Si, limits contrast techniques. SEM can of course be combined with EDX (Energy dispersive X-ray spectroscopy) to give elemental analysis, discussed above. Similarly, TEM (Transmission electron microscopy) can probe particle size, shape and roughness in greater detail, but if a material is truly microporous and crystalline, this will give limited information. EDX mapping is a useful feature, and if the resolution is suitably high can be used to identify areas where Si has built up, potentially even Si islands perhaps even isolated silicon sites. Microscopy has also been combined with other techniques, such as UV/Vis spectroscopy to identify the build-up of aromatic coke precursors within SAPOs under *in situ* and *operando* MTO reactions. The combination of microscopy with other techniques can provide vital spatially resolved information, as discussed in the MTO section.[46, 190-192]

Overall a wide range of techniques are routinely used to confirm the correct SAPO framework has formed. However, some techniques, specifically diffraction and NMR, can reveal finer details about SAPOs, and their use in catalysis. With NMR spectrometers, and synchrotron

facilities, constantly improving this will hopefully lead to more advanced techniques becoming commonplace, spurring the development of more complex and informative experiments. However, it is becoming increasingly likely that characterization methods will soon surpass our synthetic capabilities. Therefore, novel, and unique synthesis methods, with the potential to tune materials on an atomic level will always be in demand.

Methods to probe the acid strength of SAPOs

Framework topology has a significant influence on the catalytic behavior of SAPOs, though often it is overshadowed by the acid strength, quantity of acid sites and acid site location, which play a major role in the reactivity of the SAPO species.[193-195] The strength of an acid site influences which mechanistic pathways occur, and thus the product distribution. The number of acid sites will influence the reaction rate, as more sites initiate more reactions, further, acid site location determine the accessibility of acid sites to the reagents. SAPOs are generally well-defined materials, but often have multiple acid sites, which must be resolved to understand their individual behaviours.[196] Infrared (IR) spectroscopy is a commonly used technique for probing acid sites, specifically DRIFTS (Diffuse Reflectance Infrared Spectroscopy), as little sample preparation is needed, to focus on surface interactions.[16, 138, 154, 197-198] As the energy of a signal is a function of the bonds force constant and the atoms involved, one can resolve different O-H stretches, loosely based on the acid strength. The hydroxyl region of SAPO materials (4000-3000 cm^{-1}) commonly shows many features, with ever-present defect hydroxyl sites, Si-OH and P-OH, occurring at 3750 and 3680 cm^{-1} respectively.[12, 199] However, Bronsted acid sites associated with Si substitution (Al-OH-Si) occur at 3650-3500 cm^{-1}. Aside from resolving signals at different

wavenumbers, DRIFTS of the bare material provide limited information on accessibility, acid strength or acid quantity. The latter is particularly challenging, as quantification requires an absorption coefficient of that exact signal, which necessitates thorough calibration for that precise signal. As a result, probe based *in situ* IR experiments have been widely used.[11, 16, 195, 200-203]

IR probes are carefully selected, so that the molecule has distinct stretches in an unoccupied region, which are influenced by acid strength.[204] CO is a classic example, as the C-O stretch occurs between 2250-2100 cm^{-1}, which is empty for SAPOs. CO, as a weakly basic molecule, will interact with Bronsted acid sites, with the C-O stretch being sensitive to acid site strength.[25, 154, 195-196] Further, the C-O stretch has a high absorption coefficient, producing intense signals, thus CO probed IR has been widely used to examine acidity in SAPOs. Commonly spectra are collected of the bare SAPO which has been outgassed at high temperatures to remove any residual water or other impurities. Known pressures of CO are then added to the system, repeating multiple times to saturate the system. Spectra are typically shown as difference spectra, where the original dried SAPO spectrum is subtracted from each other spectra, to focus on the effects of CO interactions.[19, 195, 201, 204-206] The hydroxyl signals shift to 3500-3100 cm^{-1} when binding to CO, due to the hydrogen bonding, with a greater energy shift meaning a stronger interaction, and a stronger acid site (Figure 17). Comparing the difference spectra as a function of CO pressure one can match the disappearance and appearance of different signals to calculate the energy shift, which is compared to other systems for qualitative comparison (Figure 17). As CO binds to the system signals emerge in the CO region, with Bronsted acid-CO adducts occurring at 2190 – 2150 cm^{-1}, while Lewis acid sites are higher. As the system becomes saturated with CO it will form liquid-like physiosorbed species on surfaces and in pores,

producing a signal at 2140 cm^{-1}. While an effective method for determining the acid strength, it is challenging to quantify the total number of acid sites with CO IR due to the range of absorption coefficients for these species, though useful comparisons and trends can be made.[195, 201, 204-207]
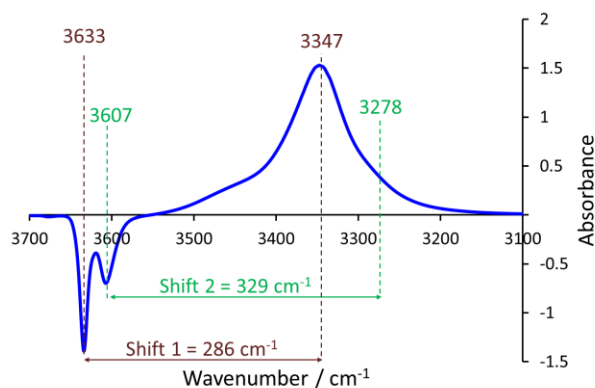
Figure 17. Difference FTIR spectra of SAPO-34 on adsorption of CO, showing the decline of O-H signals and the emergence of OH-CO bonded species, resolving two signals with distinct acidities.

To quantify the number of acid sites, probes such as pyridine, lutidine (dimethyl pyridine) and collidine (trimethyl pyridine) are often used.[16, 19, 200] These can have a range of interactions with the SAPO protons, including a full proton transfer to the probe molecule. This leads new signals appearing in the 3500-3000 cm^{-1} region, and the deviation from the original OH signal, as with CO, can be related to acid site strength. The C-C v_{8a}, v_{19a} and v_{19b} frequencies in these molecules, at 1595, 1485 and 1445 cm^{-1} respectively, and are highly sensitive to Bronsted and Lewis acids (Figure 18). More importantly the absorption coefficients have been determined for the 19a and 19b stretches, thus the peak areas can be used to determine the total acidity of the system. The 8a stretch on methyl substituted pyridines (lutidine and collidine) can also be used to measure acid

strength. Similarly, the extinction coefficients of these probes have also been determined, so can also be used to quantify the number of acid sites. Given the lower vapor pressures of these molecules, quantitative dosing is challenging. Typically, spectra of these molecules are collected by first saturating the SAPO with the probe, then collecting spectra after heating under vacuum. The difference spectra are reported on desorption at a range of temperatures, thus signals to weakly bound probes diminish first, leaving strongly bound probes (stronger acid sites) at high temperatures (Figure 18).[15-16, 19, 200, 207] In order to confidently deconvolute signals due to similar Bronsted acid sites it is important to show not just the variation in the FTIR spectra with respect to temperature,[208] but also quantify the absorption/desorption of the probe molecules as a function of temperature to differentiate between different strength acid sites.[209]
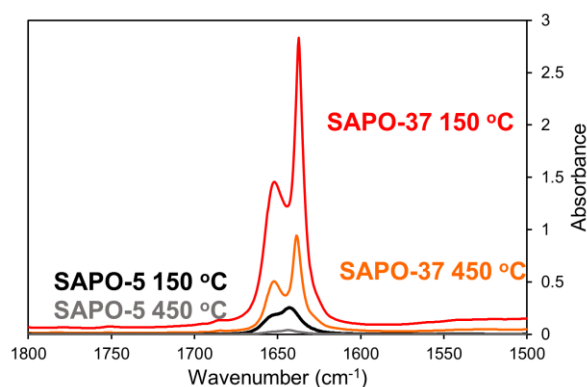
Figure 18. Collidine-probed FTIR of SAPO-37 and SAPO-5, showing the variation in accessibility and variations with desorption temperature from 150 °C (bold) and 450 °C (light). Adapted from reference [19] with permission from RSC publishing.

Accessibility is key to reactivity, especially for microporous species. With different probe molecules available, it is useful to compare larger and smaller probes, for a qualitative understanding of accessibility. This is particularly important when dealing with larger substrates,

there is little point in studying sites that cannot contribute to the reaction. As such there is often merit to using CO to probe the total acidity, then using a probe which resembles the reactant (or even the reactant itself) to develop a more realistic view of the accessible sites.[19, 25]

Probe molecules are often used in other techniques, and is fundamental to Temperature Programmed Desorption (TPD)[210-211]. Here a probe molecule, typically ammonia, saturates a dried SAPO, which is then heated, with a known temperature profile, measuring the desorption of ammonia as a function of temperature. This gives two useful quantifiable properties, the area under a signal corresponds to the total acid quantity.[19, 72] Further the temperature of the peak maxima refers to the strength of the acid site, with a higher temperature meaning a stronger acid site. This provides useful quantitative data that readily complements the IR findings. In isolation, TPD findings must be interpreted with care. Unless there is a noticeable difference in desorption temperatures it can be challenging to resolve individual TPD signals, also it cannot provide much information on accessibility of the active sites.

Thus far the TPD and IR systems discussed have only been able to provide qualitative trends on acid strength.[212] There are clear benefits to quantifying acid strength, such as predicting rates of reactions, mechanistic pathways, or validating theoretical findings. NH_3-TPD experiments can be carefully designed to give these energetic values, however this requires some simplifications and assumptions. This is also true with adsorption isotherms. One technique which can directly measure the enthalpy of adsorption is NH_3-calorimetry, here a dry, bare SAPO system is placed under vacuum, with ammonia gradually being introduced.[11, 194, 213] The heat exuded from the system, on ammonia binding, is measured as a function of the ammonia pressure. Such techniques provide valuable insight, though the strongest acid sites are often the most interesting

in a system, they bind first, therefore only a fraction of the data, in the initial stages, corresponds to these interesting sites.

All these techniques have their own advantages and disadvantages, which can be overcome by piecing the information together. An elegant solution from the zeolite world is IRMS-TPD (Infrared mass spectrometry – temperature programmed desorption),[214-217] which combines many techniques. Here ammonia-doped solid acid materials undergo TPD-MS (temperature programmed desorption – mass spectrometry), whilst the IR spectra is recorded every 10 $^{\circ}$C. In doing so one can resolve features due to each distinct active site and quantify the ammonia desorption enthalpy for each. Though this technique has only been applied to SAPO-34 it surely will provide a wealth of information on a wide range of systems.[214-217]

Theoretical studies on SAPOs

SAPOs have attracted much attention from the theoretical community, and as computing power exponentially increases, increasingly intricate and complex calculations can be performed. Some of the earliest works on SAPOs, from 1996 onwards, come from the groups of Gale,[24] Catlow,[20, 218] Angyan[21, 219] and Sauer.[220] These earlier works sought to understand the reasons behind silicon islanding and the nature of these active sites. Catlow *et al* used the molecular dynamics code GULP to compare the energetics of 5-silicon and 8-silicon islands in SAPO-5 and SAPO-34.[20, 218] This suggested the additional strain required to accommodate a 5-silicon island in AlPO-34, lead to SAPO-34 favoring isolated Si sites more than SAPO-5. These calculations also reproduced experimental findings that acid sites on the edge of silicon islands were stronger

than isolated sites, for SAPO-34, due to silicon having a lower electrostatic potential in islands.[20, 218]

Many groups working on zeolite materials sought to include the entire framework for reproducible *ab initio* calculations, as confinement and dispersion are key to zeolite reactivity, thus periodic boundary conditions became popular.[21] Sauer *et al* showed that a completely 'dry' system could not reproduce experimental findings.[220] Water was added in the pores of SAPO-34, to probe H_3O^+, with periodic boundary conditions, to model the whole framework. By considering combinations of Si loading and water probe molecules, they concluded that both Si loading and partially protonated water clusters dictated the acidic behavior. This became a common theme for many groups, who combined diffraction techniques with theoretical calculations to explore protonated water species. Gale *et al* expanded this study to compare the behavior of SAPO-34 and chabazite with methanol, as SAPO-34 cannot protonate methanol, whereas chabazite can.[24] Considering the four possible Bronsted acid sites in SAPO-34 they showed that two were favored, as per experimental findings, though neither could fully protonate methanol. Another earlier study focused on why SAPO-34 was more weakly acidic than it's zeolite counterpart; chabazite.[21] This began a surge of interest in computational calculations on the MTO process, which will be discussed in a later section.

Currently a significant body of theoretical SAPO work is still dedicated to unravelling silicon substitution,[221-225] acidity[17, 217, 226-229] and interactions with water,[230-232] showing the complexity of these problems. Fischer has investigated the influence of SAPO frameworks on the adsorption of water,[230-231] for their potential use in heat transformation applications (Table 6).[232] In doing so the interactions of six different SAPO frameworks, and their undoped AlPO counterparts, with water (> 20 molecules of water per unit cell) was calculated.[230] On saturation the SAPOs had a

stronger interaction with water than undoped AlPOs, as expected due, to hydrogen bonding from the acid site. Though there was little difference in the adsorption energy between SAPO frameworks, all six lying between -69 and -73 kJ/mol (Table 6). This suggested that topology, and the precise acid site, had little influence on water binding at saturation. Despite similar adsorption energies the framework response differed significantly between the topologies.[230] It was found that frameworks containing d6r, such as SAPO-18 and SAPO-34, had a moderate contraction of < 1.5 % of the cell volume (Table 6).[230] Whereas other frameworks were showed strong aluminum-water interactions that significantly deformed the unit cell, something which has been seen experimentally when contrasting SAPO-34 with the less stable SAPO-37.[136]

Table 6. Comparing the properties of water saturation on different SAPOs and unit cell distortion, adapted from reference [230].

SAPO framework	Interaction energy (kJ/mol)	Dispersion energy (kJ/mol)	Water molecules (per unit cell)	ΔVolume (%)
SAPO-17	-72	-24	30	-1.2
SAPO-18	-73	-24	25	-1.5
SAPO-34	-73	-25	40	-1.2
SAPO-43	-71	-28	32	-0.3
SAPO-56	-69	-24	50	-1.3
SAPO-RHO	-71	-22	25	-2.8

Beyond adsorbed water there is, as discussed previously, interest in understanding the orientation of SDAs within a SAPO pore, mimicking as-synthesized systems.[233-234] A good understanding of SDA orientations and framework interactions naturally feeds into the design of new synthesis protocols for existing and suggested frameworks. Previous work utilized a Monte-Carlo approach to consider the possible orientations of a common SDA, dipropylamine (DPA), within AlPO-11, AlPO-31, AlPO-41 and SAPO-34.[234] This showed that protonated DPA bound

far less to SAPO-34, compared to the other AlPO systems, as the SAPO-34 cage is much larger than a single DPA molecule, requiring other DPA molecules to reside within the cage to stabilize it. More recent work compared the interaction energy of SAPO-34 with dipropylamine, diisopropylamine (DIPA) and triethylamine (TEA).[233] This showed that DIPA was able to stabilize the SAPO-34 framework more than TEA and DPA, due to the stronger interaction energy. However, this study could not probe the influence of the acid-base interactions between the Bronsted sites and the SDAs. Instead the acid sites were incorporated as an 'uniform background charge' evenly distributed across the framework. While this provides a good basis, to progress further an accurate model must surely include individual acid sites.

Controlling acid strength in SAPOs has been sought for many decades, yet still uncertainty remains on which factors determine acid site strength. Many researchers have postulated theories relating to the Si—O bond length, electron density on the adjacent oxygen atoms, the framework bond angles etc. Most have reproduced experimental trends of acid strength changing as the dopant varies, for a single framework, but no single for this trend exists.[17-18, 22, 229, 235] This is unsurprising, considering the vast number of variables a metal substituent facilitates. Studies comparing the acidity of SAPO-5, TiAlPO-5 and ZrAlPO-5 by calculating ammonia interactions have been performed.[229] This confirmed that SAPO-5 produced the strongest acid sites of the three species, correlating the acid strength to the M—O—Al bond angle for these three species.[229] Similar approaches have also been used, considering the frequency of the acidic O-H bond stretch, where a lower frequency corresponds to a weaker bond, and stronger acid site.[18, 22] Researchers have also utilized the intrinsic link between catalytic activity and acid strength to benchmark calculations. Work by Studt *et al* on substituted AlPOs elegantly correlated the experimental activity for the methanol-propene step of the MTO reaction, to the calculated

ammonia adsorption energy (Figure 19).[17] The strong correlation then justified the use of

ammonia adsorption as a measure for acid strength, and thus catalytic activity.
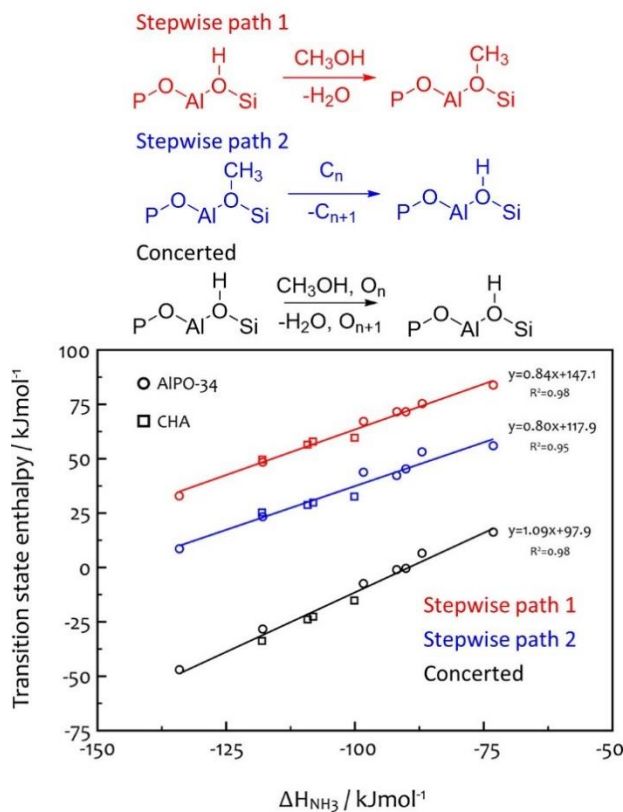
Figure 19. DFT findings correlating ammonia binding interactions with transition state enthalpy for key MTO reactions. Adapted from reference [17] with permission from ACS publishing.

The different acidity between SAPOs and zeolites is still of great interest to the community.[199] A combined ammonia IRMS-TPD and DFT study sought to compare analogous SAPOs and zeolites using Dmol^3 with periodic boundary conditions.[227] The study showed excellent agreement between experimental and theoretical values, which were within 10 kJ/mol of one another. This again highlighted that SAPOs acid strength is notably lower than zeolites. It was suggested this due to the Al-O-P bond angle would changing more on dopant substitution than a Si-O-Si angle. Thus, the greater flexibility allows the SAPO framework to better accommodate a

proton, increasing the bond strength, whereas the rigid zeolite does not bond as strongly.[227] This results in a weaker acidic OH bond in zeolites, which makes it a stronger acid site, compared to SAPOs. Similar studies where the computational findings can be 'benchmarked' against experimental findings are vital for meaningful comparisons within the SAPO community, adding significant weight to theoretical findings.

The distribution of silicon sites and the influence on acidity remains an active area of SAPO research. As the two are strongly intertwined, and the distribution of silicon sites can, to some extent, be controlled synthetically, then an improved understanding will benefit catalyst design. Investigations on SAPO-11,[225] -31,[236] -34[28, 206, 217, 221, 223, 237] and STA-7[224] have evolved to focus on the relative probabilities of silicon and proton locations, building a more accurate representation of the structure, closing in on reproducing experimental values. While such calculations have merit, they can only focus on the final configurations, they cannot, for example, account for kinetics products formed in the crystallization process. Swang et al have investigated the synthesis process, comparing $P(OAl)_4$ and $Si(OAl)_4$ formation rates.[221, 237] Considering activation and reaction energies they concluded that $Si(OH)_4$ and H_3PO_4 will insert into a $(AlOH)_3(AlOH_2)$ nest at similar rates, with activation energies of 51 and 60 kJ/mol respectively. However, the final reaction energies were significantly different at -94 and -163 kJ/mol respectively. Thus, the likelihood of Si leaving the framework again is much higher, whereas P insertion is less reversible. It was then proposed that the formation of 5-silicon islands occurs in two stages (Figure 20). The initial stage involves the sequential replacement of framework P atoms with Si, such that $Al(OP)_4$ transitions to $Al(OSi)_4$.[221] The second stage involves the central Al atom being replaced by Si, either through direct substitution, or by dealumination, leaving a defect which is subsequently 'healed' by a further $Si(OH)_4$ species. In a

further paper Swang *et al* investigated the possibility of Si being mobile and redistributed in a framework, concluding that desilication of the framework was indeed possible, leading to the redistribution of Si in the SAPO-34 species.[221, 237]
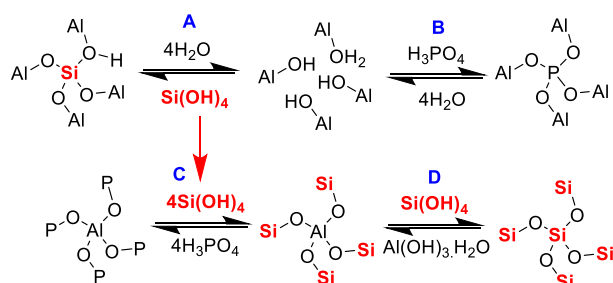
Figure 20. Stepwise mechanism of 5-silicon island formation, showing A) Isolated silicon sites desilicating from the framework B) being replaced by phosphorus to form framework species. C) Subsequent P/Si exchange leading to a Al(OSi)$_4$ site, which then undergoes D) Al/Si exchange to form a stable 5-silicon island, adapted from reference [221] with permission from ACS publishing.

A developing area of computational chemistry is the prediction of hypothetical frameworks.[238-240] Many potential new frameworks have been proposed, with their feasibility and chemical stability, still being assessed. One noteworthy example comes from Fischer, who proposed the existence of ECR-40.[241] a unique SAPO which may violate Lowensteins rule, the fundamental rule that prohibits Al-O-Al and P-O-P links in AlPOs. This example shows that the distortion created through introducing silicon (and protons) into specific positions in the framework, would lead to Al-O-Al bonds becoming feasible. Thus far this has not been achieved experimentally, though computational phenomenon such as this, can help provide inspiration for synthesis procedures for many decades.

Computational calculations on fundamental questions in SAPO chemistry such as active site location, acidity and silicon substitution still prove to be incredibly complex, even with improved computational tools. However, there is still significant scope for synergistic combined computational and experimental ventures, where either may guide the other towards improved catalyst understanding, catalyst design and unique synthesis approaches.

Catalytic case studies of SAPOs

SAPO-34 in the MTO process

SAPO-34 has been a fundamental part of the MTO process since its commercialization in the 1980s by Union Carbide.[4-5, 242] The moderate acid sites and small pore architecture of SAPO-34 allow methanol to be efficiently transformed into light olefins ethene and propene, through the shape-selective chabazite cages. A staggering amount of research is published on the MTO processes every year, making it an excellent topic for many reviews. Thus, I will not go into significant detail on the topic, though I refer interested readers to reviews that have come before.[3-4, 6, 242-244] Instead I will focus on recent advances in the field of SAPO research, and their influence on the MTO process.

As a more mature technology the operating conditions of the MTO process have been individually optimized by many different workers, resulting in seven different pilot or commercial-scale plants since 2000.[4] Most of these operate between 400-550 °C, with pressures up to 5 atmospheres, achieving quantitative conversion, and 80-85 % selectivity to C_2 and C_3 olefins.[4] The current research focus on extending the catalyst lifetime and understanding the

reaction mechanism, with emphasis on the formation of initial C-C bonds and coke precursors. The former has inspired many advances in SAPO synthesis, as many of the synthetic techniques discussed before, were explored with the notion that smaller particle size can extend the lifetime of SAPO-34.[85-86, 89-90] Most recently this has resulted in hierarchical SAPOs, a notion inspired by work on zeolites.[245-247] The micropores in SAPOs are responsible for numerous catalytic benefits, including selectivity control and confined active sites. However, small channels can hinder diffusion, preventing reactants to reach the active sites, hindering activity. Worse still it can stop products leaving the active site, triggering further reactions, leading to by-products, and ultimately coke.[248-250] Many researchers sought to overcome this by incorporating mesopores into the microporous networks, therefore having different pore sizes over multiple length scales, creating hierarchically porous (hierarchical) systems.[15, 144, 154, 197-198, 207, 251] Such systems have improved catalyst lifetime for a range of reactions, as mesopores aid product diffusion away from the active site, and act as a sacrificial site for coke build up, protecting the micropores.[252] A variety of methods have been used to incorporate mesopores into SAPOs, which can be divided into two categories. Top-down methods create mesopores post-synthetically into a microporous SAPO, typically focusing on acid or base treatments, partially eroding the microporous network to create the mesopores.[253-254] In contrast bottom-up methods form mesopores alongside the microporous framework, during synthesis, typically through a mesopore template, that is included in the synthesis gel. 'Soft' templates are hydrocarbons that can be removed on calcination, along with the microporous SDA, leaving larger pores behind (Figure 21).[255-256] Examples include surfactants and micellar agents such as Cetyltrimethylammonium bromide (CTAB), Dimethyloctadecyl[(3-(trimethoxysilyl)propyl] ammonium chloride (DMOD) or [3-(trimethoxysilyl)propyl]-octa-decyldimethylammonium chloride (TPOAC).[15, 207, 251] 'Hard'

templates typically require a separate removal step, though have the benefit of having well-defined sizes, leading to a narrow mesopore range. Carbon nanotubes,[115] nanofibers[257] and polystyrene spheres[258] have been used to excellent effect for this, with different templates influencing the mesopore location and accessibility. Hierarchical materials are very much a developing field in SAPO research, with a range of other shapes being considered,[259] including nanosheets.[260-263] While the hierarchical materials improve the catalysts MTO lifetime (Figure 21), few characterization techniques can provide quantitative information about mesopore accessibility, size, shape and links with the microporous network. As such these materials have significant potential in the MTO process, if, these factors can be controlled synthetically and quantitatively characterised.[3, 256, 264]
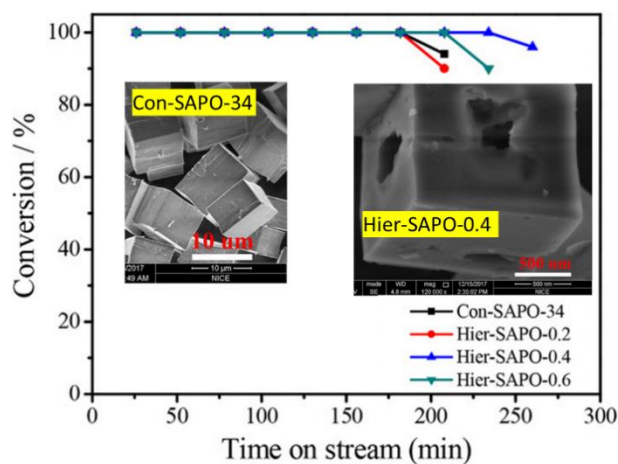
Figure 21. Comparing the MTO catalytic lifetime of conventional SAPO-34 (Con-SAPO-34) with a hierarchical 'hollow' SAPO-34 (Hier-SAPO-0.4) created with a dual template approach. Adapted from reference [255] with permission from Wiley publishing.

Theoretical studies, often combined with characterisation,[265-266] have probed the mechanism of the MTO reaction, towards an improved understanding of the process.[267-269] Given the wide

range of MTO products and intermediates, this is not trivial.[5, 270] It is generally accepted that there are four stages to the MTO process.[5] 1) Equilibration, where methanol transitions into dimethyl ether, water and surface methoxy species.[271-273] 2) Induction, these products then form C_2 and C_3 olefins alongside a growing hydrocarbon pool.[274-275] 3) Primary product formation, where the process tends towards light olefins $(C_2 - C_4)$[267] and finally, 4) Secondary product formation, where larger, aromatic products form,[276-282] leading to deactivation by either acid site leaching or pore blockage. Plessow and Studt investigated the influence of the framework on first two steps of the MTO process, using DFT calculations on both SAPO-34 and zeolite analogue SSZ-13.[283-284] This study suggests that C-C bond formation proceeds through a CO intermediate, with methanol being dehydrogenated to formaldehyde prior to CO formation, in line with many experimentally observed species. This further identified the highest energy barrier as the formation of CO, prior to C-C coupling. This study encompassed a range of frameworks, concluding that the CO pathway was favored in all cases, regardless of confinement effects.[283-284] This has since been incorporated into the work of Ding *et al*, who postulated that via the CO pathway, the first species with a stable C-C bond that should be observed experimentally was ketene, CH_2CO, with an energy barrier of 109 kJ/mol.[274] Despite CO formation being scarcely influenced by the framework, the framework was found to have a significant influence on the stability of C_3-C_6 carbonium ions, which play a major role in dictating product selectivity in the MTO process.[279] Recent research has focused on the formation of the dimethyl ether intermediate, and the influence of isolated or silicon islands on the mechanism.[271] It was found that while surface methoxy species more readily form on acid sites from silicon islands, the subsequent activation energy to form dimethyl ether was much

higher. This is likely due to the stronger acid sites on silicon islands creating too stable a species, rendering them more inert.[271]

In all cases molecular simulations and diffusion is known to play a key role in the MTO process.[285-288] This has led to Van Speybroeck *et al* carefully probing the diffusion of propene and ethene through the SAPO-34 cage, using *ab initio* molecular dynamics (Figure 22).[289] Specifically, the influence of Bronsted acid site density, diffusion temperature and the presence of other molecules was explored. Curiously, it was found that the diffusion of propene and ethene through the 8-membered rings is improved by the presence of Bronsted acid sites. Diffusion of ethene through an 8-membered ring with no acid sites had a 30 kJ/mol energy barrier, which was lowered to just 15 kJ/mol in the presence of acid sites.[289] This was attributed to the π-interaction between the alkene and the acid site, aiding 'hopping' between cages, which is observed over a wide temperature range (450–600 K). The presence of methanol and bulkier aromatic molecules from the hydrocarbon pool was also considered in this study (Figure 22). The starting cage contained one propene and four methanol molecules, whereas the adjacent cage contained four methanol and one aromatic molecules (either toluene or hexamethylbenzene). This showed that any propene (or ethene) formed within a cage, that also contained a bulky aromatic compound would be readily expelled into a neighboring cage. However, if the species became trapped (no available neighboring cages) then this would lead to rapid deactivation of the active site.[289] These insights reinforce the importance of acid site density and framework topology in catalyst design.
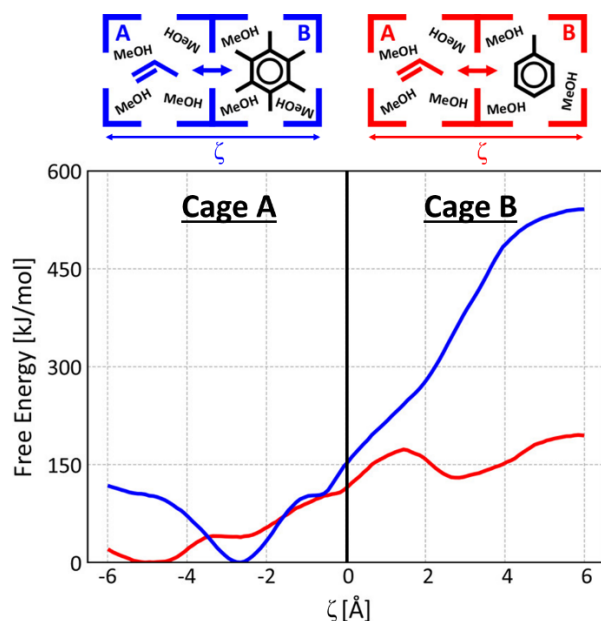
Figure 22. Energy profile of propene diffusing from one SAPO-34 cage ($\zeta < 0$), through the pore window ($\zeta = 0$), into an adjacent cage ($\zeta > 0$), containing different aromatic hydrocarbons. Adapted from reference [289] with permission from ACS publishing.

A significant contribution to the current understanding of the MTO process, its initiation, and subsequent deactivation comes from Weckhuysen and co-workers. Many of their published works have been dedicated to the development and commissioning of an array of characterization techniques and protocols, applied to the MTO process.[170, 190, 192, 290-293] Particular emphasis has been placed on microscopy and microspectroscopy, to understand spatial variations within a catalyst.[190, 265, 292, 294-295] While some of these techniques initially focused on zeolite species, many have since proven invaluable for analogous characterization of SAPO materials. One example is X-ray mapping, initially particles of conventional, and steamed, ZSM-5 were investigated,[296] but this has since expanded to focus on conventional and steamed SAPO-34.[290] Here the Al and Si K-edge were mapped using scanning transmission X-ray microscopy (STXM) to distinguish between different phases. Interestingly silicon deposits were found in both

systems, with the conventional system showing a more defined silicon environment (through XAS; X-ray absorption spectroscopy), suggesting degradation of the SAPO-34 species on steaming.[290] Similarly, the distribution and variations in carbon deposits were also examined tracking the C K-edge with STXM of the particles, as a function of time on stream. Conventional SAPO-34 showed different XAS spectra for the inner and outer areas of the particle. This revealed that the inner regions had a higher fraction of sp^2 carbons, due to more intense peaks at 286 and 287 eV, associated with coke precursors. In comparison the outer regions showed fewer coke precursors, suggesting these originate from the interior of the particle. In contrast the steamed SAPO-34 species showed little differences between the outer and inner regions, explaining its shorter induction period, but also its faster deactivation, compared to conventional SAPO-34.[290] These findings contrasted their earlier work on ZSM-5 which showed that for the zeolite species the coke precursors preferentially formed on the outer regions of the particles.[290, 296]

In many cases more information can be gained from pooling information from multiple characterization techniques. Weckhuysen *et al* have often combined *in situ* UV/Vis microspectroscopy, confocal fluorescence microscopy and *in situ* infra-red microspectroscopy.[292, 295] Focusing on the evaluate the build-up of the HCP and coke precursors across particles of SAPO-34 during the MTO process, comparing with the zeolite analogue SSZ-13.[297] This showed that the two species were similar in their behavior, both forming poly-alkylated benzenes initially, aiding the reaction, before these were converted to deactivating polyaromatic species. The use of UV-vis in this case allowed the researchers to quantify the kinetics of polyalkylated benzene (HCP species), showing that the weaker acid sites in SAPO-34 resulted in a higher activation energy compared to SSZ-13.[297]

Due to combined theoretical and experimental efforts UV/Vis spectroscopy has become a routine measurement for probing coke build-up in MTO catalysts.[265-266] This allowed distinct groups of aromatic molecules to be determined, based on characteristic UV/Vis signals. This has recently been utilized to probe both the active HCP species, and deactivating molecules on SAPO-34 as a function of time on stream and reaction temperature (Figure 23).[291, 298] Following the UV spectra as a function of time, under *operando* conditions, meant species appearing in the induction step could be linked to activity, whereas species growing as conversion decreased were associated with deactivation. At 573 K monoenyl and highly methylated benzene carbocations appeared (34000 and 26000 cm^{-1} respectively), forming the basis for the active HCP.[291] Deactivation was accompanied by signals occurring at 30000 and 24500 cm^{-1} due to low methylated benzene and methylated naphthalene carbocations, linking them to catalytic decline (Figure 23). However, at the higher temperature of 623 K, initial signals at 36000 and 24500 cm^{-1} corresponded to neutral aromatics and methylated naphthalene carbocations, suggesting the activation procedure had changed. Further deactivation was accompanied by signals at 20000 and 16700 cm^{-1} due to neutral polyaromatics and anthracene/phenanthrecene species forming, prompting deactivation (Figure 23).[291] The combination of these studies has strengthened our understanding of the MTO process, and will help guide future catalyst design towards a cleaner process.
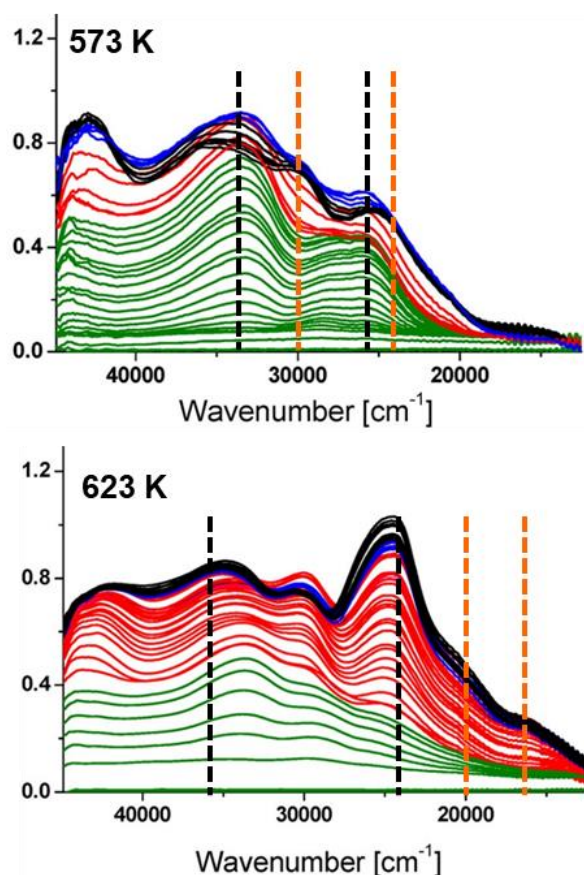
Figure 23. Showing the *operando* UV/Vis spectra of SAPO-34 during the MTO process at different temperatures. Solid lines correspond to experimental data with Green = Induction period, Red = Full conversion, Blue = Deactivation period, Black = Spent catalyst. Dashed vertical lines represent species formed during different phases, as discussed in the text. Black-dashed lines = Activating species, Orange-dashed lines = Deactivating species. Figure adapted from reference [291] with permission from ACS publishing.

Beckmann rearrangement of cyclohexanone oxime to ε-caprolactam

ε-Caprolactam is a vital precursor in the formation of Nylon-6, a recyclable form of Nylon.[207, 299-301] Currently the majority of caprolactam is formed through a variation of the Raschig process, where cyclohexane is converted to caprolactam with a series of metal salts and caustic reagents, creating significant amounts of ammonium sulfate waste.[301] Specifically, the formation of caprolactam is achieved using fuming sulfuric acid, which poses significant logistical and safety challenges. Given this step is acid catalyzed there is significant interest in using a recyclable solid-acid catalyst to negate waste production. Indeed, processes have been commercialized with this philosophy, most using a silicate-1 zeolite catalyst.[299-300] The preferred industrial approach has been a vapor phase process. Here the reagents are taken above their boiling points, typically $> 300\ ^{\circ}C$ with a solvent, which is continually passed over a bed of solid catalyst.[16, 200] Here the conversion, and to some extent the selectivity, can be influenced by the reaction temperature, giving firm control over the activity and product distribution. The vapor-phase Beckmann rearrangement is known to require moderate strength acid sites, with stronger sites promoting deactivation and cyclohexanone formation.[16, 200] As such there was interest in utilizing SAPO catalysts, with tunable acidity and framework topology for this reaction. Framework topology is of significant interest for this process, as there is fierce debate over whether the 'bulky' cyclohexanone oxime can diffuse into the pores of the MFI silicate-1 framework.[25, 207] This has led to many studies probing the true location of the active sites. As such a range of SAPO species have been tested with different pore apertures and shapes. Specifically, SAPO-5, -34, -37 and -41 were investigated, representing different combinations of large pore, small pore, 1D and 3D channels (Figure 24).[19] The total acidity of these materials was determined using NH_3-TPD and was contrasted with the number of 'accessible active sites' found from collidine-probed FTIR. As expected, this showed that the larger pored SAPO-37

(FAU) with a pore diameter of 7.4 Å had the highest proportion of accessible active sites, but the similar sized SAPO-5 (AFI) systems, 7.3 Å pore diameter, had fewer accessible sites.[19] This was attributed to SAPO-37 being a 3D cage structure, with improved accessibility, whereas SAPO-5, as a 1D channel structure, with cylindrical pores could be easily blocked at either end. Further the framework had a significant influence on the substitution of Si, with SAPO-34 and -37 favoring isolated active sites, as seen by ^{29}Si NMR, whereas SAPO-5 and -41 formed silicon islands.[19] This has influenced the amount of Si that could be incorporated into the frameworks, and therefore the total acidity of the materials. These materials were tested for the vapor phase Beckmann rearrangement between 300 and 400 ºC. At 300 and 325 ºC SAPO-37 gave the highest caprolactam yield, followed by SAPO-5 and -41, with the smaller pored SAPO-34 producing by far the lowest lactam yield.[19] This trend roughly mirrors the pore size of the materials, suggesting at the lower temperatures, diffusion and accessibility is a key metric. However, at 400 ºC SAPO-5, -34 and -41 all gave similar lactam yields (94 – 97 mol%), whereas SAPO-37 dropped to 76 mol% due to poor conversion (Figure 24).[19] While there is debate about whether cyclohexanone oxime can diffuse into silicate-1, it is clear it cannot access the 3.8 Å pores of SAPO-34. Therefore, at these higher temperatures (400 ºC) it is suggested that framework topology plays less of a role in the Beckmann rearrangement, with surface sites becoming heavily involved.
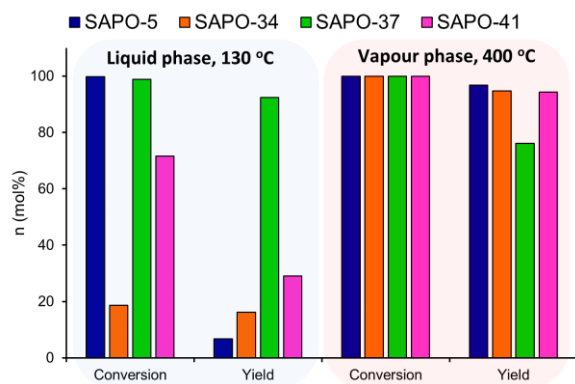
Figure 24. Contrasting liquid and vapor phase catalytic performance of different SAPO topologies for the Beckmann rearrangement of Cyclohexanone oxime to ε-Caprolactam. Adapted from reference [19] with permission from RSC publishing.

More recently interest has grown in performing the Beckmann rearrangement in the liquid phase.[19, 25, 149] While this method requires greater quantities of expensive solvent, it can be performed at significantly lower temperatures (< 150 °C), resulting in significant energy savings. Comparing SAPO-5, -34, -37 and -41 in the liquid phase process showed that the activity correlated with the pore size, like the low temperature (300 and 325 °C) vapor-phase process (Figure 24).[19] SAPO-37, achieved lactam yields of 92 mol%, due to the accessibility of the framework, warranting further investigation. The performance of SAPO-37 was found to be strongly linked to the silicon loading.[149] 2D ssNMR showed that increased silicon loading prompted silicon islanding. This then lowered the total number of acid sites, but increasing the number of strong acid sites, leading to lower lactam yields, showing that the weaker, isolated silicon sites in SAPO-37 were the active site for this reaction.[149] To confirm the efficacy of SAPO-37 was due to the combination of framework topology and specific active site, an optimized SAPO-37 system was compared with a faujasite zeolite analogue.[25] Despite these two materials possessing the same framework, they showed markedly different catalytic behavior.

Both achieved high conversions (both > 95 mol%), however the higher proportion of stronger acid sites in faujasite produced a much lower lactam selectivity of < 30 mol%, compared to > 95 mol% for SAPO-37.[25] The framework interaction with cyclohexanone oxime was also investigated through neutron scattering (Figure 25). This showed that the oxime diffused through SAPO-37 *via* 'Jump diffusion', hopping between active sites, whereas it diffused more freely through the faujasite system.[25]
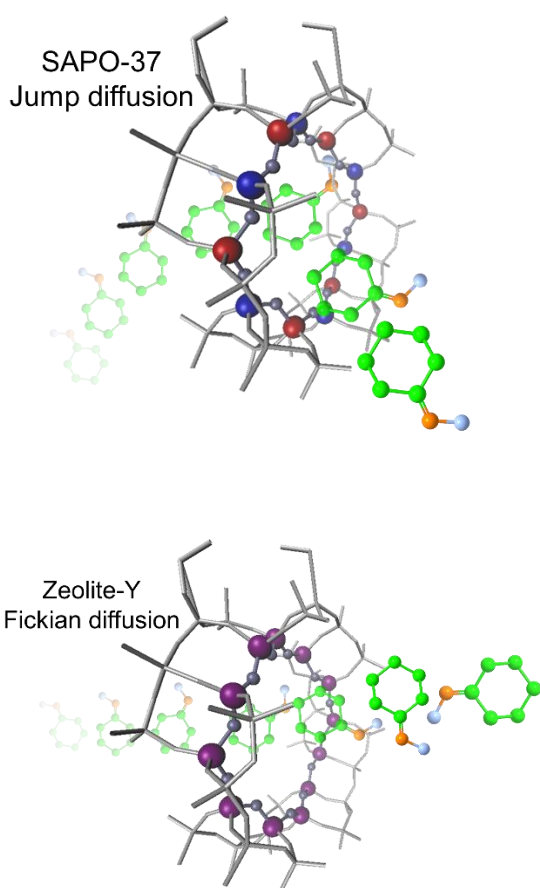
Figure 25. Differing diffusion modes identified in SAPO-37 and Zeolite-Y from reference [25] in a 9:1 mixture of catalyst to cyclohexanone oxime.

SAPO-37 has since been found to be stable and recyclable for this process, showing the benefit of combining the appropriate framework and active site within a SAPO. Further, this example

also demonstrates the importance of combining multiple characterization techniques. In this work a wide range of techniques were used to select and optimize the SAPO catalyst, which shows industrial potential.[19, 25, 149, 207]

Ethanol dehydration with SAPO-34

Ethylene is one of the most widely produced organic compounds, as it is a vital chemical in a wide range of industries, as a precursor for polymers, plastics and pharmaceuticals.[302-305] Currently ethylene is produced by steam cracking of petrochemical hydrocarbons, at temperatures above 700 ºC. It can also, in some cases, be achieved by cracking larger aromatic molecules. Few of these processes can be considered green, due to the high temperatures and reliance on crude-oil feedstocks. A proposed alternative pathway utilized ethanol, specifically fermented from bio-based feedstocks, to create a more sustainable process.[302, 305] Unlike the Beckmann rearrangement discussed above, a standout zeolite catalyst does not yet exist for ethanol dehydration. From extensive work on the MTO process, it is known that very strong acid sites promote dimerization of alkenes, leading to coking. This makes SAPOs excellent candidates for such a reaction. A study comparing the activity of large pore SAPO-5, and smaller pore SAPO-34 showed that SAPO-34 had exceptional activity for this process.[206] This was initially attributed to the acidity of the species, where the isolated Si sites in SAPO-34 were more strongly acidic than the Si islands in SAPO-5. While both species could achieve conversions > 80 mol% at 250 ºC, there were significant differences in selectivity with SAPO-34 favoring ethylene, but SAPO-5 favoring diethyl ether.[206] This led to more recent work probing the mechanism of ethanol dehydration where it was postulated diethyl ether was either a competing

by-product, or an intermediate towards ethylene formation.[205] The distinction is vital, in the former case diethyl ether production should be suppressed, whereas if it is indeed an intermediate, it's production (and subsequent activation) should be encouraged. To investigate this a mechanistic study using SAPO-34 was pursued over a range of temperatures and flow rates, conclusively showing that diethyl ether was indeed an intermediate in the process, and the formation of ethylene from diethyl ether was the rate determining step.[205] The experimental kinetic data then formed the basis of a computational fluid dynamics (CFD) study, showing that reaction temperature and bed height could play a huge role in optimizing ethylene formation.[205]

This work was also complemented by a neutron scattering (Quasi-elastic Neutron Scattering; QENS) study, probing the diffusion of the reagent (ethanol), intermediate (diethyl ether) and product (ethylene) through the SAPO-34 pore.[306] Despite the smaller pore width (3.8 Å) ethanol and ethylene readily diffused through the system. However, the 'larger' diethyl ether molecule diffused far more slowly through the pores, suggesting that once formed, diethyl ether is confined to the pores, struggling to leave the active site, forcing it to react further. This in turn goes some way to explaining the difference between SAPO-5 and SAPO-34, in the former any diethyl ether formed could readily diffuse through the larger 7.3 Å pores. In the latter it would be trapped and forced to react further.[306] In this case it is challenging to decouple the influence of the framework and the acidity, however both clearly play a key role in the process. One way this can be achieved is by modifying the acidity of the framework through the inclusion of a secondary dopant.[307] Thus far this review has purposefully limited itself to pure SAPO materials, however countless examples exist of metal-doped SAPOs. Here the inclusion of a second metal has helped modify the catalytic behavior of the system. Magnesium is known to produce stronger Bronsted acid sites than silicon.[16, 200] Therefore, including controlled quantities of magnesium

into a SAPO framework can tune the selectivity of a system. In this vein MgSAPO-34 was also

tested, containing just 0.1 wt% Mg and 3.0 wt% Si. The inclusion of magnesium was found to

increase the overall acidity of the system, leading to an increase in 'stronger' acid sites,

compared to the regular SAPO-34.[307] This lowered the activation barrier of diethyl ether

formation, increasing the rate of formation (Figure 26). The inclusion of magnesium was found

to have less of an influence on the ethylene formation step (Figure 26). However, the overall

ethylene yield was still increased due to improved intermediate formation.[307] Thus, there is

significant potential in using multiple framework dopants to tailoring the acid site, towards

sustainable processes with bio-based feedstocks.
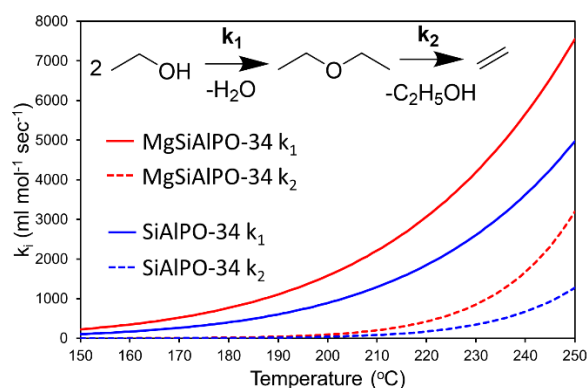
Figure 26. Showing the variation in reaction rates for ethanol dehydration to ethylene, via

diethyl ether, emphasizing the influence of a secondary Mg dopant, adapted from references [205, 307].

Concluding remarks

Over the last few decades SAPOs have been a constant feature in both applied and fundamental research for academics and industrialists alike. Since their invention SAPOs have intrigued researchers in many fields including catalysis, synthesis, characterization and theoretical chemistry. As discussed, each of these fields is constantly evolving and improving with increasingly elegant techniques, protocols and tools. However, it is only when these fields work in combination can complex challenges be solved, and significant advances be made. This field is of course fortunate that many ideas from the zeolite world can be translated to SAPOs, though these systems have repeatedly earned their vital place in society.

Some of the fundamental questions about SAPOs still remain unanswered. Why do some frameworks form islands and some form isolated sites? How can we accurately predict the acidity of these materials? How do we achieve atomic level control of the system? Can microscopy show us silicon substitution on an atomic level? These are still vital questions that will undoubtedly improve our understanding of catalyst design. Ultimately, we must aim to focus our knowledge of these materials to increasingly challenging sustainable problems such as clean energy generation and greener industrial processes for the future.

AUTHOR INFORMATION

Corresponding Author

*Matthew E. Potter, M.E.Potter@soton.ac.uk

Author Contributions

All authors have given approval to the final version of the manuscript.

REFERENCES

1.   Lok, B. M.; Messina, C. A.; Patton, R. L.; Gajek, R. T.; Cannan, T. R.; Flanigen, E. M., Silicoaluminophosphate Molecular-Sieves - Another New Class of Microporous Crystalline Inorganic Solids. *Journal of the American Chemical Society* **1984**, *106*, 6092-6093.

2.   Wilson, S. T.; Lok, B. M.; Messina, C. A.; Cannan, T. R.; Flanigen, E. M., Aluminophosphate Molecular Sieves: A New Class of Microporous Crystalline Inorganic Solids. *Journal of the American Chemical Society* **1982**, 1146-1147.

3.   Sun, Q. M.; Xie, Z. K.; Yu, J. H., The State-of-the-Art Synthetic Strategies for Sapo-34 Zeolite Catalysts in Methanol-to-Olefin Conversion. *National Science Review* **2018**, *5*, 542-558.

4.   Gogate, M. R., Methanol-to-Olefins Process Technology: Current Status and Future Prospects. *Petrol Sci Technol* **2019**, *37*, 559-565.

5.   Van Speybroeck, V.; De Wispelaere, K.; Van der Mynsbrugge, J.; Vandichel, M.; Hemelsoet, K.; Waroquier, M., First Principle Chemical Kinetics in Zeolites: The Methanol-to-Olefin Process as a Case Study. *Chem Soc Rev* **2014**, *43*, 7326-7357.

6.   Yarulina, I.; Chowdhury, A. D.; Meirer, F.; Weckhuysen, B. M.; Gascon, J., Recent Trends and Fundamental Insights in the Methanol-to-Hydrocarbons Process. *Nature Catalysis* **2018**, *1*, 398-411.

7.   Chen, J. S.; Wright, P. A.; Thomas, J. M.; Natarajan, S.; Marchese, L.; Bradley, S. M.; Sankar, G.; Catlow, C. R. A.; Gaiboyes, P. L.; Townsend, R. P.; Lok C. M., Sapo-18 Catalysts and Their Bronsted Acid Sites. *J Phys Chem-Us* **1994**, *98*, 10216-10224.

8.   Smith, L.; Cheetham, A. K.; Marchese, L.; Thomas, J. M.; Wright, P. A.; Chen, J.; Gianotti, E., A Quantitative Description of the Active Sites in the Dehydrated Acid Catalyst Hsapo-34 for the Conversion of Methanol to Olefins. *Catalysis Letters* **1996**, *41*, 13-16.

9.   Wragg, D. S.; Akporiaye, D.; Fjellvag, H., Direct Observation of Catalyst Behaviour under Real Working Conditions with X-Ray Diffraction: Comparing Sapo-18 and Sapo-34 Methanol to Olefin Catalysts. *J Catal* **2011**, *279*, 397-402.

10.   Epelde, E.; Ibáñez, M.; Valecillos, J.; Aguayo, A. T.; Gayubo, A. G.; Bilbao, J.; Castaño, P., Sapo-18 and Sapo-34 Catalysts for Propylene Production from the Oligomerization-Cracking of Ethylene or 1-Butene. *Applied Catalysis A: General* **2017**, *547*, 176-182.

11.   del Campo, A. E. S.; Gayubo, A. G.; Aguayo, A. T.; Tarrio, A.; Bilbao, J., Acidity, Surface Species, and Mechanism of Methanol Transformation into Olefins on a Sapo-34. *Industrial & Engineering Chemistry Research* **1998**, *37*, 2336-2340.

12.   Miller, S. J.; Lacheen, H. S.; Chen, C.-Y., Determining the Strength of Brønsted Acid Sites for Hydrodewaxing over Shape-Selective Catalysts. *Industrial & Engineering Chemistry Research* **2016**, *55*, 6760-6767.

13.   Hartmann, M.; Kevan, L., Transition-Metal Ions in Aluminophosphate and Silicoaluminophosphate Molecular Sieves: Location, Interaction with Adsorbates and Catalytic Properties. *Chem Rev* **1999**, *99*, 635-664.

14.   Potter, M. E.; Paterson, A. J.; Raja, R., Transition Metal Versus Heavy Metal Synergy in Selective Catalytic Oxidations. *Acs Catalysis* **2012**, *2*, 2446-2451.

15.   Raja, R.; Potter, M. E.; Newland, S. H., Predictive Design of Engineered Multifunctional Solid Catalysts. *Chem Commun (Camb)* **2014**, *50*, 5940-5957.

16.   Gianotti, E.; Manzoli, M.; Potter, M. E.; Shetti, V. N.; Sun, D.; Paterson, J.; Mezza, T. M.; Levy, A.; Raja, R., Rationalising the Role of Solid-Acid Sites in the Design of Versatile Single-Site Heterogeneous Catalysts for Targeted Acid-Catalysed Transformations. *Chemical Science* **2014**, *5*, 1810-1819.

17.   Wang, C. M.; Brogaard, R. Y.; Weckhuysen, B. M.; Norskov, J. K.; Studt, F., Reactivity Descriptor in Solid Acid Catalysis: Predicting Turnover Frequencies for Propene Methylation in Zeotypes. *J Phys Chem Lett* **2014**, *5*, 1516-1521.

18.   Saadoune, I.; Corà, F.; Catlow, C. R. A., Computational Study of the Structural and Electronic Properties of Dopant Ions in Microporous Alpos. 1. Acid Catalytic Activity of Divalent Metal Ions. *The Journal of Physical Chemistry B* **2003**, *107*, 3003-3011.

19.   Potter, M. E.; Kezina, J.; Bounds, R.; Carravetta, M.; Mezza, T. M.; Raja, R., Investigating the Role of Framework Topology and Accessible Active Sites in Silicoaluminophosphates for Modulating Acid-Catalysis. *Catalysis Science & Technology* **2018**, *8*, 5155-5164.

20.   Sastre, G.; Lewis, D. W.; Catlow, C. R. A., Modeling of Silicon Substitution in Sapo-5 and Sapo-34 Molecular Sieves. *J Phys Chem B* **1997**, *101*, 5249-5262.

21.   Jeanvoine, Y.; Angyan, J. G.; Kresse, G.; Hafner, J., Bronsted Acid Sites in Hsapo-34 and Chabazite: An Ab Initio Structural Study. *J Phys Chem B* **1998**, *102*, 5573-5580.

22.   Corà, F.; Alfredsson, M.; Barker, C. M.; Bell, R. G.; Foster, M. D.; Saadoune, I.; Simperler, A.; Catlow, C. R. A., Modeling the Framework Stability and Catalytic Activity of Pure and Transition Metal-Doped Zeotypes. *Journal of Solid State Chemistry* **2003**, *176*, 496-529.

23.   Barrer, R. M., Zeolites and Their Synthesis. *Zeolites* **1981**, *1*, 130-140.

24.   Shah, R.; Gale, J. D.; Payne, M. C., Comparing the Acidities of Zeolites and Sapos from First Principles. *Chemical Communications* **1997**, 131-132.

25.   Potter, M. E.; O'Malley, A. J.; Chapman, S.; Kezina, J.; Newland, S. H.; Silverwood, I. P.; Mukhopadhyay, S.; Carravetta, M.; Mezza, T. M.; Parker, S. F.; Catlow, C. R. A.; Raja, R., Understanding the Role of Molecular Diffusion and Catalytic Selectivity in Liquid-Phase Beckmann Rearrangement. *Acs Catalysis* **2017**, *7*, 2926-2934.

26.   Sutrisno, A.; Lucier, B. E. G.; Zhang, L.; Ding, L.; Chu, Y.; Zheng, A.; Huang, Y., Inspecting the Structure and Formation of Molecular Sieve Sapo-34 Via 17o Solid-State Nmr Spectroscopy. *The Journal of Physical Chemistry C* **2018**, *122*, 7260-7277.

27.   Ahn, S. H.; Lee, H.; Hong, S. B., Crystallization Mechanism of Cage-Based, Small-Pore Molecular Sieves: A Case Study of Cha and Lev Structures. *Chemistry of Materials* **2017**, *29*, 5583-5590.

28.   Zhang, L.; Bates, J.; Chen, D.; Nie, H.-Y.; Huang, Y., Investigations of Formation of Molecular Sieve Sapo-34. *The Journal of Physical Chemistry C* **2011**, *115*, 22309-22319.

29.   Lee, S.; Jo, C.; Park, H.; Kim, J.; Ryoo, R., Sulfonium-Based Organic Structure-Directing Agents for Microporous Aluminophosphate Synthesis. *Microporous and Mesoporous Materials* **2019**, *280*, 75-81.

30.   Yu, Y.; Qin, J.; Xiao, M.; Wang, S.; Han, D.; Meng, Y., Performance Enhanced Sapo-34 Catalyst for Methanol to Olefins: Template Synthesis Using a Co2-Based Polyurea. *Catalysts* **2018**, *9*, 16.

31.   Fan, D.; Barrier, N.; Vicente, A.; Gilson, J.-P.; Clevers, S.; Dupray, V.; Coquerel, G.; Valtchev, V., Organic Template-Free Synthesis of an Open Framework Silicoaluminophosphate (Sapo) with High Thermal Stability and High Ionic Conductivity. *Inorganic Chemistry Frontiers* **2020**, *7*, 542-553.

32.   Park, S. H.; Choi, W.; Choi, H. J.; Hong, S. B., Organic-Free Synthesis of Silicoaluminophosphate Molecular Sieves. *Angew Chem Int Ed Engl* **2018**, *57*, 9413-9418.

33.   Seo, S.; Ahn, N. H.; Lee, J. H.; Knight, L. M.; Moscoso, J. G.; Sinkler, W. A.; Prabhakar, S.; Nicholas, C. P.; Hong, S. B.; Lewis, G. J., Combined Alkali-Organoammonium Structure Direction of High-Charge-Density Heteroatom-Containing Aluminophosphate Molecular Sieves. *Angew Chem Int Ed Engl* **2019**, *58*, 9032-9037.

34.   Lewis, D. W.; Willock, D. J.; Catlow, C. R. A.; Thomas, J. M.; Hutchings, G. J., De Novo Design of Structure-Directing Agents for the Synthesis of Microporous Solids. *Nature* **1996**, *382*, 604-606.

35.   Yan, N.; Wang, L.; Liu, X.; Wu, P.; Sun, T.; Xu, S.; Han, J.; Guo, P.; Tian, P.; Liu, Z., A Novel Approach for Facilitating the Targeted Synthesis of Silicoaluminophosphates. *Journal of Materials Chemistry A* **2018**, *6*, 24186-24193.

36.   Nicholson, D. G.; Nilsen, M. H., An X-Ray Absorption Spectroscopic Study on the Local Environment of Copper in Cuapo-5. *Journal of Materials Chemistry* **2000**, *10*, 1965-1971.

37.   Martens, J. A.; Janssens, C.; Grobet, P. J.; Beyer, H. K.; Jacobs, P. A., Isomorphic Substitution of Silicon in Sapo-37. *Stud Surf Sci Catal* **1989**, *49*, 215-225.

38.   Ojo, A. F.; Dwyer, J.; Dewing, J.; Karim, K., Synthesis and Properties of Sapo-37. *J Chem Soc Faraday T* **1991**, *87*, 2679-2684.

39.   Xu, X. T.; Zhai, J. P.; Chen, Y. P.; Li, I. L.; Ruan, S. C.; Tang, Z. K., Synthesis of Large Optically Clear Sapo-47 Single Crystals Using N-Propylamine as Template. *Journal of Crystal Growth* **2015**, *426*, 123-128.

40.   Hernández-Maldonado, A. J.; Yang, R. T.; Chinn, D.; Munson, C. L., Partially Calcined Gismondine Type Silicoaluminophosphate Sapo-43: Isopropylamine Elimination and Separation of Carbon Dioxide, Hydrogen Sulfide, and Water. *Langmuir* **2003**, *19*, 2193-2200.

41.   Yan, N.; Xu, H.; Zhang, W.; Sun, T.; Guo, P.; Tian, P.; Liu, Z., Probing Locations of Organic Structure-Directing Agents (Osdas) and Host-Guest Interactions in Cha -Type Sapo-34/44. *Microporous and Mesoporous Materials* **2018**, *264*, 55-59.

42.   Dumitriu, E.; Lutic, D.; Hulea, V.; Dorohoi, D.; Azzouz, A.; Colnay, E.; Kappenstein, C., Synthesis Optimization of Chabasite-Like Sapo-47 in the Presence of Sec-Butylamine. *Microporous and Mesoporous Materials* **1999**, *31*, 187-193.

43.   Wang, L. J.; Guo, C. W.; Yan, S. R.; Huang, X. D.; Li, Q. Z., High-Silica Sapo-5 with Preferred Orientation: Synthesis, Characterization and Catalytic Applications. *Microporous and Mesoporous Materials* **2003**, *64*, 63-68.

44.   Venkatathri, N., Srivastava, R., Synthesis, Characterization and Catalytic Properties of Sapo-11, -31 and -41 Molecular Sieves. *Studies in Surface Science and Catalysis* **2004**, *154*, 978-984.

45.   Liu, G.; Tian, P.; Li, J.; Zhang, D.; Zhou, F.; Liu, Z., Synthesis, Characterization and Catalytic Properties of Sapo-34 Synthesized Using Diethylamine as a Template. *Microporous and Mesoporous Materials* **2008**, *111*, 143-149.

46.   Álvaro-Muñoz, T.; Márquez-Álvarez, C.; Sastre, E., Use of Different Templates on Sapo-34 Synthesis: Effect on the Acidity and Catalytic Activity in the Mto Reaction. *Catalysis Today* **2012**, *179*, 27-34.

47.   Xu, X. T.; Zhai, J. P.; Li, I. L.; Tang, J. N.; Ruan, S. C., Synthesis of Large Single Crystals of Sapo-47 in the Presence of Diethylamine Using Two-Step Temperature Process. *Microporous and Mesoporous Materials* **2012**, *148*, 122-130.

48.   Zamadics, M.; Kevan, L., Electron-Spin-Resonance and Electron-Spin Echo Studies of Cu(Ii) Ion Location and Coordination Geometry in Na-Sapo-42, K-Sapo-42, and Rb-Sapo-42. *J Phys Chem-Us* **1992**, *96*, 10411-10418.

49.   Xiao, T. C.; An, L. D.; Wang, H. L., Dependence of the Nature and Catalytic Performance on the Synthesis Factors of Sapo-5 Molecular-Sieve. *Appl Catal a-Gen* **1995**, *130*, 187-194.

50.   Prakash, A. M.; Unnikrishnan, S., Synthesis of Sapo-34: High Silicon Incorporation in the Presence of Morpholine as Template. *Journal of the Chemical Society, Faraday Transactions* **1994**, *90*, 2291-2296.

51.   Li, N.; Ma, Y.; Kong, W.; Guan, N.; Xiang, S., The Competition of Organic Amines and the Phosphorus Source on Directing the Formation of Aluminophosphate-Based Molecular Sieves with Chabazite Structure. *Microporous and Mesoporous Materials* **2008**, *115*, 356-363.

52.   Dumitriu, E.; Azzouz, A.; Hulea, V.; Lutic, D.; Kessler, H., Synthesis, Characterization and Catalytic Activity of Sapo-34 Obtained with Piperidine as Templating Agent. *Microporous Mater* **1997**, *10*, 1-12.

53.   Pluth, J. J.; Smith, J. V., Silicoaluminophosphate with Encapsulated Methylbutylamine Species - Chabazite Structure, Charge Coupling between Framework and Inferred Ammonium Species, and Severe Molecular Disorder. *J Phys Chem-Us* **1989**, *93*, 6516-6520.

54.   Ahn, N. H.; Seo, S.; Hong, S. B., Small-Pore Molecular Sieves Sapo-57 and Sapo-59: Synthesis, Characterization, and Catalytic Properties in Methanol-to-Olefins Conversion. *Catalysis Science & Technology* **2016**, *6*, 2725-2734.

55.   Broach, R. W.; Greenlay, N.; Jakubczak, P.; Knight, L. M.; Miller, S. R.; Mowat, J. P. S.; Stanczyk, J.; Lewis, G. J., New Abc-6 Net Molecular Sieves Znapo-57 and Znapo-59: Framework Charge Density-Induced Transition from Two- to Three-Dimensional Porosity. *Microporous and Mesoporous Materials* **2014**, *189*, 49-63.

56.   Wang, D.; Tian, P.; Fan, D.; Yang, M.; Gao, B.; Qiao, Y.; Wang, C.; Liu, Z., N-Methyldiethanolamine: A Multifunctional Structure-Directing Agent for the Synthesis of Sapo and Alpo Molecular Sieves. *J Colloid Interface Sci* **2015**, *445*, 119-126.

57.   Yang, J.; Kikhtyanin, O. V.; Wu, W.; Zhou, Y.; Toktarev, A. V.; Echevsky, G. V.; Zhang, R., Influence of the Template on the Properties of Sapo-31 and Performance of Pd-Loaded Catalysts for N-Paraffin Isomerization. *Microporous and Mesoporous Materials* **2012**, *150*, 14-24.

58.   Sinha, A. K.; Hegde, S. G.; Jacob, N. E.; Sivasanker, S., Preparation and Characterization of the Silicoaluminophosphate Sapo-39. *Zeolites* **1997**, *18*, 350-355.

59.   Meriaudeau, P.; Tuan, V. A.; Nghiem, V. T.; Lai, S. Y.; Hung, L. N.; Naccache, C., Sapo-11, Sapo-31, and Sapo-41 Molecular Sieves: Synthesis, Characterization, and Catalytic Properties in N-Octane Hydroisomerization. *J Catal* **1997**, *169*, 55-66.

60.   Kong, W.; Dai, W.; Li, N.; Guan, N.; Xiang, S., A One-Step Route to Sapo-46 Using H3po3-Containing Gel and Its Application as the Catalyst for Methanol Dehydration. *Journal of Molecular Catalysis A: Chemical* **2009**, *308*, 127-133.

61.   Sinha, A. K.; Sainkar, S.; Sivasanker, S., An Improved Method for the Synthesis of the Silicoaluminophosphate Molecular Sieves, Sapo-5, Sapo-11 and Sapo-31. *Microporous and Mesoporous Materials* **1999**, *31*, 321-331.

62.   Gao, Q. M.; Chen, J. S.; Li, S. G.; Xu, R. R., Synthesis and Characterization of Aluminophosphate Molecular Sieve Alpo4-41 from Alcohol Systems. *Microporous Mater* **1996**, *7*, 219-223.

63.   Zhang, L.; Yao, J.; Zeng, C.; Xu, N., Combinatorial Synthesis of Sapo-34 Via Vapor-Phase Transport. *Chem Commun (Camb)* **2003**, 2232-2233.

64.   Lee, C. W.; Chen, X. H.; Kevan, L., Electron-Spin-Resonance and Electron-Spin Echo Modulation Studies of Cupric Ion Location and Adsorbate Interactions in the Cu2+-Exchanged H-Sapo-11 Molecular-Sieve. *J Phys Chem-Us* **1991**, *95*, 8626-8632.

65.   Djieugoue, M.-A.; Prakash, A. M.; Zhu, Z.; Kevan, L., Electron Spin Resonance and Electron Spin Echo Modulation Studies of Ion-Exchanged Nih−Sapo-17 and Nih−Sapo-35 Molecular Sieves: Comparison with Ion-Exchanged Nih−Sapo-34 Molecular Sieve. *The Journal of Physical Chemistry B* **1999**, *103*, 7277-7286.

66.   Ashtekar, S.; Chilukuri, S. V. V.; Chakrabarty, D. K., Small-Pore Molecular-Sieves Sapo-34 and Sapo-44 with Chabazite Structure - a Study of Silicon Incorporation. *J Phys Chem-Us* **1994**, *98*, 4878-4883.

67.   Lohse, U.; Vogt, F.; Richtermendau, J., Synthesis and Characterization of the Levyne-Like Structure Sapo-35 Prepared with Cyclohexylamine as Templating Agent. *Cryst Res Technol* **1993**, *28*, 1101-1107.

68.   Suresh, S.; Reddy, I. A. K.; Venkatathri, N., Synthesis of Sapo-16 Molecular Sieve in Non-Aqueous Medium by Microwave Method Using Hexamethyleneimine as a Template. *Microporous and Mesoporous Materials* **2018**, *263*, 275-281.

69.   Venkatathri, N.; Hegde, S. G.; Rajamohanan, P. R.; Sivasanker, S., Synthesis of Sapo-35 in Non-Aqueous Gels. *J Chem Soc Faraday T* **1997**, *93*, 3411-3415.

70.   Yang, M.; Tian, P.; Liu, L.; Wang, C.; Xu, S.; He, Y.; Liu, Z., Cationic Surfactant-Assisted Hydrothermal Synthesis: An Effective Way to Tune the Crystalline Phase and Morphology of Sapo Molecular Sieves. *CrystEngComm* **2015**, *17*, 8555-8561.

71.   Wang, Y.; Chen, S.-L.; Jiang, Y.-J.; Cao, Y.-Q.; Chen, F.; Chang, W.-K.; Gao, Y.-L., Influence of Template Content on Selective Synthesis of Sapo-18, Sapo-18/34 Intergrowth and Sapo-34 Molecular Sieves Used for Methanol-to-Olefins Process. *RSC Advances* **2016**, *6*, 104985-104994.

72.   Song, X.; Bai, X.; Wu, W.; Kikhtyanin, O. V.; Zhao, A.; Xiao, L.; Su, X.; Zhang, J.; Wei, X., The Effect of Palladium Loading on the Catalytic Performance of Pd/Sapo-11 for N -Decane Hydroisomerization. *Molecular Catalysis* **2017**, *433*, 84-90.

73.   Wei, X.; Kikhtyanin, O. V.; Parmon, V. N.; Wu, W.; Bai, X.; Zhang, J.; Xiao, L.; Su, X.; Zhang, Y., Synergetic Effect between the Metal and Acid Sites of Pd/Sapo-41 Bifunctional Catalysts in N-Hexadecane Hydroisomerization. *Journal of Porous Materials* **2017**, *25*, 235-247.

74.   Hu, Y. F.; Wang, X. S.; Li, S. L.; Guo, X. W.; Sun, H. B., Effect of the Template on Synthesis of Sapo-11 for Hydroisomerization of N-Octane. *React Kinet Catal L* **2005**, *86*, 45-50.

75.   Martínez-Franco, R.; Li, Z.; Martínez-Triguero, J.; Moliner, M.; Corma, A., Improving the Catalytic Performance of Sapo-18 for the Methanol-to-Olefins (Mto) Reaction by Controlling the Si Distribution and Crystal Size. *Catalysis Science & Technology* **2016**, *6*, 2796-2806.

76.   Yoon, J. W.; Jhung, S. H.; Kim, Y. H.; Park, S. E.; Chang, J. S., Selective Crystallization of Sapo-5 and Sapo-34 Molecular Sieves in Alkaline Condition: Effect of Heating Method. *B Korean Chem Soc* **2005**, *26*, 558-562.

77.   Cheung, O.; Liu, Q.; Bacsik, Z.; Hedin, N., Silicoaluminophosphates as Co2 Sorbents. *Microporous and Mesoporous Materials* **2012**, *156*, 90-96.

78.   Pinilla-Herrero, I.; Olsbye, U.; Márquez-Álvarez, C.; Sastre, E., Effect of Framework Topology of Sapo Catalysts on Selectivity and Deactivation Profile in the Methanol-to-Olefins Reaction. *J Catal* **2017**, *352*, 191-207.

79.   Dumont, N.; Gabelica, Z.; Derouane, E. G.; Direnzo, Comparative Investigation of Different Synthesis Procedures Leading to Sapo-40. *Microporous Mater* **1994**, *3*, 71-84.

80.   Maghsoudi, H.; Soltanieh, M., Simultaneous Separation of H 2 S and Co 2 from Ch 4 by a High Silica Cha-Type Zeolite Membrane. *Journal of Membrane Science* **2014**, *470*, 159-165.

81.   Martínez-Franco, R.; Cantín, Á.; Vidal-Moya, A.; Moliner, M.; Corma, A., Self-Assembled Aromatic Molecules as Efficient Organic Structure Directing Agents to Synthesize the Silicoaluminophosphate Sapo-42 with Isolated Si Species. *Chemistry of Materials* **2015**, *27*, 2981-2989.

82.   Bakhtiar, S. u. H.; Ali, S.; Dong, Y.; Wang, X.; Yuan, F.; Li, Z.; Zhu, Y., Selective Synthesis of the Sapo-5 and Sapo-34 Mixed Phases by Controlling Si/Al Ratio and Their Excellent Catalytic Methanol to Olefins Performance. *Journal of Porous Materials* **2018**, *25*, 1455-1461.

83.   Lu, H.; Duan, W.; Zhao, X., Seed-Assisted Grinding Synthesis of Sapo-34 Catalyst and Its Prolonged Catalytic Lifetime in the Conversion of Methanol to Olefins. *Reaction Kinetics, Mechanisms and Catalysis* **2019**, *128*, 1029-1042.

84.   Lyu, M.; Yang, C.; Liu, Z.; Wang, T.; Liu, H.; Chen, X.; Sun, Y., Atmospheric Pressure Synthesis of Nano-Scale Sapo-34 Catalysts for Effective Conversion of Methanol to Light Olefins. *Sustainable Energy & Fuels* **2019**, *3*, 3101-3108.

85.   Wu, P.; Yang, M.; Sun, L.; Zeng, S.; Xu, S.; Tian, P.; Liu, Z., Synthesis of Nanosized Sapo-34 with the Assistance of Bifunctional Amine and Seeds. *Chem Commun (Camb)* **2018**, *54*, 11160-11163.

86.   Zhang, Y.; Ren, Z.; Wang, Y.; Deng, Y.; Li, J., Synthesis of Small-Sized Sapo-34 Crystals with Varying Template Combinations for the Conversion of Methanol to Olefins. *Catalysts* **2018**, *8*, 570.

87.   Doan, T.; Nguyen, K.; Dam, P.; Vuong, T. H.; Le, M. T.; Thanh, H. P., Synthesis of Sapo-34 Using Different Combinations of Organic Structure-Directing Agents. *Journal of Chemistry* **2019**, *2019*, 6197527.

88.   Yue, T.; Liu, W.; Li, L.; Zhao, X.; Zhu, K.; Zhou, X.; Yang, W., Crystallization of Ato Silicoaluminophosphates Nanocrystalline Spheroids Using a Phase-Transfer Synthetic Strategy for N-Heptane Hydroisomerization. *J Catal* **2018**, *364*, 308-327.

89.   Ma, M.; Zhao, X.; Wang, X.; Gong, F.; Yuan, F.; Li, Z.; Zhu, Y., Synthesis of Small-Sized Sapo-34 Assisted by Pluronic F127 Nonionic Surfactant and Its Catalytic Performance for Methanol to Olefins (Mto). *Catalysis Communications* **2020**, *133*, 105839.

90.   Luo, M.; Wang, D.; Fu, Y.; Mao, G.; Wang, B., Three-Stage Crystallization: An Effective Way to Reduce the Crystal Size and Improve the Catalytic Performance of Sapo-34 for Mto. *European Journal of Inorganic Chemistry* **2018**, *2018*, 3491-3495.

91.   Shalmani, F. M.; Askari, S.; Halladj, R., Microwave Synthesis of Sapo Molecular Sieves. *Reviews in Chemical Engineering* **2013**, *29*, 99-122.

92.   Jhung, S. H.; Chang, J.-S.; Hwang, J. S.; Park, S.-E., Selective Formation of Sapo-5 and Sapo-34 Molecular Sieves with Microwave Irradiation and Hydrothermal Heating. *Microporous and Mesoporous Materials* **2003**, *64*, 33-39.

93.   Venna, S. R.; Carreon, M. A., Microwave Assisted Phase Transformation of Silicoaluminophosphate Zeolite Crystals. *Journal of Materials Chemistry* **2009**, *19*, 3138-3140.

94.   Bértolo, R.; Silva, J. M.; Ribeiro, M. F.; Martins, A.; Fernandes, A., Microwave Synthesis of Sapo-11 Materials for Long Chain N -Alkanes Hydroisomerization: Effect of Physical Parameters and Chemical Gel Composition. *Applied Catalysis A: General* **2017**, *542*, 28-37.

95.   Yang, S.-T.; Kim, J.-Y.; Chae, H.-J.; Kim, M.; Jeong, S.-Y.; Ahn, W.-S., Microwave Synthesis of Mesoporous Sapo-34 with a Hierarchical Pore Structure. *Materials Research Bulletin* **2012**, *47*, 3888-3892.

96.   Chew, T. L.; Ahmad, A. L.; Bhatia, S., Rapid Synthesis of Thin Sapo-34 Membranes Using Microwave Heating. *Journal of Porous Materials* **2010**, *18*, 355-360.

97.   Gharibeh, M.; Tompsett, G. A.; Conner, W. C.; Yngvesson, K. S., Microwave Synthesis of Sapo-11 and Alpo-11: Aspects of Reactor Engineering. *Chemphyschem* **2008**, *9*, 2580-2591.

98.   Dang, T. T. H.; Hoang, D.-L.; Schneider, M.; Hunger, M.; Martin, A., Impact of Conventional and Microwave Heating on Sapo-5 Formation and Brønsted Acidic Properties. *Zeitschrift für anorganische und allgemeine Chemie* **2014**, *640*, 1576-1584.

99.   Álvaro-Muñoz, T.; Sastre, E.; Márquez-Álvarez, C., Microwave-Assisted Synthesis of Plate-Like Sapo-34 Nanocrystals with Increased Catalyst Lifetime in the Methanol-to-Olefin Reaction. *Catal. Sci. Technol.* **2014**, *4*, 4330-4339.

100.   Gharibeh, M.; Tompsett, G. A.; Conner, W. C., Microwave Reaction Enhancement: The Rapid Synthesis of Sapo-11 Molecular Sieves. *Topics in Catalysis* **2008**, *49*, 157-166.

101.   Shalmani, F. M.; Halladj, R.; Askari, S., Effect of Contributing Factors on Microwave-Assisted Hydrothermal Synthesis of Nanosized Sapo-34 Molecular Sieves. *Powder Technology* **2012**, *221*, 395-402.

102.   Bonaccorsi, L.; Calabrese, L.; Freni, A.; Proverbio, E., Hydrothermal and Microwave Synthesis of Sapo (Cha) Zeolites on Aluminium Foams for Heat Pumping Applications. *Microporous and Mesoporous Materials* **2013**, *167*, 30-37.

103.   Ng, E.-P.; Awala, H.; Komaty, S.; Mintova, S., Microwave-Green Synthesis of Alpo-N and Sapo-N (N = 5 and 18) Nanosized Crystals and Their Assembly in Layers. *Microporous and Mesoporous Materials* **2019**, *280*, 256-263.

104.   Cooper, E. R.; Andrews, C. D.; Wheatley, P. S.; Webb, P. B.; Wormald, P.; Morris, R. E., Ionic Liquids and Eutectic Mixtures as Solvent and Template in Synthesis of Zeolite Analogues. *Nature* **2004**, *430*, 1012-1016.

105.   Xu, Y. P.; Tian, Z. J.; Wang, S. J.; Hu, Y.; Wang, L.; Wang, B. C.; Ma, Y. C.; Hou, L.; Yu, J. Y.; Lin, L. W., Microwave-Enhanced Ionothermal Synthesis of Aluminophosphate Molecular Sieves. *Angew Chem Int Ed Engl* **2006**, *45*, 3965-3970.

106.   Feng, J.; Guo, L.; Wang, Z.; Wang, B.; Wang, J.; Lu, T.; Xu, J.; Zhan, Y.; Rawal, A.; Zhao, C.; Han, L., Effect of Ionothermal Synthesis on the Acidity and Catalytic Performance of a Sapo-5 Molecular Sieve. *ChemistrySelect* **2019**, *4*, 10520-10524.

107.   Sánchez-Sánchez, M.; Romero, Á. A.; Pinilla-Herrero, I.; Sastre, E., Ionothermal Preparation of Triclinic Sapo-34 and Its Catalytic Performance in the Mto Process. *Catalysis Today* **2017**, *296*, 239-246.

108.   Azim, M. M.; Stark, A., The First Systematic Study on the Conditions Affecting the Ionothermal Synthesis of Silicoaluminophosphates. *ChemistrySelect* **2018**, *3*, 12495-12503.

109.   Cai, R.; Sun, M.; Chen, Z.; Munoz, R.; O'Neill, C.; Beving, D. E.; Yan, Y., Ionothermal Synthesis of Oriented Zeolite Ael Films and Their Application as Corrosion-Resistant Coatings. *Angew Chem Int Ed Engl* **2008**, *47*, 525-528.

110.   Lin, Y.; Wei, Y.; Zhang, L.; Guo, K.; Wang, M.; Huang, P.; Meng, X.; Zhang, R., Facile Ionothermal Synthesis of Sapo-Lta Zeotypes with High Structural Stability and Their Catalytic Performance in Mto Reaction. *Microporous and Mesoporous Materials* **2019**, *288*, 109611.

111.   Azim, M. M.; Mohsin, U., An Efficient Method for the Ionothermal Synthesis of the Lta Framework Type of Silicoaluminophosphates. *Chemistry Letters* **2018**, *47*, 1029-1031.

112.   Almeida, G.; Variani, Y. M.; Gómez-Hortigüela, L.; Rivas Mercury, J. M.; Rojas, A., Performance of Three Different Cations Based on Imidazolium Ring as Structure Directing Agents in the Synthesis of Aluminophosphates and Silicoaluminophosphates Microporous Materials. *Microporous and Mesoporous Materials* **2020**, *294*, 109861.

113.   Zhao, X.; Wang, H.; Kang, C.; Sun, Z.; Li, G.; Wang, X., Ionothermal Synthesis of Mesoporous Sapo-5 Molecular Sieves by Microwave Heating and Using Eutectic Solvent as Structure-Directing Agent. *Microporous and Mesoporous Materials* **2012**, *151*, 501-505.

114.   Zhao, X.; Wen, J.; Zhao, J.; Li, A.; Li, G.; Wang, X., Hierarchically Structured Sapo-5 Molecular Sieve Catalysts with Tailored Mesoporosity for Alkylation Reaction. *Journal of Porous Materials* **2015**, *22*, 577-584.

115.   Rimaz, S.; Halladj, R.; Askari, S., Synthesis of Hierarchal Sapo-34 Nano Catalyst with Dry Gel Conversion Method in the Presence of Carbon Nanotubes as a Hard Template. *J Colloid Interface Sci* **2016**, *464*, 137-46.

116.   Zheng, J.; Zhang, W.; Liu, Z.; Huo, Q.; Zhu, K.; Zhou, X.; Yuan, W., Unraveling the Non-Classic Crystallization of Sapo-34 in a Dry Gel System Towards Controlling Meso-

Structure with the Assistance of Growth Inhibitor: Growth Mechanism, Hierarchical Structure Control and Catalytic Properties. *Microporous and Mesoporous Materials* **2016**, *225*, 74-87.

117. Lyu, Y.; Liu, Y.; He, X.; Xu, L.; Liu, X.; Yan, Z., The Regulation of Si Distribution and Surface Acidity of Sapo-11 Molecular Sieve. *Applied Surface Science* **2018**, *453*, 350-357.

118. Jin, Y.; Sun, Q.; Qi, G.; Yang, C.; Xu, J.; Chen, F.; Meng, X.; Deng, F.; Xiao, F. S., Solvent-Free Synthesis of Silicoaluminophosphate Zeolites. *Angew Chem Int Ed Engl* **2013**, *52*, 9172-9175.

119. Du, Y.; Feng, B.; Jiang, Y.; Yuan, L.; Huang, K.; Li, J., Solvent-Free Synthesis and N-Hexadecane Hydroisomerization Performance of Sapo-11 Catalyst. *European Journal of Inorganic Chemistry* **2018**, *2018*, 2599-2606.

120. Liu, Y.; Lyu, Y.; Zhao, X.; Xu, L.; Mintova, S.; Yan, Z.; Liu, X., Silicoaluminophosphate-11 (Sapo-11) Molecular Sieves Synthesized Via a Grinding Synthesis Method. *Chem Commun (Camb)* **2018**, *54*, 10950-10953.

121. Askari, S.; Halladj, R., Effects of Ultrasound-Related Variables on Sonochemically Synthesized Sapo-34 Nanoparticles. *Journal of Solid State Chemistry* **2013**, *201*, 85-92.

122. Askari, S.; Halladj, R., Ultrasonic Pretreatment for Hydrothermal Synthesis of Sapo-34 Nanocrystals. *Ultrason Sonochem* **2012**, *19*, 554-559.

123.   Azarhoosh, M. J.; Halladj, R.; Askari, S.; Aghaeinejad-Meybodi, A., Performance Analysis of Ultrasound-Assisted Synthesized Nano-Hierarchical Sapo-34 Catalyst in the Methanol-to-Lights-Olefins Process Via Artificial Intelligence Methods. *Ultrason Sonochem* **2019**, *58*, 104646.

124.   Zhang, P.; Liu, H.; Zhu, H.; Oyama, S. T.; Bao, X., Synthesis and Catalytic Application of Alumina@Sapo-11 Composite Via the in Situ Assembly of Silicoaluminophosphate Nanoclusters at an Alumina Substrate. *Catalysis Science & Technology* **2018**, *8*, 4209-4218.

125.   Jin, W.; Ma, J.; Ma, H.; Li, X.; Wang, Y., Hydrothermal Synthesis of Core-Shell Zsm-5/Sapo-34 Composite Zeolites and Catalytic Performance in Methanol-to-Aromatics Reaction. *Journal of Solid State Chemistry* **2018**, *267*, 6-12.

126.   Wragg, D. S.; O'Brien, M. G.; Bleken, F. L.; Di Michiel, M.; Olsbye, U.; Fjellvag, H., Watching the Methanol-to-Olefin Process with Time- and Space-Resolved High-Energy Operando X-Ray Diffraction. *Angew Chem Int Ed Engl* **2012**, *51*, 7956-7959.

127.   Kalantzopoulos, G. N.; Lundvall, F.; Lind, A.; Arstad, B.; Chernyshov, D.; Fjellvåg, H.; Wragg, D. S., Sapo-37 Microporous Catalysts: Revealing the Structural Transformations During Template Removal. *Catalysis, Structure & Reactivity* **2017**, *3*, 79-88.

128.   Buragadda, V. R.; Yu, L.; Alabarse, F. G.; Haidoux, A.; Levelut, C.; van der Lee, A.; Cambon, O.; Haines, J., High Temperature and High Pressure X-Ray Diffraction Study of Sapo-

37: Effect of Chemical Composition on the Mechanical Properties of Faujasite-Type Materials. *RSC Advances* **2013**, *3*, 9911-9915.

129.   Wragg, D. S.; Johnsen, R. E.; Norby, P.; Fjellvåg, H., The Adsorption of Methanol and Water on Sapo-34: In Situ and Ex Situ X-Ray Diffraction Studies. *Microporous and Mesoporous Materials* **2010**, *134*, 210-215.

130.   Wragg, D. S.; Johnsen, R. E.; Balasundaram, M.; Norby, P.; Fjellvåg, H.; Grønvold, A.; Fuglerud, T.; Hafizovic, J.; Vistad, Ø. B.; Akporiaye, D., Sapo-34 Methanol-to-Olefin Catalysts under Working Conditions: A Combined in Situ Powder X-Ray Diffraction, Mass Spectrometry and Raman Study. *J Catal* **2009**, *268*, 290-296.

131.   Zokaie, M.; Wragg, D. S.; Grønvold, A.; Fuglerud, T.; Cavka, J. H.; Lillerud, K. P.; Swang, O., Unit Cell Expansion Upon Coke Formation in a Sapo-34 Catalyst: A Combined Experimental and Computational Study. *Microporous and Mesoporous Materials* **2013**, *165*, 1-5.

132.   Wragg, D. S.; Grønvold, A.; Voronov, A.; Norby, P.; Fjellvåg, H., Combined Xrd and Raman Studies of Coke Types Found in Sapo-34 after Methanol and Propene Conversion. *Microporous and Mesoporous Materials* **2013**, *173*, 166-174.

133.   Vistad, Ø. B.; Akporiaye, D. E.; Lillerud, K. P., Identification of a Key Precursor Phase for Synthesis of Sapo-34 and Kinetics of Formation Investigated by in Situ X-Ray Diffraction. *The Journal of Physical Chemistry B* **2001**, *105*, 12437-12447.

134. Sławiński, W. A.; Wragg, D. S.; Akporiaye, D.; Fjellvåg, H., Intergrowth Structure Modelling in Silicoaluminophosphate Sapo-18/34 Family. *Microporous and Mesoporous Materials* **2014**, *195*, 311-318.

135. Smith, R. L.; Sławiński, W. A.; Lind, A.; Wragg, D. S.; Cavka, J. H.; Arstad, B.; Fjellvåg, H.; Attfield, M. P.; Akporiaye, D.; Anderson, M. W., Nanoporous Intergrowths: How Crystal Growth Dictates Phase Composition and Hierarchical Structure in the Cha/Aei System. *Chemistry of Materials* **2015**, *27*, 4205-4215.

136. Kalantzopoulos, G. N.; Lundvall, F.; Thorshaug, K.; Lind, A.; Vajeeston, P.; Dovgaliuk, I.; Arstad, B.; Wragg, D. S.; Fjellvåg, H., Factors Determining Microporous Material Stability in Water: The Curious Case of Sapo-37. *Chemistry of Materials* **2020**, *32*, 1495-1505.

137. Lo, B. T. W.; Ye, L.; Chang, G. G. Z.; Purchase, K.; Day, S.; Tang, C. C.; Mei, D.; Tsang, S. C. E., Dynamic Modification of Pore Opening of Sapo-34 by Adsorbed Surface Methoxy Species During Induction of Catalytic Methanol-to-Olefins Reactions. *Applied Catalysis B: Environmental* **2018**, *237*, 245-250.

138. Arstad, B.; Lind, A.; Cavka, J. H.; Thorshaug, K.; Akporiaye, D.; Wragg, D.; Fjellvåg, H.; Grønvold, A.; Fuglerud, T., Structural Changes in Sapo-34 Due to Hydrothermal Treatment. A Nmr, Xrd, and Drifts Study. *Microporous and Mesoporous Materials* **2016**, *225*, 421-431.

139. Wragg, D. S.; O'Brien, M. G.; Di Michiel, M.; Lønstad-Bleken, F., Rietveld Analysis of Computed Tomography and Its Application to Methanol to Olefin Reactor Beds. *Journal of Applied Crystallography* **2015**, *48*, 1719-1728.

140. Bull, L. M.; Cheetham, A. K.; Hopkins, P. D.; Powell, B. M., A Neutron-Diffraction Study of Acid Sites in H-Sapo-37. *J Chem Soc Chem Comm* **1993**, 1196-1198.

141. Bull, L. M.; Cheetham, A. K.; Powell, B. M.; Ripmeester, J. A.; Ratcliffe, C. I., The Interaction of Sorbates with Acid Sites in Zeolite Catalysts: A Powder Neutron Diffraction and 2h Nmr Study of Benzene in H-Sapo-37. *Journal of the American Chemical Society* **1995**, *117*, 4328-4332.

142. Kalantzopoulos, G. N.; Lundvall, F.; Checchia, S.; Lind, A.; Wragg, D. S.; Fjellvag, H.; Arstad, B., In Situ Flow Mas Nmr Spectroscopy and Synchrotron Pdf Analyses of the Local Response of the Bronsted Acidic Site in Sapo-34 During Hydration at Elevated Temperatures. *Chemphyschem* **2018**, *19*, 519-528.

143. Martis, M.; Smith, A. J.; Tang, C.; Parker, J. E.; Hyde, T. I.; Watson, M. J.; Baucherel, X.; Kohara, S.; Wakihara, T.; Sankar, G., Tracking the Structural Changes in Pure and Heteroatom Substituted Aluminophosphate, Aipo-18, Using Synchrotron Based X-Ray Diffraction Techniques. *Phys Chem Chem Phys* **2013**, *15*, 11766-11774.

144. Potter, M. E.; Light, M. E.; Irving, D. J. M.; Oakley, A. E.; Chapman, S.; Chater, P.; Cutts, G.; Watts, A.; Wharmby, M.; Vandegehuchte, B. D.; Schreiber, M. W.; Raja, R., Exploring the Origins of Crystallisation Kinetics in Hierarchical Materials Using in Situ X-Ray Diffraction and Pair Distribution Function Analysis. *Phys Chem Chem Phys* **2020**, DOI: 10.1039/d0cp00670j.

145. Buchholz, A.; Wang, W.; Xu, M.; Arnold, A.; Hunger, M., Thermal Stability and Dehydroxylation of Brønsted Acid Sites in Silicoaluminophosphates H-Sapo-11, H-Sapo-18, H-Sapo-31, and H-Sapo-34 Investigated by Multi-Nuclear Solid-State Nmr Spectroscopy. *Microporous and Mesoporous Materials* **2002**, *56*, 267-278.

146. Shen, W.; Li, X.; Wei, Y.; Tian, P.; Deng, F.; Han, X.; Bao, X., A Study of the Acidity of Sapo-34 by Solid-State Nmr Spectroscopy. *Microporous and Mesoporous Materials* **2012**, *158*, 19-25.

147. Buchholz, A.; Wang, W.; Xu, M.; Arnold, A.; Hunger, M., Sequential Steps of Ammoniation of the Microporous Silicoaluminophosphates H-Sapo-34 and H-Sapo-37 Investigated by in Situ Cf Mas Nmr Spectroscopy. *The Journal of Physical Chemistry B* **2004**, *108*, 3107-3113.

148. Jung, H. J.; Shin, C. H.; Hong, S. B., Si Distribution in Silicoaluminophosphate Molecular Sieves with the Lev Topology: A Solid-State Nmr Study. *J Phys Chem B* **2005**, *109*, 20847-20853.

149.	Potter, M. E.; Chapman, S.; O'Malley, A. J.; Levy, A.; Carravetta, M.; Mezza, T. M.; Parker, S. F.; Raja, R., Understanding the Role of Designed Solid Acid Sites in the Low-Temperature Production of ϵ-Caprolactam. *ChemCatChem* **2017**, *9*, 1897-1900.

150.	Su, X.; Xu, S.; Tian, P.; Li, J.; Zheng, A.; Wang, Q.; Yang, M.; Wei, Y.; Deng, F.; Liu, Z., Investigation of the Strong Brønsted Acidity in a Novel Sapo-Type Molecular Sieve, Dnl-6. *The Journal of Physical Chemistry C* **2015**, *119*, 2589-2596.

151.	Hunger, M.; Seiler, M.; Buchholz, A., In Situ Mas Nmr Spectroscopic Investigation of the Conversion of Methanol to Olefins on Silicoaluminophosphates Sapo-34 and Sapo-18 under Continuous Flow Conditions. *Catalysis Letters* **2001**, *74*, 61-68.

152.	Dai, W.; Wang, C.; Dyballa, M.; Wu, G.; Guan, N.; Li, L.; Xie, Z.; Hunger, M., Understanding the Early Stages of the Methanol-to-Olefin Conversion on H-Sapo-34. *ACS Catalysis* **2014**, *5*, 317-326.

153.	Chen, T.-H.; Wouters, B. H.; Grobet, P. J., Enhanced Resolution of Aluminum and Proton Sites in the Molecular Sieve Sapo-37 By27al Multiple Quantum Magic Angle Spinning And1h Spin Echo Editing Nmr. *The Journal of Physical Chemistry B* **1999**, *103*, 6179-6184.

154.	Miletto, I.; Ivaldi, C.; Paul, G.; Chapman, S.; Marchese, L.; Raja, R.; Gianotti, E., Hierarchical Sapo-34 Architectures with Tailored Acid Sites Using Sustainable Sugar Templates. *ChemistryOpen* **2018**, *7*, 297-301.

155.   Tian, P.; Li, B.; Xu, S.; Su, X.; Wang, D.; Zhang, L.; Fan, D.; Qi, Y.; Liu, Z., Investigation of the Crystallization Process of Sapo-35 and Si Distribution in the Crystals. *The Journal of Physical Chemistry C* **2013**, *117*, 4048-4056.

156.   Akolekar, D.; Bhargava, S.; Gorman, J.; Paterson, P., Formation of Small Pore Sapo-44 Type Molecular Sieve. *Colloids and Surfaces A: Physicochemical and Engineering Aspects* **1999**, *146*, 375-386.

157.   Zhang, L.; Huang, Y., New Insights into Formation of Molecular Sieve Sapo-34 for Mto Reactions. *The Journal of Physical Chemistry C* **2016**, *120*, 25945-25957.

158.   Tan, J.; Liu, Z.; Bao, X.; Liu, X.; Han, X.; He, C.; Zhai, R., Crystallization and Si Incorporation Mechanisms of Sapo-34. *Microporous and Mesoporous Materials* **2002**, *53*, 97-108.

159.   Vistad, Ø. B.; Hansen, E. W.; Akporiaye, D. E.; Lillerud, K. P., Multinuclear Nmr Analysis of Sapo-34 Gels in the Presence and Absence of Hf: The Initial Gel. *The Journal of Physical Chemistry A* **1999**, *103*, 2540-2552.

160.   Yan, Z.; Chen, B.; Huang, Y., A Solid-State Nmr Study of the Formation of Molecular Sieve Sapo-34. *Solid State Nucl Magn Reson* **2009**, *35*, 49-60.

161.   Zhang, L.; Huang, Y., Crystallization and Catalytic Properties of Molecular Sieve Sapo-34 by a Vapor-Phase Transport Method. *Journal of Materials Chemistry A* **2015**, *3*, 4522-4529.

162.   Zhang, L.; Chen, D.; Nie, H.-Y.; Huang, Y., A Study of the Formation of Microporous Material Sapo-37. *Microporous and Mesoporous Materials* **2013**, *175*, 147-156.

163.   Ashbrook, S. E.; Smith, M. E., Solid State 17o Nmr-an Introduction to the Background Principles and Applications to Inorganic Materials. *Chem Soc Rev* **2006**, *35*, 718-735.

164.   Bignami, G. P. M.; Dawson, D. M.; Seymour, V. R.; Wheatley, P. S.; Morris, R. E.; Ashbrook, S. E., Synthesis, Isotopic Enrichment, and Solid-State Nmr Characterization of Zeolites Derived from the Assembly, Disassembly, Organization, Reassembly Process. *J Am Chem Soc* **2017**, *139*, 5140-5148.

165.   Vistad, Ø. B.; Akporiaye, D. E.; Taulelle, F.; Lillerud, K. P., In Situ Nmr of Sapo-34 Crystallization. *Chemistry of Materials* **2003**, *15*, 1639-1649.

166.   Peng, Q.; Wang, G.; Wang, Z.; Jiang, R.; Wang, D.; Chen, J.; Huang, J., Tuning Hydrocarbon Pool Intermediates by the Acidity of Sapo-34 Catalysts for Improving Methanol-to-Olefins Reaction. *ACS Sustainable Chemistry & Engineering* **2018**, *6*, 16867-16875.

167.   Xiao, D.; Han, X.; Bao, X.; Hou, G.; Blanc, F., Identification of Different Carbenium Ion Intermediates in Zeolites with Identical Chabazite Topology Via13c–13c through-Bond Nmr Correlations. *RSC Advances* **2019**, *9*, 12415-12418.

168.   Zhang, W.; Zhi, Y.; Huang, J.; Wu, X.; Zeng, S.; Xu, S.; Zheng, A.; Wei, Y.; Liu, Z., Methanol to Olefins Reaction Route Based on Methylcyclopentadienes as Critical Intermediates. *ACS Catalysis* **2019**, *9*, 7373-7379.

169.   Salehirad, F.; Anderson, M. W., Solid-State13c Mas Nmr Study of Methanol-to-Hydrocarbon Chemistry over H-Sapo-34. *J Catal* **1996**, *164*, 301-314.

170.   Chowdhury, A. D.; Paioni, A. L.; Houben, K.; Whiting, G. T.; Baldus, M.; Weckhuysen, B. M., Bridging the Gap between the Direct and Hydrocarbon Pool Mechanisms of the Methanol-to-Hydrocarbons Process. *Angew Chem Int Ed Engl* **2018**, *57*, 8095-8099.

171.   Chowdhury, A. D.; Houben, K.; Whiting, G. T.; Mokhtar, M.; Asiri, A. M.; Al-Thabaiti, S. A.; Basahel, S. N.; Baldus, M.; Weckhuysen, B. M., Initial Carbon-Carbon Bond Formation During the Early Stages of the Methanol-to-Olefin Process Proven by Zeolite-Trapped Acetate and Methyl Acetate. *Angew Chem Int Ed Engl* **2016**, *55*, 15840-15845.

172.   Wang, W.; Seiler, M.; Hunger, M., Role of Surface Methoxy Species in the Conversion of Methanol to Dimethyl Ether on Acidic Zeolites Investigated by in Situ Stopped-Flow Mas Nmr Spectroscopy. *The Journal of Physical Chemistry B* **2001**, *105*, 12553-12558.

173.   Wang, W.; Jiang, Y.; Hunger, M., Mechanistic Investigations of the Methanol-to-Olefin (Mto) Process on Acidic Zeolite Catalysts by in Situ Solid-State Nmr Spectroscopy. *Catalysis Today* **2006**, *113*, 102-114.

174.   Jiang, Y.; Huang, J.; Reddy Marthala, V. R.; Ooi, Y. S.; Weitkamp, J.; Hunger, M., In Situ Mas Nmr–Uv/Vis Investigation of H-Sapo-34 Catalysts Partially Coked in the Methanol-to-Olefin Conversion under Continuous-Flow Conditions and of Their Regeneration. *Microporous and Mesoporous Materials* **2007**, *105*, 132-139.

175.   Weiland, E.; Springuel-Huet, M.-A.; Nossov, A.; Gédéon, A., 129xenon Nmr: Review of Recent Insights into Porous Materials. *Microporous and Mesoporous Materials* **2016**, *225*, 41-65.

176.   Koskela, T.; Jokisaari, J.; Satyanarayana, C., Correlation of 129xe Nmr Shielding Data with the Pore Structures of Various Aluminophosphate Molecular Sieves. *Microporous and Mesoporous Materials* **2004**, *67*, 113-122.

177.   Koskela, T.; Ylihautala, M.; Jokisaari, J., Microporous Channel and Crystallite Surface Effects on Xenon Atoms as Studied by Nmr: Shielding and Exchange of Xenon in Sapo-11 and Alpo4-11 Molecular Sieves. *Microporous and Mesoporous Materials* **2001**, *46*, 99-110.

178. Gao, S.; Xu, S.; Wei, Y.; Qiao, Q.; Xu, Z.; Wu, X.; Zhang, M.; He, Y.; Xu, S.; Liu, Z., Insight into the Deactivation Mode of Methanol-to-Olefins Conversion over Sapo-34: Coke, Diffusion, and Acidic Site Accessibility. *J Catal* **2018**, *367*, 306-314.

179. Gao, S.; Xu, S.; Wei, Y.; Liu, Z.; Zheng, A.; Wu, P.; Liu, Z., Direct Probing of Heterogeneity for Adsorption and Diffusion within a Sapo-34 Crystal. *Chem Commun (Camb)* **2019**, *55*, 10693-10696.

180. Mehlhorn, D.; Valiullin, R.; Karger, J.; Cho, K.; Ryoo, R., Exploring Mass Transfer in Mesoporous Zeolites by Nmr Diffusometry. *Materials (Basel)* **2012**, *5*, 699-720.

181. Dai, W.; Scheibe, M.; Li, L.; Guan, N.; Hunger, M., Effect of the Methanol-to-Olefin Conversion on the Pfg Nmr Self-Diffusivities of Ethane and Ethene in Large-Crystalline Sapo-34. *The Journal of Physical Chemistry C* **2012**, *116*, 2469-2476.

182. Zheng, A.; Liu, S. B.; Deng, F., Acidity Characterization of Heterogeneous Catalysts by Solid-State Nmr Spectroscopy Using Probe Molecules. *Solid State Nucl Magn Reson* **2013**, *55-56*, 12-27.

183. Ishimaru, S. i.; Gotoh, K.; Ichikawa, M.; Ikeda, R., Dynamic Behavior of Acetonitrile Molecules Adsorbed in Alpo4-5 and Sapo-5 Studied by H and H Nmr. *Microporous and Mesoporous Materials* **2002**, *51*, 17-22.

184.	Brunauer, S.; Emmett, P. H.; Teller, E., Adsorption of Gases in Multimolecular Layers. *Journal of the American Chemical Society* **1938**, *60*, 309-319.

185.	Cychosz, K. A.; Thommes, M., Progress in the Physisorption Characterization of Nanoporous Gas Storage Materials. *Engineering* **2018**, *4*, 559-566.

186.	Lastoskie, C.; Gubbins, K. E.; Quirke, N., Pore Size Distribution Analysis of Microporous Carbons: A Density Functional Theory Approach. *The Journal of Physical Chemistry* **1993**, *97*, 4786-4796.

187.	Olivier, J. P.; Conklin, W. B.; Szombathely, M. v., Determination of Pore Size Distribution from Density Functional Theory: A Comparison of Nitrogen and Argon Results. *Studies in Surface Science and Catalysis* **1994**, *87*, 81-89.

188.	Barrett, E. P.; Joyner, L. G.; Halenda, P. P., The Determination of Pore Volume and Area Distributions in Porous Substances. I. Computations from Nitrogen Isotherms. *Journal of the American Chemical Society* **1951**, *73*, 373-380.

189.	Wang, P.; Lv, A.; Hu, J.; Xu, J. a.; Lu, G., The Synthesis of Sapo-34 with Mixed Template and Its Catalytic Performance for Methanol to Olefins Reaction. *Microporous and Mesoporous Materials* **2012**, *152*, 178-184.

190.   Schmidt, J. E.; Peng, L.; Paioni, A. L.; Ehren, H. L.; Guo, W.; Mazumder, B.; Matthijs de Winter, D. A.; Attila, O.; Fu, D.; Chowdhury, A. D.; Houben, K.; Baldus, M.; Poplawsky, J. D.; Weckhuysen, B. M., Isolating Clusters of Light Elements in Molecular Sieves with Atom Probe Tomography. *J Am Chem Soc* **2018**, *140*, 9154-9158.

191.   Chen, D.; Moljord, K.; Holmen, A., A Methanol to Olefins Review: Diffusion, Coke Formation and Deactivation on Sapo Type Catalysts. *Microporous and Mesoporous Materials* **2012**, *164*, 239-250.

192.   Karwacki, L.; van der Bij, H. E.; Kornatowski, J.; Cubillas, P.; Drury, M. R.; de Winter, D. A.; Anderson, M. W.; Weckhuysen, B. M., Unified Internal Architecture and Surface Barriers for Molecular Diffusion of Microporous Crystalline Aluminophosphates. *Angew Chem Int Ed Engl* **2010**, *49*, 6790-6794.

193.   Masukawa, T.; Komatsu, T.; Yashima, T., Strong Acid Sites Generated in Aluminosilicate Region of Sapo-5. *Zeolites* **1997**, *18*, 10-17.

194.   Aguayo, A. T.; Gayubo, A. G.; Vivanco, R.; Olazar, M.; Bilbao, J., Role of Acidity and Microporous Structure in Alternative Catalysts for the Transformation of Methanol into Olefins. *Applied Catalysis A: General* **2005**, *283*, 197-207.

195.   Bordiga, S.; Regli, L.; Cocina, D.; Lamberti, C.; Bjorgen, M.; Lillerud, K. P., Assessing the Acidity of High Silica Chabazite H-Ssz-13 by Ftir Using Co as Molecular Probe: Comparison with H-Sapo-34. *J Phys Chem B* **2005**, *109*, 2779-2784.

196.   Martins, G. A. V.; Berlier, G.; Coluccia, S.; Pastore, H. O.; Superti, G. B.; Gatti, G.; Marchese, L., Revisiting the Nature of the Acidity in Chabazite-Related Silicoaluminophosphates: Combined Ftir And29si Mas Nmr Study. *The Journal of Physical Chemistry C* **2007**, *111*, 330-339.

197.   Chapman, S.; O'Malley, A. J.; Miletto, I.; Carravetta, M.; Cox, P.; Gianotti, E.; Marchese, L.; Parker, S. F.; Raja, R., Integrated Theoretical and Empirical Studies for Probing Substrate-Framework Interactions in Hierarchical Catalysts. *Chemistry* **2019**, *25*, 9938-9947.

198.   Miletto, I.; Paul, G.; Chapman, S.; Gatti, G.; Marchese, L.; Raja, R.; Gianotti, E., Mesoporous Silica Scaffolds as Precursor to Drive the Formation of Hierarchical Sapo-34 with Tunable Acid Properties. *Chemistry* **2017**, *23*, 9952-9961.

199.   Halasz, I.; Moden, B.; Petushkov, A.; Liang, J.-J.; Agarwal, M., Delicate Distinction between Oh Groups on Proton-Exchanged H-Chabazite and H-Sapo-34 Molecular Sieves. *The Journal of Physical Chemistry C* **2015**, *119*, 24046-24055.

200. Potter, M. E.; Sun, D.; Gianotti, E.; Manzoli, M.; Raja, R., Investigating Site-Specific Interactions and Probing Their Role in Modifying the Acid-Strength in Framework Architectures. *Phys Chem Chem Phys* **2013**, *15*, 13288-13295.

201. Bleken, F.; Bjørgen, M.; Palumbo, L.; Bordiga, S.; Svelle, S.; Lillerud, K.-P.; Olsbye, U., The Effect of Acid Strength on the Conversion of Methanol to Olefins over Acidic Microporous Catalysts with the Cha Topology. *Topics in Catalysis* **2009**, *52*, 218-228.

202. Hemelsoet, K.; Ghysels, A.; Mores, D.; De Wispelaere, K.; Van Speybroeck, V.; Weckhuysen, B. M.; Waroquier, M., Experimental and Theoretical Ir Study of Methanol and Ethanol Conversion over H-Sapo-34. *Catalysis Today* **2011**, *177*, 12-24.

203. Usman, M.; Zhu, J.; Chuiyang, K.; Arslan, M. T.; Khan, A.; Galadima, A.; Muraza, O.; Khan, I.; Helal, A.; Al-Maythalony, B. A.; Yamani, Z. H., Propene Adsorption-Chemisorption Behaviors on H-Sapo-34 Zeolite Catalysts at Different Temperatures. *Catalysts* **2019**, *9*, 919.

204. Bordiga, S.; Lamberti, C.; Bonino, F.; Travert, A.; Thibault-Starzyk, F., Probing Zeolites by Vibrational Spectroscopies. *Chem Soc Rev* **2015**, *44*, 7262-341.

205. Potter, M. E.; Armstrong, L.-M.; Raja, R., Combining Catalysis and Computational Fluid Dynamics Towards Improved Process Design for Ethanol Dehydration. *Catalysis Science & Technology* **2018**, *8*, 6163-6172.

206.	Potter, M. E.; Cholerton, M. E.; Kezina, J.; Bounds, R.; Carravetta, M.; Manzoli, M.; Gianotti, E.; Lefenfeld, M.; Raja, R., Role of Isolated Acid Sites and Influence of Pore Diameter in the Low-Temperature Dehydration of Ethanol. *ACS Catalysis* **2014**, *4*, 4161-4169.

207.	Chapman, S.; Potter, M. E.; Raja, R., The Molecular Design of Active Sites in Nanoporous Materials for Sustainable Catalysis. *Molecules* **2017**, *22*, 2127.

208.	Yadav, R.; Singh, A. K.; Sakthivel, A., Mesoporous Silico-Aluminophosphates Derived from Microporous Precursors as Promising Catalyst for Hydroisomerization. *Catalysis Today* **2015**, *245*, 155-162.

209.	Jin, F.; Li, Y., A Ftir and Tpd Examination of the Distributive Properties of Acid Sites on Zsm-5 Zeolite with Pyridine as a Probe Molecule. *Catalysis Today* **2009**, *145*, 101-107.

210.	Fitzgerald, S. A.; Shinbrough, K.; Rigdon, K. H.; Rowsell, J. L. C.; Kapelewski, M. T.; Pang, S. H.; Lawler, K. V.; Forster, P. M., Temperature-Programmed Desorption for Isotope Separation in Nanoporous Materials. *The Journal of Physical Chemistry C* **2018**, *122*, 1995-2001.

211.	Gould, N. S.; Xu, B., Temperature-Programmed Desorption of Pyridine on Zeolites in the Presence of Liquid Solvents. *ACS Catalysis* **2018**, *8*, 8699-8708.

212. Hu, B.; Wang, D.; Gao, S.; Zhang, X.; Mao, G.; Wang, B.; Luo, M., Nh3competitive Adsorbed Ftir: A Potential Method to Investigate the Confined Species-Acidic Sites Interaction in Sapo-34 Catalyst. *ChemistrySelect* **2016**, *1*, 5493-5496.

213. Oliveira, A. C.; Essayem, N.; Tuel, A.; Clacens, J.-M.; Taarit, Y. B., Studies on Meapso-5: An Investigation of Physicochemical and Acidic Properties. *Catalysis Today* **2008**, *133-135*, 56-62.

214. Katada, N., Analysis and Interpretation of Acidic Nature of Aluminosilicates. *Molecular Catalysis* **2018**, *458*, 116-126.

215. Katada, N.; Tamagawa, H.; Niwa, M., Quantitative Analysis of Acidic Oh Groups in Zeolite by Ammonia Irms-Tpd and Dft: Application to Bea. *Catalysis Today* **2014**, *226*, 37-46.

216. Niwa, M.; Katada, N., New Method for the Temperature-Programmed Desorption (Tpd) of Ammonia Experiment for Characterization of Zeolite Acidity: A Review. *Chem Rec* **2013**, *13*, 432-455.

217. Suzuki, K.; Nishio, T.; Katada, N.; Sastre, G.; Niwa, M., Ammonia Irms-Tpd Measurements on Bronsted Acidity of Proton-Formed Sapo-34. *Phys Chem Chem Phys* **2011**, *13*, 3311-3318.

218. Sastre, G.; Lewis, D. W.; Catlow, C. R. A., Structure and Stability of Silica Species in Sapo Molecular Sieves. *The Journal of Physical Chemistry* **1996**, *100*, 6722-6730.

219. Jeanvoine, Y.; Ángyán, J. G.; Kresse, G.; Hafner, J., On the Nature of Water Interacting with Brønsted Acidic Sites. Ab Initio Molecular Dynamics Study of Hydrated Hsapo-34. *The Journal of Physical Chemistry B* **1998**, *102*, 7307-7310.

220. Termath, V.; Haase, F.; Sauer, J.; Hutter, J.; Parrinello, M., Understanding the Nature of Water Bound to Solid Acid Surfaces. Ab Initio Simulation on Hsapo-34. *Journal of the American Chemical Society* **1998**, *120*, 8512-8516.

221. Fjermestad, T.; Svelle, S.; Swang, O., Mechanism of Si Island Formation in Sapo-34. *The Journal of Physical Chemistry C* **2015**, *119*, 2086-2095.

222. Zokaie, M.; Olsbye, U.; Lillerud, K. P.; Swang, O., A Computational Study on Heteroatom Distribution in Zeotype Materials. *Microporous and Mesoporous Materials* **2012**, *158*, 175-179.

223. Zokaie, M.; Olsbye, U.; Lillerud, K. P.; Swang, O., Stabilization of Silicon Islands in Silicoaluminophosphates by Proton Redistribution. *The Journal of Physical Chemistry C* **2012**, *116*, 7255-7259.

224.   Deroche, I.; Maurin, G.; Llewellyn, P. L.; Castro, M.; Wright, P. A., Silicon Distribution in Sapo Materials: A Computational Study of Sta-7 Combined to 29si Mas Nmr Spectroscopy. *Microporous and Mesoporous Materials* **2008**, *107*, 268-275.

225.   Grenev, I. V.; Gavrilov, V. Y., Silicon Distribution in Sapo-11 Molecular Sieves: Simulation and Experimental Adsorption Study. *Microporous and Mesoporous Materials* **2020**, *294*, 109906.

226.   Li, Q.-M.; Zhang, M.; Wang, C.-M.; Zhu, Y.-A.; Zhou, X.-G.; Xie, Z.-K., Effects of Methylating Agent and Brønsted Acidity on Methylation Activity of Olefins in Cha-Structured Zeolites: A Periodic Dft Study. *Molecular Catalysis* **2018**, *446*, 106-114.

227.   Katada, N.; Nouno, K.; Lee, J. K.; Shin, J.; Hong, S. B.; Niwa, M., Acidic Properties of Cage-Based, Small-Pore Zeolites with Different Framework Topologies and Their Silicoaluminophosphate Analogues. *The Journal of Physical Chemistry C* **2011**, *115*, 22505-22513.

228.   Zheng, A.; Han, B.; Li, B.; Liu, S. B.; Deng, F., Enhancement of Bronsted Acidity in Zeolitic Catalysts Due to an Intermolecular Solvent Effect in Confined Micropores. *Chem Commun (Camb)* **2012**, *48*, 6936-6938.

229.   Elanany, M.; Vercauteren, D. P.; Kubo, M.; Miyamoto, A., The Acidic Properties of H-Mealpo-5 (Me=Si, Ti, or Zr): A Periodic Density Functional Study. *Journal of Molecular Catalysis A: Chemical* **2006**, *248*, 181-184.

230.   Fischer, M., Interaction of Water with (Silico)Aluminophosphate Zeotypes: A Comparative Investigation Using Dispersion-Corrected Dft. *Phys Chem Chem Phys* **2016**, *18*, 15738-15750.

231.   Fischer, M., Water Adsorption in Sapo-34: Elucidating the Role of Local Heterogeneities and Defects Using Dispersion-Corrected Dft Calculations. *Phys Chem Chem Phys* **2015**, *17*, 25260-25271.

232.   Fasano, M.; Falciani, G.; Brancato, V.; Palomba, V.; Asinari, P.; Chiavazzo, E.; Frazzica, A., Atomistic Modelling of Water Transport and Adsorption Mechanisms in Silicoaluminophosphate for Thermal Energy Storage. *Applied Thermal Engineering* **2019**, *160*, 114075.

233.   Fan, D.; Tian, P.; Xu, S.; Wang, D.; Yang, Y.; Li, J.; Wang, Q.; Yang, M.; Liu, Z., Sapo-34 Templated by Dipropylamine and Diisopropylamine: Synthesis and Catalytic Performance in the Methanol to Olefin (Mto) Reaction. *New Journal of Chemistry* **2016**, *40*, 4236-4244.

234.   Han, B.; Shin, C. H.; Cox, P. A.; Hong, S. B., Molecular Conformations of Protonated Dipropylamine in Alpo4-11, Alpo4-31, Sapo-34, and Alpo4-41 Molecular Sieves. *J Phys Chem B* **2006**, *110*, 8188-8193.

235.   Elanany, M.; Koyama, M.; Kubo, M.; Selvam, P.; Miyamoto, A., Periodic Density Functional Investigation of Brønsted Acidity in Isomorphously Substituted Chabazite and Alpo-34 Molecular Sieves. *Microporous and Mesoporous Materials* **2004**, *71*, 51-56.

236.   Ruiz-Salvador, A. R.; Gomez, A.; Diaz, B. N.; Ortega, Y.; Lewis, D. W., Si Atoms in Sapo-31: A Computational Study. *Recent Advances in the Science and Technology of Zeolites and Related Materials, Pts a - C* **2004**, *154*, 1439-1447.

237.   Fjermestad, T.; Svelle, S.; Swang, O., Desilication of Sapo-34: Reaction Mechanisms from Periodic Dft Calculations. *The Journal of Physical Chemistry C* **2015**, *119*, 2073-2085.

238.   Kapko, V.; Dawson, C.; Treacy, M. M.; Thorpe, M. F., Flexibility of Ideal Zeolite Frameworks. *Phys Chem Chem Phys* **2010**, *12*, 8531-8541.

239.   Earl, D. J.; Deem, M. W., Toward a Database of Hypothetical Zeolite Structures. *Industrial & Engineering Chemistry Research* **2006**, *45*, 5449-5454.

240.   Li, Y.; Yu, J.; Xu, R., Criteria for Zeolite Frameworks Realizable for Target Synthesis. *Angew Chem Int Ed Engl* **2013**, *52*, 1673-1677.

241.   Fischer, M., Proton Acidity and Proton Mobility in Ecr-40, a Silicoaluminophosphate That Violates Lowenstein's Rule. *Chemistry* **2019**, *25*, 13579-13590.

242.   Kianfar, E., Comparison and Assessment of Zeolite Catalysts Performance Dimethyl Ether and Light Olefins Production through Methanol: A Review. *Rev Inorg Chem* **2019**, *39*, 157-177.

243.   Ali, M. A.; Ahmed, S.; Al-Baghli, N.; Malaibari, Z.; Abutaleb, A.; Yousef, A., A Comprehensive Review Covering Conventional and Structured Catalysis for Methanol to Propylene Conversion. *Catalysis Letters* **2019**, *149*, 3395-3424.

244.   Yang, M.; Fan, D.; Wei, Y.; Tian, P.; Liu, Z., Recent Progress in Methanol-to-Olefins (Mto) Catalysts. *Adv Mater* **2019**, *31*, e1902181.

245.   Mehlhorn, D.; Valiullin, R.; Karger, J.; Cho, K.; Ryoo, R., Intracrystalline Diffusion in Mesoporous Zeolites. *Chemphyschem* **2012**, *13*, 1495-1499.

246.   Na, K.; Choi, M.; Ryoo, R., Recent Advances in the Synthesis of Hierarchically Nanoporous Zeolites. *Microporous and Mesoporous Materials* **2013**, *166*, 3-19.

247.   Na, K.; Jo, C.; Kim, J.; Cho, K.; Jung, J.; Seo, Y.; Messinger, R. J.; Chmelka, B. F.; Ryoo, R., Directing Zeolite Structures into Hierarchically Nanoporous Architectures. *Science* **2011**, *333*, 328-332.

248.	Hartmann, M., Hierarchical Zeolites: A Proven Strategy to Combine Shape Selectivity with Efficient Mass Transport. *Angew Chem Int Ed Engl* **2004**, *43*, 5880-5882.

249.	Parlett, C. M.; Wilson, K.; Lee, A. F., Hierarchical Porous Materials: Catalytic Applications. *Chem Soc Rev* **2013**, *42*, 3876-3893.

250.	Yang, X. Y.; Chen, L. H.; Li, Y.; Rooke, J. C.; Sanchez, C.; Su, B. L., Hierarchically Porous Materials: Synthesis Strategies and Structure Design. *Chem Soc Rev* **2017**, *46*, 481-558.

251.	Newland, S. H.; Sinkler, W.; Mezza, T.; Bare, S. R.; Carravetta, M.; Haies, I. M.; Levy, A.; Keenan, S.; Raja, R., Expanding Beyond the Micropore: Active-Site Engineering in Hierarchical Architectures for Beckmann Rearrangement. *ACS Catalysis* **2015**, *5*, 6587-6593.

252.	Potter, M. E.; Riley, L. N.; Oakley, A. E.; Mhembere, P. M.; Callison, J.; Raja, R., The Influence of Porosity on Nanoparticle Formation in Hierarchical Aluminophosphates. *Beilstein J Nanotechnol* **2019**, *10*, 1952-1957.

253.	Liu, Z.; Sun, Z.; Qin, D.; Yang, G., Sulfonic Acid-Functionalized Hierarchical Sapo-34 for Fructose Dehydration to 5-Hydroxymethylfurfural. *Reaction Kinetics, Mechanisms and Catalysis* **2019**, *128*, 523-538.

254.   Pan, Y.; Chen, G.; Yang, G.; Chen, X.; Yu, J., Efficient Post-Synthesis of Hierarchical Sapo-34 Zeolites Via Organic Amine Etching under Hydrothermal Conditions and Their Enhanced Mto Performance. *Inorganic Chemistry Frontiers* **2019**, *6*, 1299-1303.

255.   Yang, H.; Miao, P.; Sun, Q.; Zhang, Y.; Tian, D., Dual Templating Fabrication of Hollow Sapo-34 Molecular Sieves for Enhanced Mto Catalytic Activity and Selectivity. *Cryst Res Technol* **2019**, *54*, 1800132.

256.   Mousavi, S. H.; Fatemi, S.; Razavian, M., Synthesis and Stability Evaluation of Hierarchical Silicoaluminophosphates with Different Structural Frameworks in the Methanol to Olefins Process. *Particuology* **2018**, *37*, 43-53.

257.   Soltanali, S.; Darian, J. T., Synthesis of Mesoporous Sapo-34 Catalysts in the Presence of Mwcnt, Cnf, and Go as Hard Templates in Mto Process. *Powder Technology* **2019**, *355*, 127-134.

258.   Liu, Y.; Wang, L.; Zhang, J.; Chen, F.; Anpo, M., Preparation of Macroporous Sapo-34 Microspheres by a Spray Drying Method Using Polystyrene Spheres as Hard Template. *Research on Chemical Intermediates* **2011**, *37*, 949-959.

259.   Zhang, S.; Wen, Z.; Yang, L.; Duan, C.; Lu, X.; Song, Y.; Ge, Q.; Fang, Y., Controllable Synthesis of Hierarchical Porous Petal-Shaped Sapo-34 Zeolite with Excellent Dto Performance. *Microporous and Mesoporous Materials* **2019**, *274*, 220-226.

260.   Sun, Q.; Ma, Y.; Wang, N.; Li, X; Xi, D.; Xu, J.; Deng, F.; Yoon, K. B.; Oleynikov, P.; Terasaki, O.; Yu, J.,   High Performance Nanosheet-Like Silicoaluminophosphate Molecular Sieves: Synthesis, 3d Edt Structural Analysis and Mto Catalytic Studies. *J. Mater. Chem. A* **2014**, *2*, 17828-17839.

261.   Wang, C.; Yang, M.; Tian, P.; Xu, S.; Yang, Y.; Wang, D.; Yuan, Y.; Liu, Z., Dual Template-Directed Synthesis of Sapo-34 Nanosheet Assemblies with Improved Stability in the Methanol to Olefins Reaction. *Journal of Materials Chemistry A* **2015**, *3*, 5608-5616.

262.   Zhang, F.; Liu, Y.; Sun, Q.; Dai, Z.; Gies, H.; Wu, Q.; Pan, S.; Bian, C.; Tian, Z.; Meng, X.; Zhang, Y.; Zou, X.; Yi, X.; Zheng, A.; Wang, L.; Xiao, F. S., Design and Preparation of Efficient Hydroisomerization Catalysts by the Formation of Stable Sapo-11 Molecular Sieve Nanosheets with 10-20 Nm Thickness and Partially Blocked Acidic Sites. *Chem Commun (Camb)* **2017**, *53*, 4942-4945.

263.   Zhu, S.; Liang, S.; Wang, Y.; Zhang, X.; Li, F.; Lin, H.; Zhang, Z.; Wang, X., Ultrathin Nanosheets of Molecular Sieve Sapo-5: A New Photocatalyst for Efficient Photocatalytic Reduction of Co 2 with H 2 O to Methane. *Applied Catalysis B: Environmental* **2016**, *187*, 11-18.

264.   Sun, Q.; Wang, N.; Bai, R.; Chen, G.; Shi, Z.; Zou, Y.; Yu, J., Mesoporogen-Free Synthesis of Hierarchical Sapo-34 with Low Template Consumption and Excellent Methanol-to-Olefin Conversion. *ChemSusChem* **2018**, *11*, 3812-3820.

265.   Hemelsoet, K.; Qian, Q.; De Meyer, T.; De Wispelaere, K.; De Sterck, B.; Weckhuysen, B. M.; Waroquier, M.; Van Speybroeck, V., Identification of Intermediates in Zeolite-Catalyzed Reactions by in Situ Uv/Vis Microspectroscopy and a Complementary Set of Molecular Simulations. *Chemistry* **2013**, *19*, 16595-16606.

266.   Van Speybroeck, V.; Hemelsoet, K.; De Wispelaere, K.; Qian, Q.; Van der Mynsbrugge, J.; De Sterck, B.; Weckhuysen, B. M.; Waroquier, M., Mechanistic Studies on Chabazite-Type Methanol-to-Olefin Catalysts: Insights from Time-Resolved Uv/Vis Microspectroscopy Combined with Theoretical Simulations. *ChemCatChem* **2013**, *5*, 173-184.

267.   Hemelsoet, K.; Van der Mynsbrugge, J.; De Wispelaere, K.; Waroquier, M.; Van Speybroeck, V., Unraveling the Reaction Mechanisms Governing Methanol-to-Olefins Catalysis by Theory and Experiment. *Chemphyschem* **2013**, *14*, 1526-1545.

268.   Ilias, S.; Bhan, A., Mechanism of the Catalytic Conversion of Methanol to Hydrocarbons. *ACS Catalysis* **2012**, *3*, 18-31.

269.   Sastre, G., Confinement Effects in Methanol to Olefins Catalysed by Zeolites: A Computational Review. *Frontiers of Chemical Science and Engineering* **2016**, *10*, 76-89.

270.   Alwahabi, S. M.; Froment, G. F., Single Event Kinetic Modeling of the Methanol-to-Olefins Process on Sapo-34. *Industrial & Engineering Chemistry Research* **2004**, *43*, 5098-5111.

271.   Sierraalta, A.; Añez, R.; Coll, D. S.; Alejos, P., Conversion of Methanol to Dimethyl Ether over Silicoaluminophosphates: Isolated Acid Sites and the Influence of Silicon Islands. A Dft-Oniom Study. *Microporous and Mesoporous Materials* **2020**, *292*, 109732.

272.   Zang, K.; Zhang, W.; Huang, J.; Feng, P., Chabazite Architecture Dominates the Structure of Sapo-34's Surface Methoxy Species. *Catalysis Letters* **2019**, *149*, 2104-2109.

273.   Li, H.; Guo, C.; Huang, L.; Long, J.; Fu, X.; Chu, W.; Xiao, J., Toward a Comparative Description between Transition Metal and Zeolite Catalysts for Methanol Conversion. *Phys Chem Chem Phys* **2020**, *22*, 5293-5300.

274.   Zang, K.; Zhang, W.; Huang, J.; Feng, P.; Ding, J., First Molecule with Carbon–Carbon Bond in Methanol-to-Olefins Process. *Chemical Physics Letters* **2019**, *737*, 136844.

275.   Li, J.; Wei, Z.; Chen, Y.; Jing, B.; He, Y.; Dong, M.; Jiao, H.; Li X.; Qin, Z.; Wang, J.; Fan, W., A Route to Form Initial Hydrocarbon Pool Species in Methanol Conversion to Olefins over Zeolites. *J Catal* **2014**, *317*, 277-283.

276.   Li, J.; Wei, Y.; Chen, J.; Xu, S.; Tian, P.; Yang, X.; Li, B.; Wang, J.; Liu, Z., Cavity Controls the Selectivity: Insights of Confinement Effects on Mto Reaction. *ACS Catalysis* **2014**, *5*, 661-665.

277.   Hemelsoet, K.; Nollet, A.; Van Speybroeck, V.; Waroquier, M., Theoretical Simulations Elucidate the Role of Naphthalenic Species During Methanol Conversion within H-Sapo-34. *Chemistry* **2011**, *17*, 9083-9093.

278.   Wang, C.-M.; Wang, Y.-D.; Du, Y.-J.; Yang, G.; Xie, Z.-K., Similarities and Differences between Aromatic-Based and Olefin-Based Cycles in H-Sapo-34 and H-Ssz-13 for Methanol-to-Olefins Conversion: Insights from Energetic Span Model. *Catalysis Science & Technology* **2015**, *5*, 4354-4364.

279.   Liu, J.; Yin, Y.; Fu, X.-Z.; Luo, J.-L., Stability of C3-C6 Carbonium Ions inside Zeolites: A First Principles Study. *Applied Surface Science* **2020**, *503*, 144148.

280.   De Wispelaere, K.; Hemelsoet, K.; Waroquier, M.; Van Speybroeck, V., Complete Low-Barrier Side-Chain Route for Olefin Formation During Methanol Conversion in H-Sapo-34. *J Catal* **2013**, *305*, 76-80.

281.   Martinez-Espin, J. S.; De Wispelaere, K.; Westgård Erichsen, M.; Svelle, S.; Janssens, T. V. W.; Van Speybroeck, V.; Beato, P.; Olsbye, U., Benzene Co-Reaction with Methanol and Dimethyl Ether over Zeolite and Zeotype Catalysts: Evidence of Parallel Reaction Paths to Toluene and Diphenylmethane. *J Catal* **2017**, *349*, 136-148.

282. Liu, J.; Liu, Z.-F.; Feng, G.; Kong, D., Dimerization of Propene Catalyzed by Brønsted Acid Sites inside the Main Channel of Zeolite Sapo-5: A Computational Study. *The Journal of Physical Chemistry C* **2014**, *118*, 18496-18504.

283. Plessow, P. N.; Studt, F., Theoretical Insights into the Effect of the Framework on the Initiation Mechanism of the Mto Process. *Catalysis Letters* **2018**, *148*, 1246-1253.

284. Plessow, P. N.; Studt, F., Unraveling the Mechanism of the Initiation Reaction of the Methanol to Olefins Process Using Ab Initio and Dft Calculations. *ACS Catalysis* **2017**, *7*, 7987-7994.

285. De Wispelaere, K.; Ensing, B.; Ghysels, A.; Meijer, E. J.; Van Speybroeck, V., Complex Reaction Environments and Competing Reaction Mechanisms in Zeolite Catalysis: Insights from Advanced Molecular Dynamics. *Chemistry* **2015**, *21*, 9385-9396.

286. De Wispelaere, K.; Bailleul, S.; Van Speybroeck, V., Towards Molecular Control of Elementary Reactions in Zeolite Catalysis by Advanced Molecular Simulations Mimicking Operating Conditions. *Catalysis Science & Technology* **2016**, *6*, 2686-2705.

287. Sastre, G., Computational Study of Diffusion of Propane in Small Pore Acidic Zeotypes Afx and Aei. *Catalysis Today* **2014**, *226*, 25-36.

288.   Bailleul, S.; Rogge, S. M. J.; Vanduyfhuys, L.; Van Speybroeck, V., Insight into the Role of Water on the Methylation of Hexamethylbenzene in H-Sapo-34 from First Principle Molecular Dynamics Simulations. *ChemCatChem* **2019**, *11*, 3993-4010.

289.   Cnudde, P.; Demuynck, R.; Vandenbrande, S.; Waroquier, M.; Sastre, G.; Speybroeck, V. V., Light Olefin Diffusion During the Mto Process on H-Sapo-34: A Complex Interplay of Molecular Factors. *J Am Chem Soc* **2020**, *142*, 6007-6017.

290.   Aramburo, L. R.; Ruiz-Martínez, J.; Sommer, L.; Arstad, B.; Buitrago-Sierra, R.; Sepúlveda-Escribano, A.; Zandbergen, H. W.; Olsbye, U.; de Groot, F. M. F.; Weckhuysen, B. M., X-Ray Imaging of Sapo-34 Molecular Sieves at the Nanoscale: Influence of Steaming on the Methanol-to-Hydrocarbons Reaction. *ChemCatChem* **2013**, *5*, 1386-1394.

291.   Borodina, E.; Sharbini Harun Kamaluddin, H.; Meirer, F.; Mokhtar, M.; Asiri, A. M.; Al-Thabaiti, S. A.; Basahel, S. N.; Ruiz-Martinez, J.; Weckhuysen, B. M., Influence of the Reaction Temperature on the Nature of the Active and Deactivating Species During Methanol-to-Olefins Conversion over H-Sapo-34. *ACS Catal* **2017**, *7*, 5268-5281.

292.   Mores, D.; Stavitski, E.; Kox, M. H.; Kornatowski, J.; Olsbye, U.; Weckhuysen, B. M., Space- and Time-Resolved in-Situ Spectroscopy on the Coke Formation in Molecular Sieves: Methanol-to-Olefin Conversion over H-Zsm-5 and H-Sapo-34. *Chemistry* **2008**, *14*, 11320-11327.

293.   Ristanovic, Z.; Weckhuysen, B. M., Breakthroughs in Hard X-Ray Diffraction: Towards a Multiscale Science Approach in Heterogeneous Catalysis. *Angew Chem Int Ed Engl* **2014**, *53*, 8556-8558.

294.   Mores, D.; Kornatowski, J.; Olsbye, U.; Weckhuysen, B. M., Coke Formation During the Methanol-to-Olefin Conversion: In Situ Microspectroscopy on Individual H-Zsm-5 Crystals with Different Bronsted Acidity. *Chemistry* **2011**, *17*, 2874-2884.

295.   Qian, Q.; Ruiz-Martinez, J.; Mokhtar, M.; Asiri, A. M.; Al-Thabaiti, S. A.; Basahel, S. N.; van der Bij, H. E.; Kornatowski, J.; Weckhuysen, B. M., Single-Particle Spectroscopy on Large Sapo-34 Crystals at Work: Methanol-to-Olefin Versus Ethanol-to-Olefin Processes. *Chemistry* **2013**, *19*, 11204-11215.

296.   Aramburo, L. R.; de Smit, E.; Arstad, B.; van Schooneveld, M. M.; Sommer, L.; Juhin, A.; Yokosawa, T.; Zandbergen, H. W.; Olsbye, U.; de Groot F. M.; Weckhuysen, B. M., X-Ray Imaging of Zeolite Particles at the Nanoscale: Influence of Steaming on the State of Aluminum and the Methanol-to-Olefin Reaction. *Angew Chem Int Ed Engl* **2012**, *51*, 3616-3619.

297.   Qian, Q.; Ruiz-Martínez, J.; Mokhtar, M.; Asiri, A. M.; Al-Thabaiti, S. A.; Basahel, S. N.; Weckhuysen, B. M., Single-Catalyst Particle Spectroscopy of Alcohol-to-Olefins Conversions: Comparison between Sapo-34 and Ssz-13. *Catalysis Today* **2014**, *226*, 14-24.

298.   Goetze, J.; Meirer, F.; Yarulina, I.; Gascon, J.; Kapteijn, F.; Ruiz-Martinez, J.; Weckhuysen, B. M., Insights into the Activity and Deactivation of the Methanol-to-Olefins Process over Different Small-Pore Zeolites as Studied with Operando Uv-Vis Spectroscopy. *ACS Catal* **2017**, *7*, 4033-4046.

299.   Kumar, R.; Chowdhury, B., Comprehensive Study for Vapor Phase Beckmann Rearrangement Reaction over Zeolite Systems. *Industrial & Engineering Chemistry Research* **2014**, *53*, 16587-16599.

300.   Izumi, Y.; Ichihashi, H.; Shimazu, Y.; Kitamura, M.; Sato, H., Development and Industrialization of the Vapor-Phase Beckmann Rearrangement Process. *Bulletin of the Chemical Society of Japan* **2007**, *80*, 1280-1287.

301.   Dahlhoff, G.; Niederer, J. P. M.; Hoelderich, W. F., ϵ-Caprolactam: New by-Product Free Synthesis Routes. *Catalysis Reviews* **2001**, *43*, 381-441.

302.   Fan, D.; Dai, D. J.; Wu, H. S., Ethylene Formation by Catalytic Dehydration of Ethanol with Industrial Considerations. *Materials (Basel)* **2012**, *6*, 101-115.

303.   Galadima, A.; Muraza, O., Zeolite Catalysts in Upgrading of Bioethanol to Fuels Range Hydrocarbons: A Review. *Journal of Industrial and Engineering Chemistry* **2015**, *31*, 1-14.

304.   Sun, J.; Wang, Y., Recent Advances in Catalytic Conversion of Ethanol to Chemicals. *ACS Catalysis* **2014**, *4*, 1078-1090.

305.   Zhang, M.; Yu, Y., Dehydration of Ethanol to Ethylene. *Industrial & Engineering Chemistry Research* **2013**, *52*, 9505-9514.

306.   Potter, M. E.; Aswegen, S. V.; Gibson, E. K.; Silverwood, I. P.; Raja, R., Spectroscopic Investigation into the Design of Solid-Acid Catalysts for the Low Temperature Dehydration of Ethanol. *Phys Chem Chem Phys* **2016**, *18*, 17303-17310.

307.   Potter, M. E.; Armstrong, L. M.; Carravetta, M.; Mezza, T. M.; Raja, R., Designing Multi-Dopant Species in Microporous Architectures to Probe Reaction Pathways in Solid-Acid Catalysis. *Front Chem* **2020**, *8*, 171.

For Table of Contents Only
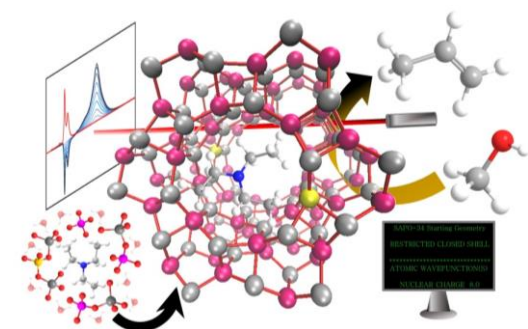
Since their discovery, SAPOs have been a highly active area of research. This review discusses recent developments in synthesis, characterisation, theoretical studies and catalysis in the field of SAPO research.